

Mechanical Performance and Failure of Laminated Composites Made by
Automated Fibre Placement (AFP) Process

Mohammadhossein Ghayour

A Thesis

In the Department

Of

Mechanical, Industrial and Aerospace Engineering

Presented in Partial Fulfillment of the Requirements

For the Degree of

Doctor of Philosophy Mechanical Engineering at

Concordia University

Montreal, Quebec, Canada

October 2021

© Mohammadhossein Ghayour, 2021

CONCORDIA UNIVERSITY
SCHOOL OF GRADUATE STUDIES

This is to certify that the thesis prepared

By: Mohammad Hossein Ghayour

Entitled: **Mechanical Performance and Failure of Laminated Composites Made by Automated Fibre Placement (AFP) Process**

and submitted in partial fulfillment of the requirements for the degree of

Doctor Of Philosophy (Mechanical Engineering)

complies with the regulations of the University and meets the accepted standards with respect to originality and quality.

Signed by the final examining committee:

_____	Chair
Dr. Sébastien Le Beux	
_____	External Examiner
Dr. Rachid Boukhili	
_____	External to Program
Dr. Khaled Galal	
_____	Examiner
Dr. Suong Van Hoa	
_____	Examiner
Dr. Farjad Shadmehri	
_____	Thesis Co-Supervisor
Dr. Mehdi Hojjati	
_____	Thesis Co-Supervisor
Dr. Rajamohan Ganesan	

Approved by

Dr. Ivan Contreras, Graduate Program Director

9/15/2021

Dr. Mourad Debbabi, Dean
Gina Cody School of Engineering and Computer Science

ABSTRACT

Mechanical Performance and Failure of Laminated Composites Made by Automated Fibre Placement (AFP) Process

Mohammadhossein Ghayour, Ph.D.

Concordia University, 2021

Automated Fibre Placement (AFP) is a new robot technology that has the advantages of both the rapid manufacturing process and reducing material waste. However, new types of defects are introduced into the composite structures when using the fibre tows instead of composite prepreg sheets. These defects can cause geometrical discontinuities and local material inhomogeneities. Although the effect of these defects on the in-plane mechanical performance of composite structures can be found in the literature, there is still a lack of knowledge in studying the out-of-plane and impact response of the composite laminates.

The main objective of this research study is to investigate the effect of induced tow-gaps on the Low-Velocity Impact (LVI) response and Compression After Impact (CAI) response of the thin composite plates. For this purpose, defective quasi-isotropic composite plates have been manufactured with the AFP technique. Two millimetres of tow-gaps are embedded in all composite plies to provide an average of 8% of pre-cured volumetric gaps in all specimens.

The test specimens are subjected to impact loads with impact energies of 5 J, 10 J, and 15 J, and the corresponding impact response and projected delamination of the defective plates are compared with the baseline sample. Delamination areas are measured using the Ultrasonic C-scan technique. CAI tests are carried out to evaluate the residual compressive strengths of the defective impacted samples. Furthermore, Digital Image Correlation (DIC) technique is used during the CAI tests to measure the in-plane strains of the specimen under compressive loading. Effect of the curing process on the gap formation is evaluated by measuring the Induced Gap Shrinkage Factor (IGSF) using microscopic observation. This factor is used for numerical simulation of the defective composite plates. Additional tests on beams are performed to evaluate the out-of-plane response of the defective beams. Three-point bending tests are carried out on both short and standard beams to measure the interlaminar shear strength and flexural stiffness/strength of the composite beams with tow-gaps.

Furthermore, Induced Defect Layer Method (IDL), a robust meso-macro model, is developed for damage analysis of the defective laminates. This method uses a geometrical parameter to incorporate induced gaps in the elastic, inelastic, and softening behaviour of the material. The main advantage of the proposed method is that a novel homogenization technique is used to include tow gaps in composite damage analysis of defective laminates. In addition, IDL evaluates the mechanical response of the defective laminates with acceptable precision and less computational time compared to the current numerical models.

Results indicate that tow-gaps can reduce the impact resistance of the composite plates by about 17% for low levels of impact energy. It is also shown that the interaction of induced gaps and impact damage at the compressive residual strength reduction of impacted thin composite plates is significant and cannot be neglected. Numerical results show that the IDL is a robust method for damage analysis of the composite laminates with induced gaps.

Acknowledgement

I am most grateful for the support, guidance, wisdom, and inspiration I received from my Supervisors, Professor Mehdi Hojjati and Professor Rajamohan Ganesan, Concordia University. They trusted my ideas and kindly devoted hours of their time to guide me through my challenging PhD program logically.

I feel indebted to the dedication and support of Professor Suong Van Hoa, who established Concordia Centre for Composites (CONCOM). I sincerely acknowledge the FRQNT Scholarship (BX2) for supporting my PhD candidature at Concordia University. I would like to thank Bombardier Aerospace for providing the advanced materials and Natural Sciences and Engineering Research Council of Canada (NSERC) for providing research facilities, without which it would have been impossible to complete my studies.

A big recognition goes to Mr Marc Genest and Mr Trent Gillies from National Research Council (NRC), Ottawa, for performing the Ultra-Sonic C-scan tests. I am particularly thankful to the highly experienced technical staff, Dr Daniel Rosca, Dr Heng Wang, all my colleagues and friends, Nima, Muhsan, Massimo, Shambhu, Alireza, Ali and Sandesh.

Dedication

Dedication

I would like to dedicate this thesis to my beloved family.

To my love, Fahimeh, who I am willing to commence the new sweet chapter of my life with her.

To my parents, Mehri and Morteza and my siblings, Elham and Mahdi, for all their love, endless support, guidance and for being a ray of sunshine.

To my nephew, Iliya, who was always calling me during my work and was making me remember that life is beautiful and there is so much to smile about.

List of papers/conference presentations

Journal Papers

- [1] Ghayour M, Ganesan R, Hojjati M., "Impact Damage assessment of thin impacted defective composite laminates manufactured by Automated Fibre Placement", Submitted to *Journal of Composite Structures*.
- [2] Ghayour M, Hojjati M., Ganesan R, "Induced Defect Layer Method to characterize the effect of fibre tow gaps for the laminates manufactured by Automated Fibre Placement Technique". *J Compos Mater*, 2021, <https://doi.org/10.1177/00219983211031649> 2021; 002199832110316.
- [3] Ghayour M, Ganesan R, Hojjati M., "Flexural response of composite beams made by Automated Fibre Placement process: Effect of fibre tow gaps". *Compos Part B Eng* 2020; 201: 108368.
- [4] Ghayour M, Hojjati M, Ganesan R., "Effect of Tow Gaps on Impact Strength of Thin Composite Laminates Made by Automated Fibre Placement: Experimental and Semi-Analytical Approaches". *Compos Struct* 2020; 248: 112536.

Conference Papers/Presentations

- [1] Ghayour M., Hojjati M. and Ganesan R., "Residual Stress State of Composite Laminates with Automated Induced-Gap Subjected to Hemi-Spherical Impact Loading", Proceedings of the American Society for Composites—Thirty-Sixth Technical Conference on Composite Materials, 19-22 September 2021.
- [2] Ghayour M., Ganesan R. and Hojjati M., "Statistical Characterization of the Microstructure of the Composite Plates with Induced Defects in Automated Manufacturing", in *23rd International Conference on Composite Structures (ICCS23)*, Porto, Portugal 01-04 September 2020.
- [3] Ghayour M., Hojjati M. and Ganesan R., "Effect of Gaps on the Damage Initiation and Failure of Thin Composite Laminates Manufactured by AFP Under Out-of-Plane Loading", in *SAMPE 2020*, Seattle, USA, 04-07 May 2020.
- [4] Ghayour M., Ganesan R. and Hojjati M., "Interlaminar Shear Strength of the Carbon/Epoxy Composites Containing Gaps Induced by Automated Fibre Placement Process", in *11th Canadian-International Conference on Composites*, CANCOM 2019, Kelowna, Canada. 22-25 July 2019.
- [5] Ghayour M., Hojjati M. and Ganesan R., "Effect of Manufacturing Flaws on the Behaviour of Composite Beams Manufactured by Automated Fibre Placement (AFP) Process, in *Fourth International Symposium on Automated Composites Manufacturing, ACM4*, Montreal, Canada, 25-26 May 2019.

Table of Content

List of Figures	iv
List of Tables	viii
CHAPTER 1	1
1. Introduction and Motivation	2
1.1 Automated Manufacturing in Composite Industry.....	2
1.2 AFP Process Description.....	4
1.3 AFP Induced Defects	5
1.4 Experimental Tests of the Laminates Made by AFP Technique.....	6
1.5 Computational Modeling of the Laminates Made by AFP Technique	6
1.6 Research Motivation	7
1.7 Research Objective.....	7
1.8 Research Scope	8
1.9 Thesis Layout	8
CHAPTER 2	10
2. Literature Review.....	11
2.1 AFP Manufacturing Defects.....	11
2.2 Experimental Observation.....	12
2.3 Numerical Simulations.....	14
2.4 Concluding Remarks	16
CHAPTER 3	17
3. Effect of Tow Gaps on Impact Strength of Thin Defective Composite Laminates Manufactured by AFP technique	18
Summary	19
3.1 Introduction	19
3.2 Materials and Manufacturing	20
3.2.1 AFP Layup Process.....	20
3.2.2 Vacuuming and Curing Process.....	21
3.3 Quality of the Cured Plates	24
3.3.1 Differential Scanning Calorimetry Test.....	25
3.3.2 Ultrasonic C-Scan tests	26

Contents

3.3.3	Microscopic Observation of the Cured Samples	27
3.4	Experimental Procedure	28
3.5	Semi-Analytical Approach.....	29
3.6	Results and Discussion.....	32
3.7	Concluding Remarks	40
CHAPTER 4	42
4.	Flexural Response of Defective Composite Beams.....	43
	Summary.....	44
4.1	Introduction	44
4.2	Experimental Investigation	45
4.3	Numerical Simulation	47
4.3.1	Material Damage Model	49
4.1	Nonlinear Shear Model	50
4.1.1	Epoxy Material Model	53
4.1.2	Damage Law for Cohesive Elements.....	55
4.2	Results and Discussion.....	57
4.2.2	Short Beam Shear Test.....	59
4.3	Flexural Test.....	63
4.4	Concluding Remarks	67
CHAPTER 5	69
5.	Induced Defect Layer Method	70
	Summary.....	71
5.1	Introduction	71
5.2	Induced Defect Layer Method (IDLM).....	73
5.2.1	Generalized Method of Cell.....	76
5.2.2	Composite damage model.....	77
5.2.3	Epoxy Material Model	78
5.3	Results and Discussion.....	80
5.3.1	Single Material Point	80
5.3.2	Multiscale Analysis of Defective Composite Laminates.....	83
5.4	Concluding Remarks	89
CHAPTER 6	91
6.	Impact Damage Assessment of Defective Composite Laminates: Experimental Studies and Numerical Simulations.....	92

Contents

Summary	93
6.1 Introduction	93
6.2 Experimental Investigation	95
6.2.1 Fabrication Process	95
6.2.2 Impact Test.....	96
6.2.3 Compression after impact test.....	96
6.3 Numerical Studies	97
6.4 Results and Discussion.....	99
6.4.1 Induced Gap shrinkage factor (IGSF) and Consolidation Factor (CF).....	99
6.4.2 Low-Velocity Impact Results	101
6.4.3 Effect of Induced gap on Delamination Initiation and Propagation	104
6.4.4 Compression After Impact (CAI)	106
6.5 Concluding Remarks	110
CHAPTER 7	112
7. Conclusions and Future Work	113
7.1 Conclusions	113
7.2 Future Work	114
References.....	116

List of Figures

Figure 1-1 Main Components of AFP system [8].....	3
Figure 1-2 A graphical view of the change in composite manufacturing methods comparing with the composite weight ratio in aircraft [9].....	3
Figure 1-3 Adoption of AFP technique over traditional manufacturing technique [12]	4
Figure 1-4 A schematic view of AFP head [15]	4
Figure 1-5 AFP steered tows on a mould [16].....	5
Figure 1-6 Different types of AFP manufacturing defect (reproduced from Ref. [19])	5
Figure 2-1 Advanced Composite Structures Inspection System [22].....	11
Figure 2-2 Non-staggered tow-defects at mid-ply of a composite laminate	12
Figure 2-3 Cross-section view of a composite plate with a 3.175 mm gap (a) no caul plate (2) with caul plate [35]	12
Figure 2-4 Effect of AFP defects on the strength reduction of Carbon/Epoxy laminates. Reproduced from Ref. [28]	13
Figure 2-5 Delamination initiation from the gap after 10 ⁵ cycles [42].....	13
Figure 2-6 Effect of tow-gaps on the projected delamination pattern of variable stiffness laminates under medium impact loads [33]	14
Figure 2-7 Microscopic and schematic views of different types of gap shapes after the curing process.....	15
Figure 2-8 Microscopic and FE models of the gap and overlap based on observation [43].....	16
Figure 3-1 Schematic illustration of placing widespread periodical gaps during AFP (a) Robot arm(b) Top view (c) Cross-section view	21
Figure 3-2 Principal elements of the vacuuming process	22
Figure 3-3 sandpaper the base tool and the caul plate	23
Figure 3-4 Vacuumed composite plate	23
Figure 3-5 Curing Cycle of CYCOM 977-2 HTS 40	24
Figure 3-6 (a) Circular band saw machine (b) Drying the samples in the oven	24
Figure 3-7 MDSC TA Q200 DSC machine.....	25
Figure 3-8 Heat flow versus temperature for the uncured selected material	26
Figure 3-9 Heat flow versus temperature of the cured sample (AFP-G sample).....	26
Figure 3-10 (a) manufactured by AFP AFP-G (b) manufactured by HL technique (baseline)	27
Figure 3-11 Immersed samples in the resin epoxy	27
Figure 3-12 Polishing machine	28
Figure 3-13 Microscopy image of the intact laminate	28
Figure 3-14 LVI test; Fixture and boundary condition.....	29
Figure 3-15: Two-Degree of freedom of Mass-Spring model.....	30
Figure 3-16 Effect of fibre tow gaps on the thickness change of Quasi-isotropic composite laminates	31
Figure 3-17 Gap area after the curing process for (a) interlayers (b) outer layers.....	32
Figure 3-18 Thickness reduction of the composite plates with widespread induced fibre tow gaps	33
Figure 3-19 Comparison of the (a) Impact responses and (b) projected delamination patterns for AFP-G and baseline samples at different levels of impact energy	35

List of Figures

Figure 3-20 A comparison of the maximum impact force between the samples with widespread gaps and baseline samples for different impact energy levels.....	36
Figure 3-21 A comparison between the projected delamination of AFP-G with baseline at different levels of impact energy (a) Longest delamination diagonal length(b) Projected delamination area (c) Projected delamination shape	36
Figure 3-22 Impact depth versus impact energies for baseline and AFP-G samples	37
Figure 3-23 (a) Force versus impactor Displacement (b) Impact Energy versus time for different levels of IEs.....	39
Figure 3-24 Delamination pattern and matrix cracking in the middle section of the samples for impact energy (a) 10 J (b) 15 J.....	39
Figure 3-25 Delamination initiation in the composite plates under impact loading at gap area (Resin-rich area).....	40
Figure 4-1 Automated Fibre Placement process (a) Fibre deposition by a 6-axis articulated robot arm (b) Fibre tow gap between the fibre courses.....	46
Figure 4-2 Dimensions and boundary conditions of the specimens for the (a) three-point bending test and (b) short-beam shear test (All dimensions are in <i>mm</i>).....	47
Figure 4-3 Isometric view of the FE models for (a) Short beam shear test (b) Flexural test	49
Figure 4-4 Non-linear shear stress and shear damage parameter versus shear strain.....	53
Figure 4-5 (a) A graphical view of the yield surface of the epoxy resin material (b) Stress-strain curve of the epoxy resin under uniaxial loading condition.....	55
Figure 4-6 Traction-displacement relationship for cohesive surface under mixed fracture modes	57
Figure 4-7 Effect of fibre tow gaps on thickness reduction of Carbon/Epoxy composite laminate (a) in the present study (b) (Reproduced Figure from Ref. [32] from <i>Automated Composites Manufacturing (ACM4), Proceedings of the Fourth International Symposium of ACM, Montreal, Canada, 2019</i> . Lancaster, PA: DEStech Publications, Inc.).....	58
Figure 4-8 Local thickness reduction at the gap area	58
Figure 4-9 Distribution of the Fibre Volume Fraction and fibre distributions at the gap zone in 45° lamina.....	58
Figure 4-10 Applied force versus. Out-of-plane displacement of short beams for (a) Baseline (b) AFP-G samples. The final failure of the short beams under flexural loading: (c) Experimental observation (d) Numerical simulation	60
Figure 4-11 Comparison of ILSS between the experimental and numerical results	61
Figure 4-12 Effect of fibre tow gap on the shear stress contour and the delamination of the short beam under transverse loading. Shear stress (τ_{13}) for (a) baseline (b) AFP-G samples right before the failure. Delamination pattern at section <i>B</i> for (c) baseline(d) AFP-G samples	62
Figure 4-13 Effect of tow gap on the through-the-thickness shear stress at section <i>A</i>	62
Figure 4-14 Effect of the tow gap on the interlaminar shear stress of the short beams in section <i>B</i>	63
Figure 4-15 Delamination initiation from the gap area	63
Figure 4-16 Applied force versus out-of-plane displacement for (a) Baseline (b) AFP-G samples. Comparison of the failure of the beams under out-of-plane loading between (c) Experimental observation and (d) Numerical study.....	65
Figure 4-17 (a) Experimental setup (b) load-displacement curve for $[90_2/-45_2/0_2/45_2]_s$ (c) damaged beam after the failure	66

List of Figures

Figure 4-18 Comparison of the crack density of 90° plies versus longitudinal strain for AFP-G and baseline samples with the stacking sequence of [90 ₂ /-45 ₂ /0 ₂ /45 ₂] _s under flexural loading	67
Figure 4-19 (a) Delamination initiation in the standard beam under transverse loading (b) Contour of the plastic strain at the gap area at the cross-head displacement of 15 mm.....	67
Figure 5-1 Cross-section view of a composite laminate with the induced gap	74
Figure 5-2 (a) Fabrication of a composite plate with AFP robot (b) ply-by-ply mapping induced gaps to FE meshes (c) Definition of Gap Percentage at macro FE model.....	75
Figure 5-3 (a) macro meso gap percentage transfer from the selected element (b) Representative Unit Cell of the IDLM method (<i>C</i> and <i>R</i> stand for composite material and resin, respectively) .	75
Figure 5-4 (a) A multiphase composite with periodic microstructure and (b) corresponding RUC (c) Discretized RUC with eight sub-cells labelled as α , β , $\gamma=1,2$ [107].....	77
Figure 5-5. Stress-strain curves of the epoxy resin under (a) uniaxial (b) in-plane shear loading condition	80
Figure 5-6 Effect of GP on the stiffness reduction of Cycom 977-2/ HTS 40 unidirectional ply	81
Figure 5-7 Effect of GP (a) on the stress-strain behaviour in longitudinal direction and (b) transverse direction, and (c) on in-plane shear stress-strain	82
Figure 5-8 Effect of GP on the failure envelope for in-plane stresses in the fibre direction	82
Figure 5-9 Effect of GP on the failure envelope for in-plane transverse stress (direction 2)	83
Figure 5-10 Top view of the numerical model with gaps.....	84
Figure 5-11 Contour of GP for different mesh sizes for zero and 90° plies for (a) 2.0 mm (b) 1.0 mm (c) 0.5 mm of the approximate global mesh size (only a quarter of the samples have been shown).....	85
Figure 5-12 Effect of mesh size and gap on the tensile response of the FE numerical model presented in Figure 5-10	86
Figure 5-13 Comparison of the Compressive strength of the defective composite laminate; present study versus the experiment.....	86
Figure 5-14 Effect of gap on the in-plane stress distribution (σ_{11}) at zero-degree plies for G-Zero-Ninety case before the failure	86
Figure 5-15 Comparison of the flexural load versus displacement of the defective composite beams; present study versus the experiment.....	87
Figure 5-16 Distributed partial gaps and the corresponding max principal stress for 90° ply (a) with AFP tow gaps (b) without gaps.....	88
Figure 5-17 (a) Comparison of the tensile strength of the defective composite laminate; present study versus the experiment [34] (b) fibre breakage and matrix crack pattern at zero and ninety plies.....	89
Figure 5-18 (a) Comparison of the compressive strength of the defective composite laminate; present study versus the experiment [34] (b) gap pattern of the defective specimens at zero plies	89
Figure 6-1 (a) Fibre deposition by AFP robot head (b) 2.0 mm tow-gap between the fibre courses	96
Figure 6-2 (a) CEAST 9340 Instron machine for impact test (b) CAI test setup, 100 kN MTS machine, and DIC camera.....	97
Figure 6-3 Boundary conditions for (a) low-velocity impact (b) Compression after impact simulation.....	99
Figure 6-4 (a) Top view of Composite plate FE mesh (b) Tetrahedral elements for rigid body impactor	99

List of Figures

Figure 6-5 Gap shrinkage due to in-ply and out-of-ply fibres movement	100
Figure 6-6 Resin pocket at gap zones at 90° ply	101
Figure 6-7 Statistical results of the tow-gap length obtained from the different spots of the AFP-G samples.....	101
Figure 6-8 Comparison of impact force versus; experimental and numerical results for IE= 5 J, 10 J, and 15 J.....	102
Figure 6-9 Numerical results of the impact energy versus time for both baseline and defective samples.....	103
Figure 6-10 Numerical results of the projected delamination pattern for baseline and AFP-G samples.....	103
Figure 6-11 (a) Cross-section view of the deformed specimen under impact loading for IE = 15 J (b) Resin failure at gap areas close to the impact zone(c) Gap areas mapped on the FE elements	104
Figure 6-12 Effect of tow-gaps on the delamination patterns of the laminated under IE = 10 J	105
Figure 6-13 Effect of upper and lower ply gap lines on the delamination propagation of the laminates under low-velocity impact loads.....	106
Figure 6-15 Compressive stress versus longitudinal strain for the specimens under (a) IE = 5 J, (b) IE = 10 J, (c) IE = 15 J.....	107
Figure 6-16 Residual strength versus (a) Impact Energy (b) Maximum delamination length ...	108
Figure 6-17 Observed failure modes of the impacted samples (a) Lateral gage away from damage (b) Widespread delamination.....	108
Figure 6-18 Comparison of in-plane strain contours between non-impacted and impacted samples under IE = 5 J at displacement load equal to 1.15 mm	109
Figure 6-19 In-plane strain contours for impacted samples under IE = 15 J at displacement load equal to 1.03 mm.....	110

List of Tables

List of Tables

Table 3-1: Properties of the experimental samples.....	21
Table 4-1. Properties of the test samples	46
Table 4-2 Material properties of Cycom 977-2/ HTS 40 unidirectional ply [79, 80].....	49
Table 4-3 Hashin Failure Criteria	49
Table 4-4 Damage evolution parameters for composite ply [82]	52
Table 4-5 General characteristics of the FE models of the short beam	59
Table 4-6 Experimental results of the flexural tests for both baseline and AFP-G samples	65

CHAPTER 1

Introduction and Motivation

1. Introduction and Motivation

1.1 Automated Manufacturing in Composite Industry

Since inventing carbon fibres in the early 1960s, there has been an increased demand for advanced composite materials in the aircraft and automotive industries. Although weight reduction has been the primary objective of utilizing composite materials in aircraft structures, reducing carbon footprint has become a significant reason for the climate change crisis. For example, composite material is contained in more than 50% of the structural weight of Aircrafts such as Airbus A350XWB and Boeing 787. Furthermore, Airbus [1] and Boeing [2] forecast an annual increase of 4.3% and 4.6% in air transportation demand between 2019 to 2038, respectively, leading to new aircraft demands, and consequently, it increases the demand for composite material. Thus, the hand-layup technique widely used in the aircraft industry due to the limited number of productions may not be cost- and time-effective anymore for the future of the composite industry.

Automated manufacturing as one of the elements of Industry 4.0 is one of the solutions to reduce labour costs and improve product quality. Because typically, 40% to 60% of composite manufacturing costs relate to ply collation and cutting [3]. Implementing the automated technology in the composite industry started by inventing the Filament Winding (FW) technique in the late 1960s [4]. However, the application of FW is limited to create hollow composite structures such as pipes [5]. Automated Tape Laying (ATL) was then developed for the fabrication of composite components. ATL uses wide prepreg tape ($>305\text{ mm}$), making it suitable for large flat or low curve structures such as wing skin. Nevertheless, this technique could not be applied to complex shapes.

Automated Fibre Placement (AFP) is a hybrid technique initially developed in the early 1980s to overcome the limitation of ATL and FW techniques [6]. Figure 1-1 shows an AFP system's main components: a head with a compaction roller, fibre feeding system, a robotic arm, and a control panel. AFP has two main advantages over than ATL technique.

- (1) The wide tape has been replaced by fibre tows: The tows have a nominal width of 6.35 mm . AFP allows the individual tows to be cut or stopped during the fabrication process. This feature adds more flexibility to the AFP technique. Although the productivity of the AFP might be decreased by replacing the tape, today's AFP robots can place up to 32 tows in one layup process.
- (2) AFP facilitates a six-degrees-of-freedom articulated robot arm: The robot arm makes the AFP method a robust method for laying up the fibre tows on complex moulds [7].

The flexibility of mounting two modular layup heads for thermoplastic and thermoset composite fibre tows and fibre steering are other exciting features of the AFP technique.

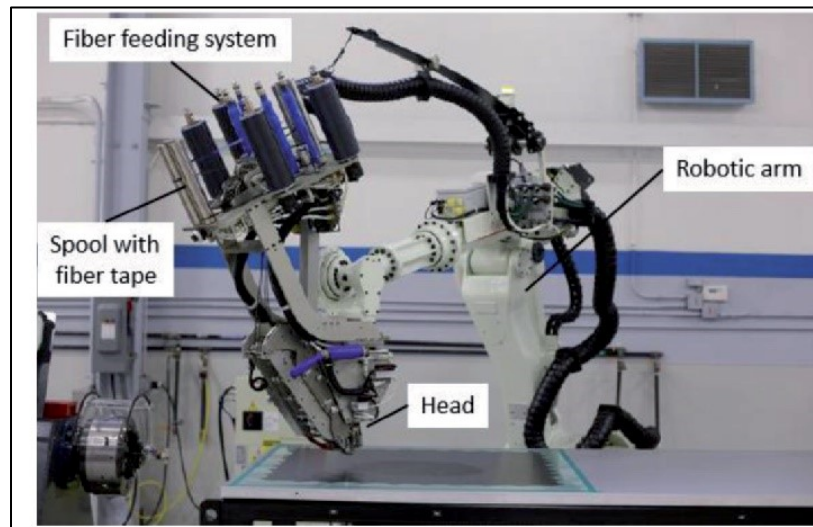


Figure 1-1 Main Components of AFP system [8]

Figure 1-2 shows a graphical view of the change in the composite manufacturing method in the last fifty years by comparing it with the composite weight percentage in aircraft. It is shown that AFP has become one of the pioneer methods in the last twenty years.

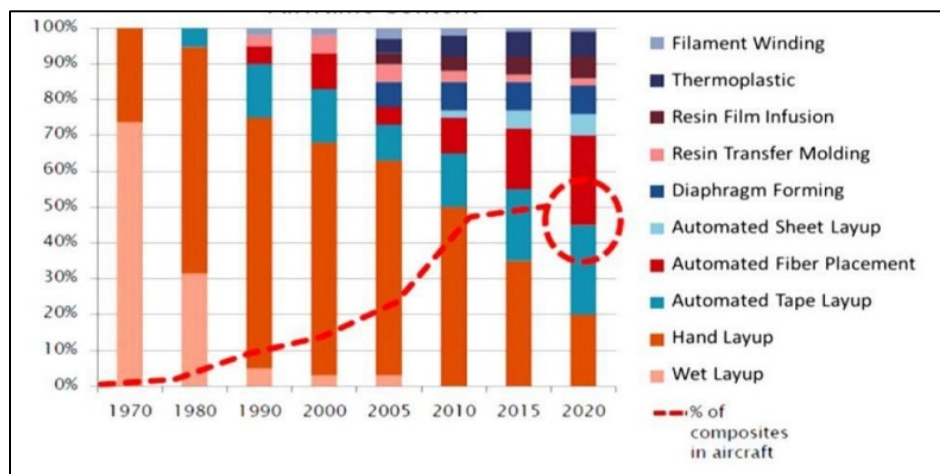


Figure 1-2 A graphical view of the change in composite manufacturing methods comparing with the composite weight ratio in aircraft [9]

Comparing the AFP with the traditional manual lay-up, a lay-up rate of 30 meters/min was reported [10], which yields 1.9 kg/h for Carbon Fibre Reinforced Plastics (CFRP) materials. This productivity was compared to the 0.7 kg/h productivity of hand-layup for the same component. Initially, the AFP application was limited to manufacturing engine inlet fairing of large aircraft with complex geometry. However, due to recent advancements in AFP systems, AFP is used for a broad range of aircraft structures, such as the A350 fuselage [11]. Figure 1-3 shows the pie chart of the adoption of AFP over traditional techniques. While only 7% of the composite components were manufactured by AFP in 1990, the AFP technique was adopted to manufacture 35% of composite structures in 2020.

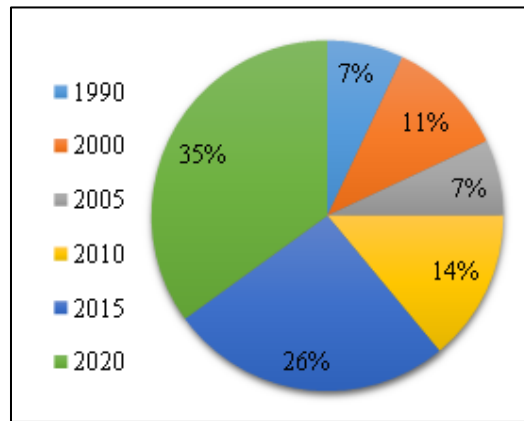


Figure 1-3 Adoption of AFP technique over traditional manufacturing technique [12]

1.2 AFP Process Description

One of the main differences between AFP and ATL is the width of fibres laid on the tools. The typical fibre tow width is 3.2 mm , 6.4 mm , and 12.7 mm . However, depending on the machine, AFP can deliver up to 32 tows in a single sequence. The advantage of having several tows in one sequence rather than a wide prepreg (that is used in ATL) is that each tow can be driven individually during the layup position. In other words, single tows can be individually cut, restarted, and clamped [13], as shown in Figure 1-4. This advantage makes AFP a convenient method for fabricating structures with complex shapes in conjunction with the fibre steering capability. In addition, using fibre tows instead of wide prepreg sheets reduces material waste.

AFP steering was primarily invented to improve the lay-up deposition over the double curvature structures. AFP can steer the fibre tows because it can run the tows at an individual speed [14]. It was later found that the steering can be applied to fabricate the variable stiffness structures [15–18] that bear a higher buckling load than the regular composite laminates. Figure 1-5 shows the steered tows on a mould. In order to lay the steered tows, the inner and outer tows should be run with different feeding rates to prevent the fibre courses from local buckling and wrinkling.

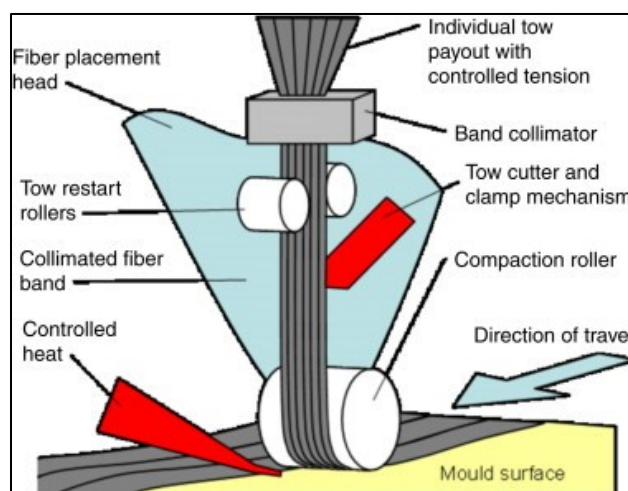


Figure 1-4 A schematic view of AFP head [15]

Fibre steering brings the advantages of using the AFP technique. However, the fibre tows deposition on complex geometric is challenging. The process of laying down the several tows on a curved path with different curvature radiuses creates inevitable manufactured induced imperfections. The lay-up quality and the mechanical performance of the final part can be significantly affected by the inherent flaws. The amount and the dimension of the flaws are the determinant parameters for accepting or rejecting the fabricated composite structures.



Figure 1-5 AFP steered tows on a mould [16]

1.3 AFP Induced Defects

Inherent defects can be categorized as gap, overlap, missing tow, upfolding, tow wrinkling [17, 18], twisted tow, bridging, and crowning, as shown in Figure 1-6. Gap and overlap are the most probable types of defects that may occur during the automated fibre deposition which their effect on the durability of the structures cannot be neglected [10].

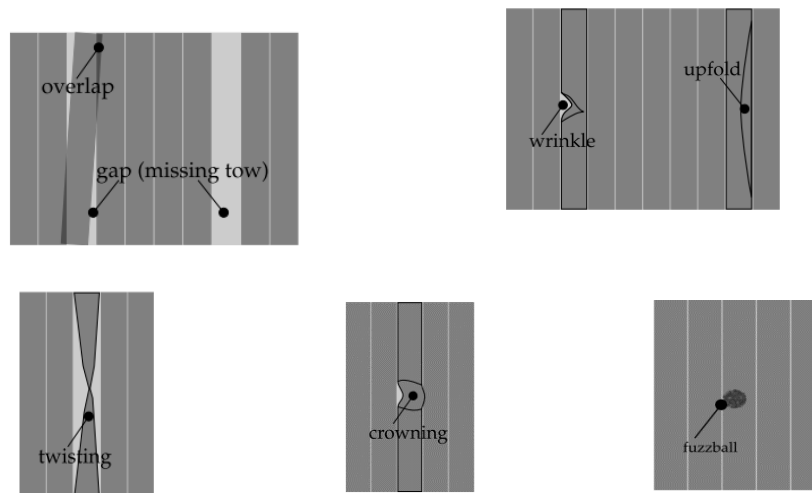


Figure 1-6 Different types of AFP manufacturing defect (reproduced from Ref. [19])

While gaps and overlap are inherent defects, the laying up process by the robot head can be programmed to avoid overlaps in many practical applications. That is because overlaps can create a significant through-the-thickness geometrical discontinuity that causes mechanical instability in compressive loading conditions. Furthermore, overlaps affect the surface quality of the final components and cause local bumpy areas that are not acceptable for aircraft exterior components.

On the other hand, gaps create relatively large resin pockets in the structures. One of the main challenges with induced gaps is that the shape and size of the formed gaps are functions of many parameters such as material system, curing process, stacking sequence, and the complexity of the component. Furthermore, the effect gap on the failure and damage of the structures might be different in different loading conditions. Thus, applying a knockdown factor for the stress analysis of the defective structures does not guarantee the safety of the structures.

1.4 Experimental Tests of the Laminates Made by AFP Technique

AFP induced gaps cause local material inhomogeneities and geometrical discontinuities in final products. Based on the fact that the mechanical performance of the heterogeneous materials is highly dependent on microstructure, these two effects affect the mechanical performance and durability of the structure. Therefore, one of the main challenges in the experimental studies of the laminates with defects is the scenario of pre-setting the gaps into the laminates. Although fabricating a laminate with distributed gaps of different sizes might be a preferred test scenario, the complexity of the defect-damage interaction makes it difficult to interpret the effect of the gaps on the mechanical performance of the structures. For that reason, experimental tests are mainly designed to fabricate the test specimens, including the controlled gaps with a homogenic distribution.

Because the tow gaps create out-of-plane waviness and resin pockets and do not affect the fibre's material properties, most research studies focus on reducing the compressive and shear strength of the defective laminates. However, there is still a lack of knowledge in the out-of-plane, impact, and post-impact behaviour of the composite structures with the defect. More details on the current progress in the experimental studies of the defective laminate are discussed in section 2.2.

1.5 Computational Modeling of the Laminates Made by AFP Technique

Composite laminates are categorized as heterogenous materials that are constituted by fibre and resin materials. However, due to the assumption of the uniform dispersion of the fibres into the resin, analytical approaches such as Classical Lamination Theory (CLT) and the composite failure criteria [20] in the macro-scale can be used for stress and failure analyses of composite structures. These theories have been used for decades to analyze and design composite structures, and several Finite Element (FE) packages have been facilitated with finite element analysis of composite materials. However, these techniques and methods can no longer be used for stress analysis of the laminates manufactured by the AFP technique because the assumption of the uniform distribution of the fibres is not valid for the defective laminates with distributed manufacturing defects. Gap areas create local stress singularity in the laminates. Besides, the resin failure and plasticity at the

gap area are new failures that have not been an issue for the regular composite laminates. However, it needs to be considered in stress analysis and damage assessment of defective laminates.

This issue can be resolved by decomposing the composite areas with uniform distribution and the gap areas in the numerical calculations. Several research studies used this approach to evaluate the gap effect on the material strength. However, this approach is practical for virtual tests on specimens with a limited number of defects. More details on the computational modelling of the laminates with defects are discussed in Section 2.3.

1.6 Research Motivation

It was mentioned earlier in this chapter that the in-plane loading response of the defective laminates has been the subject of several research studies. However, to the authors' knowledge, there is still a lack of knowledge in understanding the failure mechanism of the defective laminates subjected to the out-of-plane and impact loadings. Therefore, the main question of this thesis relates to the investigation of the gap effect on the out-of-plane behaviour of the composite laminates manufactured by the AFP technique.

From the numerical aspect of the studies, the heterogeneous assumption of the composite material with uniform distribution of the fibre and resin is no longer valid in the gap areas. That is why a robust meso-macro method is required to incorporate the effect of induced tow-gaps in damage assessment of the composite structures under complex loading.

1.7 Research Objective

The first objective of this research is to investigate experimentally the impact/post-impact behaviour of the composite laminates with inherent tow-gaps manufactured by the AFP technique. This research also aims to understand the interaction of the manufacturing defects and impact damage at reducing the compressive residual strength of the composite plates that have been internally damaged by an impactor at a low level of energy. In other words, this research will address the level of importance or negligibility of the AFP defects for analysis of damage tolerance of the damaged Carbon/Epoxy composite plates. For this purpose, several experimental tests, including the flexural tests, impact, and compression after impact tests, are performed to extend our current knowledge in the damage assessment of the laminated manufactured by AFP technique.

The second objective of this work is to empower the current FE tools with a robust method for damage assessment and failure analysis of defective laminates manufactured by the AFP technique. Because the distributed defects invalidate the homogenized distribution of fibres in the resin, a local damage analysis is required for stress analysis of defective laminates. Thus, this research aims to develop an efficient method to capture the defect patterns in the laminated plies and take them into account for the failure analysis of the laminated under general loading conditions.

1.8 Research Scope

This research study focuses on the low-velocity impact and compression after impact behaviours of the composite plates manufactured by the AFP technique. The test specimens are made of CYCOM 977-2/ HTS 40, a high-strength standard material system in the aerospace industry. The fabricated samples are categorized as thin laminates with a total thickness of around 2.0 *mm*. Note that thin and thick laminates expose dissimilar impact and CAI behaviours. The reason for choosing the thin laminate rather than a thick one is that these laminates are used widely in aerospace applications.

Although various selections for the induced gap distribution inside the laminates can be considered, a homogenic distribution of gap with the gap width of 2.0 *mm* was selected for this study. The homogenic defect distribution assures that all tests specimens contain almost the same induced gap percentage, which is essential for qualitative comparison of the test samples.

Three levels of Impact Energy (IE) were selected, IE = 5 J, 10 J, and 15 J. The impact test results include the impact force versus time graph, projected delamination pattern, impact indentation, and microscopic images of impact zones. CAI results include the comparative graph of compressive forces versus in-plane strain between the baseline and defective samples, in-plane strain contours extracted from the Digital Image Correlations (DIC) technique, and the failure modes of the test samples under compressive loads.

Additional tests are performed on the standard and short beam to evaluate the out-of-plane behaviour of the beam with induced gaps. For this purpose, the -gap effect on flexural stiffness/strength of standard beam and interlaminar shear strength of short beams is experimentally and numerically investigated.

From the numerical aspect of this research study, a robust computational model is developed for failure analysis and damage assessment of the defective composite structures with the arbitrary gap distributions. The so-called Induced Defect Layer Method (IDLMM) method is a meso-macro method that can be integrated into finite element software packages for 3D stress and damage analysis of defective structures. Using this method, the effect of the gap on the failure envelopes of a single material point and failure analysis of the laminates with defects can be assessed.

1.9 Thesis Layout

This thesis follows the Concordia manuscript-based thesis guideline and is divided into seven chapters as below:

Chapter 2: The background of this research study and reviews of research works conducted on the AFP manufacturing defects are provided.

Chapter 3: Experimental results of the low-velocity impact tests and the proposed semi-analytical approach are presented.

Chapter 4: Out-of-plane behaviour of standard and short beams with the induced gap is studied.

Chapter 1

Chapter 5: Induced Defect Layer Method (IDLM), a robust meso-macro method for considering tow-gaps in the damage assessment of composite structures, is developed.

Chapter 6: Experimental results of Compression After Impact tests (CAI) and the numerical results of impact and CAI are presented.

Chapter 7: Conclusions of this research study are presented, and the potential future work is discussed.

CHAPTER 2
Literature Review

2. Literature Review

In this chapter, the current progress in the study of AFP manufacturing defects is reviewed. The literature review is narrowed to the AFP induced gaps and their effect on the mechanical performance of the composite laminates, which is the main objective of this study. It is important to note that the AFP is an advanced recent technique, and a limited number of research laboratories have been facilitated with this technology. Thus, the number of research work in this field is lesser than similar fields in composite research studies.

2.1 AFP Manufacturing Defects

AFP processing induced-defects have been a significant challenge of automated manufacturing in the composite industry. These defects can reduce the loading capacity of composite structures and also affect the surface quality of the final products. Induced- defects can be categorized as (1) defects that can be avoided by modifying the current AFP technique (2) defects that cannot be avoided.

Missing tow, upfolding, twisted tow, wrinkle [17, 21], and crowning can be avoided or fixed during the laying up process by utilizing advanced in-process inspection techniques [22–25] or by adjusting the main AFP parameters, including consolidation force, melting temperature, and feed rate [12, 26, 27]. Figure 2-1 shows an advanced inspection system facilitated with a neural network algorithm for in-fly fabrication detection of the defects. On the other hand, gap and overlap are the most observed defects that must be included in designing and analyzing complex composite components. Therefore, AFP steering parameters can be adjusted to minimize the effect of (1) gap (100% overlap), (2) overlap (100% gap), or to make a balance between the gap and overlap densities in laminates (half gap/overlap) [28, 29]. The scenario of 100% overlap may be used where the local higher stiffness is required [30, 31]; however, this scenario is not preferable in many practical applications due to mechanical instability and poor surface quality [32].

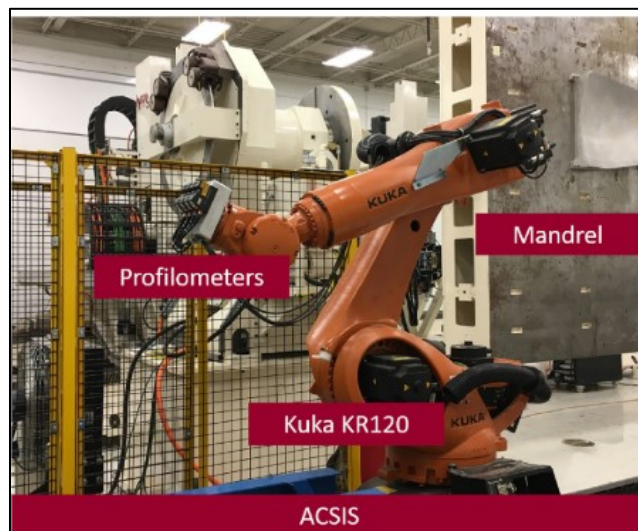


Figure 2-1 Advanced Composite Structures Inspection System [22]

2.2 Experimental Observation

Gap/overlap are structural level defects that make it challenging to consider in mechanical design and analysis. The complexity relates to the (1) geometry and distribution of the defects, (2) post-cured effects (3) loading conditions. Large defect areas could cause a significant ply waviness and creates relatively large resin pockets. Furthermore, inducing defects might form a larger flaw if ply-staggering does not occur, which was shown is a crucial factor during the lay-up process [33, 34]. Figure 2-2 shows an induced gap formed in four -45° adjacent plies during a non-staggered ply disposition. The curing process affects the final forming of the defects. For instance, it is expected that the post-cured size of an induced gap would be larger than the gap in a flat plate with the same pre-cured dimension due to using a caul plate on top of the sample during the curing process [35]. Figure 2-3 shows the effect of using a caul plate on the quality of cured plate with a 3.175 mm gap. The thermoplastic material may also suffer from flaws than thermoset materials because of lack of autoclave cures pressure that might shrink the defect size [32, 34].

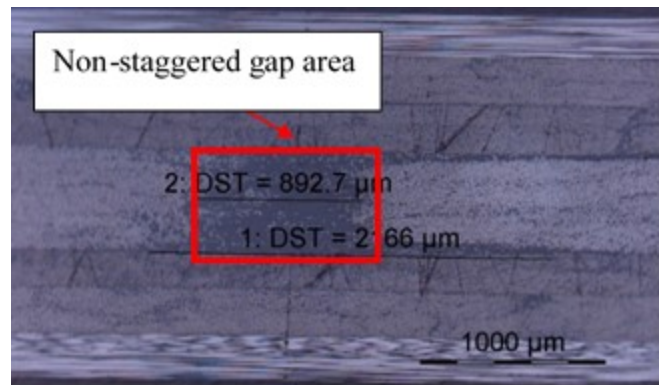
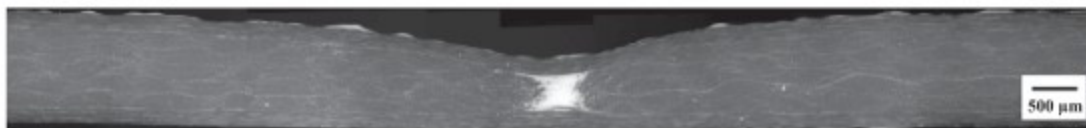


Figure 2-2 Non-staggered tow-defects at mid-ply of a composite laminate



(a)



(b)

Figure 2-3 Cross-section view of a composite plate with a 3.175 mm gap (a) no caul plate (2) with caul plate [35]

The effect of flaws on the integrity of the structure might change by the in-service loading condition. For instance, gap/overlap negligibly affects the tensile strength [28, 35]. However, it

Chapter 2

reduces the compressive strength of the defective laminates. Sawicki and Minguett [36] did extensive experimental tests on the compression behaviour of different laminate configurations. It was revealed that gap/overlap could reduce the compression strength of the laminates by 5-30% for the laminates with a minimum of 0.75 mm of gaps and overlaps width. An enhanced experimental work on the effect of several AFP defects on the strength reduction of the flat coupons was performed in Ref. [28]. The tests were conducted on samples with gap, overlap, half gap/overlap, twisted-tow in tension, compression, in-plane shear loads. Results showed that an average strength reduction of 3-15% could be expected due to the presence of the defect. However, the rate of reduction depends on the loading condition and defect type. A detailed description of the obtained results has been shown in Figure 2-4. The similar mechanical behaviour but with a different pre-set of inducing the defect also shows that gap and overlap play a significant role in the compressive strength of the composite structure [37, 38].

		Gap	Overlap	Half Gap/Overlap	Twisted Tow
Tension		—	—	↘	↗
Compression		—	↗	—	—
In-Plane Shear	Length	—	—	↘	↘
	Width	↗	↘	↘	↘
OHT		—	—	—	
OHC	Length	↗	↗	↗	
	Width	↘	↘	↘	

↗ ≥ 3% increase (up to 13%)
 — ±3% variation
 ↘ ≥ 3% decrease (up to 12%)

Figure 2-4 Effect of AFP defects on the strength reduction of Carbon/Epoxy laminates. Reproduced from Ref. [28]

Effect of defects in stress raiser applications such as open holes has also been an interesting topic. Experimental results [28, 38–40] demonstrate that stress concentration might diminish the effect of defects, especially under tensile loading. Fatigue life and durability of the composite plate with a single missing tow were evaluated in Ref. [41] by performing a series of fatigue tests on the unidirectional laminates [41, 42]. It was concluded that the effect of the gap becomes more severe with increasing the maximum applied stress; however, this effect can be neglected for a low level of fatigue stress. It was also shown that the gap areas are prone to be a source of delamination initiation, as shown in Figure 2-5.

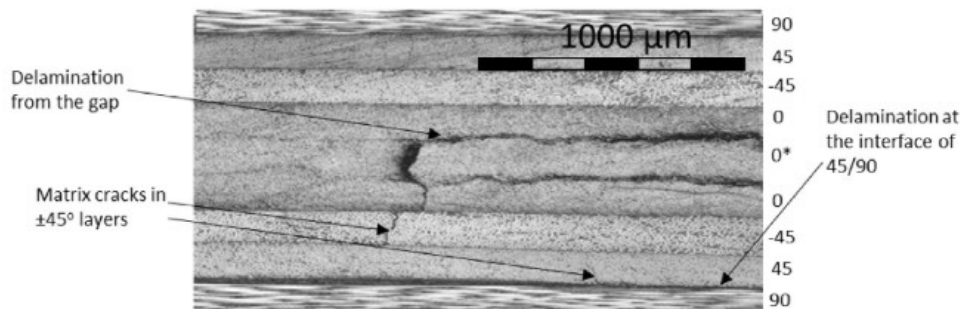


Figure 2-5 Delamination initiation from the gap after 10^5 cycles [42]

The interaction of fibre tow gap and impacted damage is also of interest. However, a few research works can be found that address the effect of the gap on the impact and post-impact behaviour of composite laminates. Effect of fibre tow-drop gaps on damage resistance of variable stiffness composite plates was carried on in Ref. [33] with performing a series of impact tests with medium to high Impact energy (15 J-45 J). Results show that the influence of the gap is more relevant to the low level of impact energy. However, induced gaps can affect the projected delamination pattern of composite plates under impact loads, as shown in Figure 2-6. It was also found that the compressive residual strength of the composite plates is more sensitive to the damage caused by impact rather than manufacturing defects. A similar study on the compression after the impact of the composite structure was conducted in Ref. [37]. It was shown that the location and dimension of the gaps significantly affect the damage resistance of the structure.

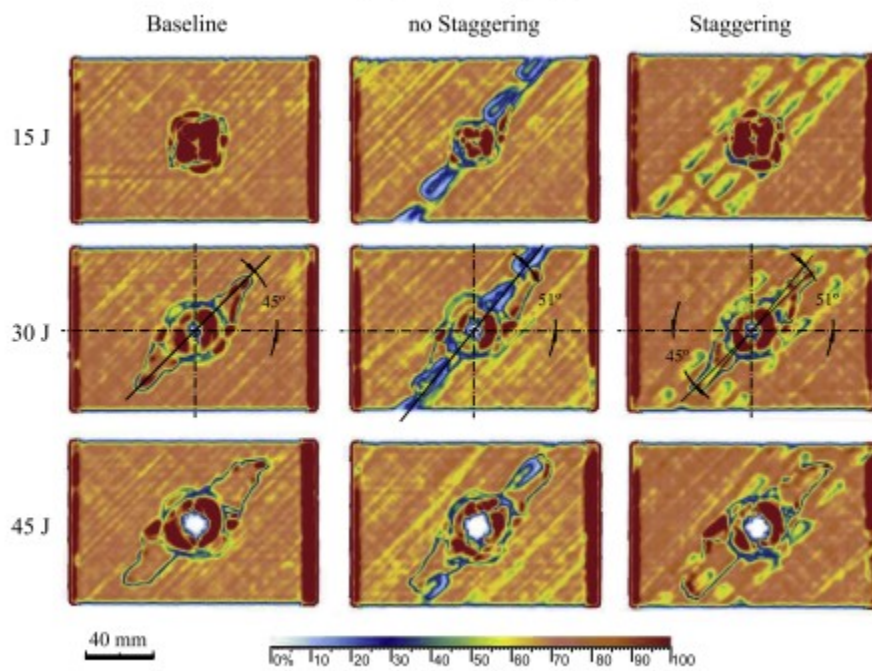


Figure 2-6 Effect of tow-gaps on the projected delamination pattern of variable stiffness laminates under medium impact loads [33]

2.3 Numerical Simulations

Numerical stress analysis of defective composite structures is a significant challenge due to the vast scenario of the defect patterns in the structures. The main issues relate to the difficulty of the numerical simulations;

- (1) Gap area reshapes after the curing process: Although many numerical models assume that the gap area and shape remain the same as before the curing process, the gap shape can change. Figure 2-7 shows three different types of post-cured gap shapes. While some gaps

might form in rectangular and trapezoid shapes, multiple smaller gaps can also be observed due to the adjacent plies' interference into the gap zones.

- (2) Defect distribution is a multivariant phenomenon: AFP defects are inherent defects. Thus, it is required expensive inspection techniques to detect these defects during the lay-up process. Because many of the AFP robots in the research laboratories have not been facilitated with the inspection tools, there is still a lack of databases for providing sufficient data for numerical model validations.
- (3) Defects can cause uncertainty in different scales of structure: AFP gap/overlap forms in the meso level of the structures. However, the consequence of ply waviness affects the macro-scale behaviour of the structures.

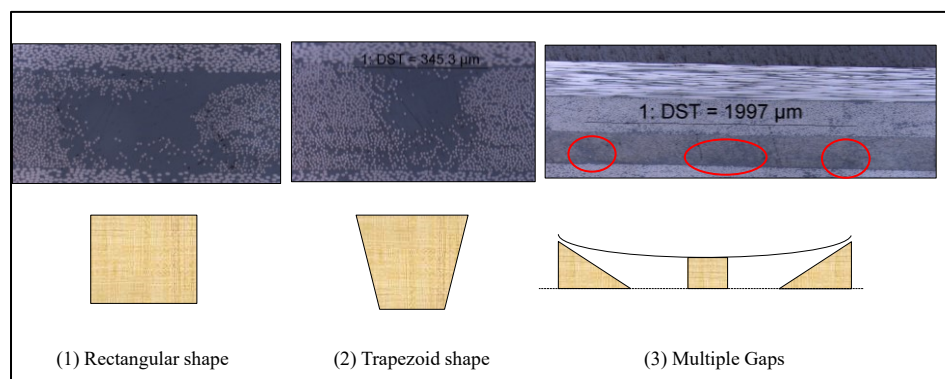


Figure 2-7 Microscopic and schematic views of different types of gap shapes after the curing process

The mentioned issues limited the virtual testing of the defective structures to the coupon tests with few pre-set gaps and overlap. Sawicki and Minguet [36] developed a 2D FE model to account for the gap and overlap. The FE model was based on experimental observation and stress localization and redistribution at the defect zones. A FE model for estimating the stiffness and strength of the variable stiffness composite laminates was developed by Blom et al. [16], based on a progressive damage model with a LaRC failure criterion. However, the result shows deviations from the experimental results. The same procedure for estimating the strength of the plates with a hole under tensile loading was followed in Ref. [40]. However, the developed model requires high mesh density at the defect area to obtain a satisfactory result. Li et al. [43] developed an FE model for simulating the gaps and overlaps based on the observation for both hard and soft tooling with thickness scaling at the defect zones of the structure. However, implementing the thickness scaling for overlap increases the local strength of the structure at the overlap zones, which results in overestimating the strength [44]. Figure 2-8 shows the FE model of gap and overlap based on microscopic observation. The Ply-by-Ply simulation approach is another FE technique to consider the effect of both resin-rich areas and ply waviness [45, 46]. In this technique, composite plies are modelled individually, and the desired waviness and the gap area are created. The next ply is programmed to follow the curve of the previously simulated ply.

Although the discussed methods applied different failure models and different approaches to address the induced defects, the common assumption is that the pre-set gaps are considered individual resin FE elements. Furthermore, the FE model based on observation is limited to the

selected studied samples. These assumptions can help study the mechanical behaviour of the structures in micro and meso-scale. Still, the effectiveness of these methods for simulating the continuous fibre-reinforced composite with widespread distribution of the gaps in the structural level is uncertain and limited.

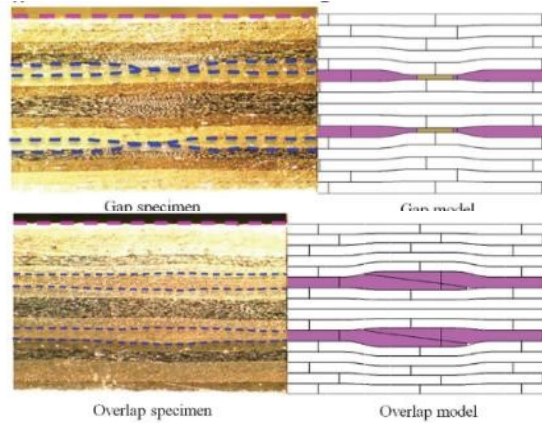


Figure 2-8 Microscopic and FE models of the gap and overlap based on observation [43]

A meso-macro linear model was developed [30] for the instability analysis of variable stiffness laminates. The homogenization process of this method is based on the FE simulations on a defined Unit-Cell. This method eliminates the mentioned drawbacks of the other methods by introducing a non-dimensional defect length for material points. But, the method implements an elastic homogenization technique that restricts the method to the linear elastic analysis of defective composite structures.

2.4 Concluding Remarks

In this chapter, a review of the AFP induced-defects and their effect on the mechanical performance of composite laminates was conducted. It was shown that despite the research progress in this field of study in recent decades, there is still much room for studying the AFP defects. For instance, while many experimental works focused on the in-plane behaviour of defective laminates, a few research can be found in the literature addressing the out-of-plane response of laminates with manufacturing defects. To be more precise, it was discussed that, up to the authors' knowledge, there is still a lack of knowledge in the study of low-velocity impact (LVI) of the composite plates with induced manufacturing defects.

Furthermore, despite advancements in experimental studies, few works dealt with the challenge of numerical simulation of defective structures. The authors believed that this challenge is complex due to the interactive mechanism of the defects in both structural and material levels. Thus, up to the authors' knowledge, there is still no practical method that can assess the structural integrity of the composite structures in the presence of the automated manufacturing induced gaps under general loading conditions.

CHAPTER 3

Effect of Tow Gaps on Impact Strength of Thin Defective Composite Laminates Manufactured by AFP technique

This work has been published in:

Ghayour M, Hojjati M, Ganesan R. "Effect of Tow Gaps on Impact Strength of Thin Composite Laminates Made by Automated Fibre Placement: Experimental and Semi-Analytical Approaches". *Compos Struct* 2020; 248: 112536.

<https://doi.org/10.1016/j.compstruct.2020.112536>

3. Effect of Tow Gaps on Impact Strength of Thin Defective Composite Laminates Manufactured by AFP technique

In this chapter, the effect of induced tow gaps on the impact response of the composite laminates is experimentally investigated. For this purpose, several impact tests were performed on the standard size composite plates manufactured by AFP and hand lay-up techniques. A low-velocity impact test was chosen for this study to investigate the interaction of the gap and impact damages. Because the LVI causes internal damages (matrix cracks and delamination) at the resin level, the LVI test is more suitable than the high-velocity impact test for evaluating the impact-gap interaction. Three levels of Impact energies (IE) were chosen for the impact tests, IE = 5 J, 10 J, and 15 J, to investigate whether the IE's level affects the gap-damage interaction.

In this chapter, the manufacturing process of the composite laminates with defects is explained in detail. It includes fibre ply deposition, gap embedding, vacuuming, and curing processes. The quality of the laminates is then evaluated using several techniques, including Differential Scanning Calorimetry (DSC) test, ultrasonic C-scan test, and microscopic observations. It is shown that the final cured laminates have been well cured with no voids and flaws.

The results include the (1) graphs of the impact forces versus time that are helpful for measuring the maximum impact force, delamination threshold load, and total impact time. These graphs are the output of the impact machine without requiring postprocessing tools. (2) Projected delamination patterns on the impacted samples show the severity of the impact on the laminate delamination, which is the critical damage mode of the impacted samples. These graphs are derived using the Ultrasonic C-scan technique. (3) Impact depth graphs using a digital indicator and (4) microscopic images of the impacted plate at the impact area.

A semi-analytical approach is developed in this chapter using the mass-spring model to incorporate the effect of the gaps on the impact response of thin laminates under LVI. The main advantage of the developed method is that no experimental impact tests are required for the defective laminates to simulate the impact response of the composite laminates.

Results indicate that the effect of manufacturing induced tow-gaps on the impact strength and the impact damage is significant and cannot be neglected.

Summary

In this chapter, the effect of periodically induced gaps on the low-velocity impact response of the thin composite plates has been experimentally investigated. For this purpose, quasi-isotropic Carbon/Epoxy polymer composite plates have been manufactured with the AFP process, including periodical patterns of gaps, and the obtained impact responses of the plates have been compared with the results of the baseline samples. The baseline sample is a similar sample that has been manufactured by the hand lay-up technique. Furthermore, a two-degree of freedom mass-spring model is also proposed to account for the effect of the manufacturing defect on the impact response of the laminates with induced defects. The model includes a non-linear damage model to account for the delamination propagation during the impact process. Ultrasonic C-Scan analysis has also been performed to capture the projected delamination pattern. Results indicate that the AFP manufacturing defects can reduce the impact resistance of the composite plates by about 17% and affect the delamination area of the samples for low levels of impact energy. Microscopic observation is further performed to investigate the interaction of manufacturing defects and damage caused by impact. It is shown that delamination initiation likely occurs in the gap area.

3.1 Introduction

Advanced robotic manufacturing has attracted interest in the manufacturing industry early in the decade, and Automated Fibre Placement (AFP) technique has found its way to be one of the well-established composite fabrication techniques in aerospace and automotive industries. This technique has the advantage of reducing material waste and also speeding up the fabrication process. However, using fibre tows instead of composite prepreg sheets, new types of defects are introduced into the composite structures during the fabrication process. These defects can cause geometrical discontinuities and local material inhomogeneities at the structure, which affect the mechanical performance and durability of the structure in service load [10]. Fibre Tow Gap is one of the probable types of defects that may occur during automated fibre deposition, especially for complex shapes like doubly curved structures [19]. These gaps create resin-rich areas in the structure prone to be the sources of damage initiation [7].

Mechanical performance of the composite structures with defects is highly dependent on the scenario of introducing the pre-set gaps into the structure, curing process, stacking sequence, and material properties. For instance, it was shown in Ref. [35] that using a caul plate (hard tool) during the curing process can significantly reduce the out-of-plane fibre waviness, which has a consequent effect on the compressive strength of the composite samples. The fabrication process for embedding the gaps in Ref. [38] has been designed to place the gaps between individual tows in the laminates, which is unlikely to occur in manufacturing the structures, and the results would be conservative. Fibre tow-drop is another scenario for investigating the effect of the gap on structural integrity [33, 41]. However, due to advancements in AFP robot technology and quality control, this type of defect is unlikely to happen. A study on the compressive strength after impact was done in Ref. [47], and it was shown that the location and dimension of the gaps have a significant effect on the damage resistance of the structure.

Experimental studies show that the effect of the gap on the tensile strength is negligible [28, 35]. Sawicki and Minguett [36] did extensive experimental tests on the effect of gap and overlap on the

compression behaviour of different laminate configurations. Results show that gap and overlap can reduce the compression strength of the laminates by 5-27% for the laminates with a minimum of 0.75 mm of gaps and overlaps. However, the scenario for embedding the defects had been designed to cause the most significant out-of-plane waviness. The same trend but with different intentional induced defects also shows that the gaps play a significant role in the compressive strength of the composite structure [28, 37, 38]. Effect of defects in Open Hole Tension (OHT) and Open Hole Compression (OHC) strengths can also be found in Ref. [28, 38–40]. Results reveal that the effect of defects for composite plates with the hole under tensile load seems to be negligible due to stress concentration. Effect of the gap on the durability of the structure was examined by performing a series of fatigue tests on the unidirectional laminates [41]. It was concluded that with increasing the maximum applied stress, the effect of the gap becomes more severe. However, this effect is negligible for low levels of fatigue stress.

Effect of fibre tow gaps on impact response and damage resistance of variable stiffness composite plates was carried on in Ref. [33] with performing a series of impact tests with medium levels of impact energy (15 J-45 J). Results show that the influence of the gap is more relevant to the low-velocity impact energies. It was also found that the compressive residual strength of the composite plates is more sensitive to the damage caused by impact rather than manufacturing defects. However, to the authors' knowledge, there is still a lack of knowledge in studying Low-Velocity Impact (LVI) of the composite structures with induced defects.

The main objective of this chapter is to investigate the effect of fibre tow gaps on the impact response of and damage in thin composite plates. For this purpose, Carbon/Epoxy composite plates are subjected to three levels of impact energy less than 15 J. Impact resistance and delamination threshold load of the plates are measured and compared with that of the baseline samples, which have been fabricated by conventional hand lay-up technique. Furthermore, the effect of gaps in the projected delamination area is investigated using both the ultra-sonic C-Scan technique and microscopic observations. Additionally, a semi-analytical approach based on two degrees of freedom (2DOF) mass-spring model is proposed to simulate the effect of the manufacturing defect on the impact response of the composite plate with induced defects. The proposed model can consider the effect of the manufacturing induced gaps and delamination propagation on the overall bending stiffness of the composite plate.

3.2 Materials and Manufacturing

3.2.1 AFP Layup Process

The material system used here was 6.35 mm (1/4 in) 977-2/35-12K HTS-145 unidirectional prepreg. In this material system, 12K of high-strength grade carbon fibres (HTS-145) are impregnated in the CYCOM 977-2 epoxy resin system, designed for autoclave curing or press moulding.

Both hand-layup (HL) and AFP techniques were applied for the fabrication of the composite plates. A plate with the size of 43 cm by 48 cm was manufactured using prepreg materials and the hand lay-up technique, representing defect-free samples, and will be considered the baseline. During the ply deposition, the debulking process was performed to ensure an even consolidation in the plate and remove trapped air between plies. This process was carried out after ply one, every subsequent three plies, and the final ply.

Chapter 3

AFP was used to fabricate the samples with gaps that represent the samples with defects (AFP-G). AFP proceeds with a ZX130L Kawasaki 6-axis articulated arm robot. This robot has a capacity of 125 kg payload, and it can place four fibre tows per course. The tow-preg materials with a width of 6.35 mm were used, which provide a total width of 25.4 mm (1.0 inches) in each course.

A quasi-isotropic stacking sequence with the sixteen layers has been selected for the experimental studies. Table 3-1 shows the properties of the composite samples designed for this study.

Table 3-1: Properties of the experimental samples

Sample Dimension	Stacking Sequence	Material	Curing Type
150 × 100 mm ²	[0 ₂ /45 ₂ /90 ₂ /-45 ₂] _s	Cycom 977-2 HTS 40 (Fibre Volume Fraction = 58%)	Autoclave

Intentional periodic gaps between the fibre courses were further embedded in all layers of the plates. In order to place gaps between fibre tows, the fibre placement software needs to be adjusted for a predefined tow width, which is more than the actual fibre tow's width. In this study, an average of 2.0 mm was chosen for the width of the periodic gaps between fibre courses, generating 8% of free space (gap percentage) in the whole laminate during the fibre placement. Figure 3-1 shows a schematic illustration of the location of the gaps in the composite plate.

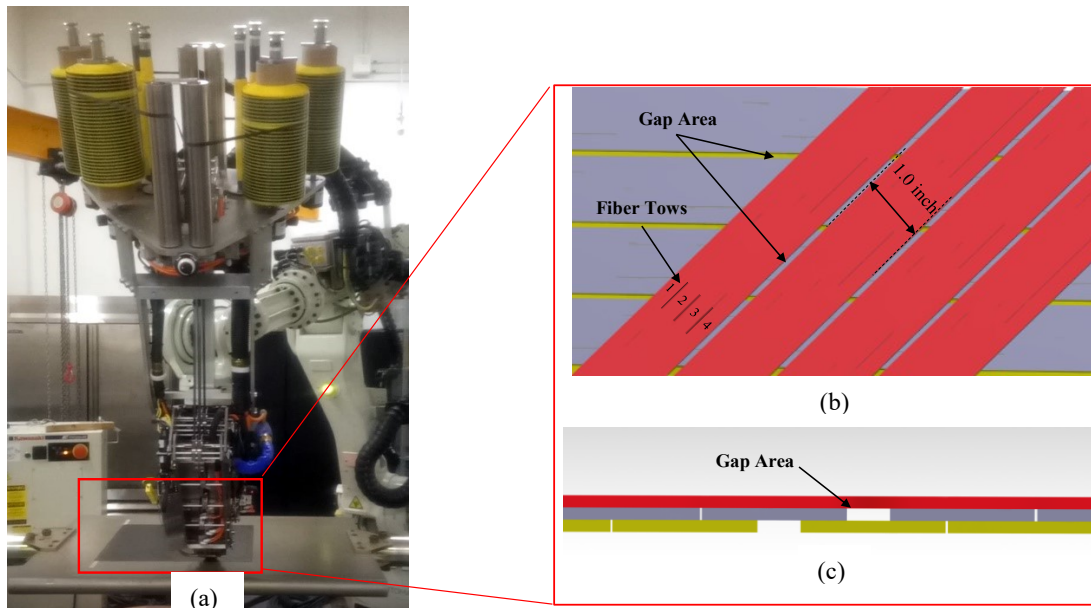


Figure 3-1 Schematic illustration of placing widespread periodical gaps during AFP (a) Robot arm (b) Top view (c) Cross-section view

3.2.2 Vacuuming and Curing Process

Thermoset composite materials must be vacuumed before curing in an autoclave to eliminate the voids and flaws in the final part. Vacuuming is the challenging step of composite manufacturing. It is an irreversible step that cannot be modified or repaired during the curing. In other words, if a

poor vacuum causes an air leakage during the curing, the process should be continued, and the quality of the structures should be evaluated for the final part.

Figure 3-2 shows the principal elements of a vacuumed laminate. The composite plate was placed on an aluminium tool. The top side of the tool was wiped with the release agent to avoid sticking the tool to the composite plate during the curing process. The release film was then placed on top of the composite plate. Fibreglass fabric strips works as an excess resin absorber. It is essential to make sure that the composite plate is not in contact with the breather. A caul plate was then placed on the top of the composite plate. Using a caul plate reduces the out-of-plane waviness and provides a smooth surface. The caul plate and tool surfaces were sandpapered using an electric sandpaper machine to provide smooth surfaces (Figure 3-3). A thermocouple was installed under the edge composite plate to monitor the plate temperature during the curing process. In this study, the plate temperature was the selected temperature for curing rather than the autoclave temperature. Note that because the composite plate is a thin laminate, one thermocouple is sufficient for temperature monitoring of the plate. In other words, it is assumed that the surface temperature of the plate is almost equal to the plate temperature, which is a reasonable assumption for thin laminates. Figure 3-4 shows the final vacuumed plate. Two vacuum bag connectors were installed to pull out the excess air and bubbles trapped in the resins. The vacuumed plate was then tested for leakage before the curing. Figure 3-5 shows the graphs of the curing cycle and the autoclave pressure of the curing process. It is shown that the plates have been cured at 350 °C under a pressure of 90 psi for 350 minutes.

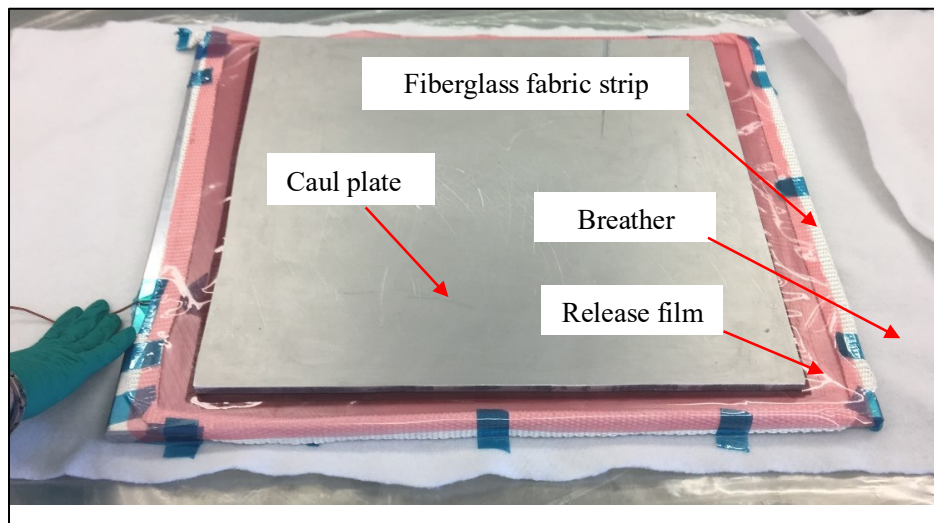


Figure 3-2 Principal elements of the vacuuming process

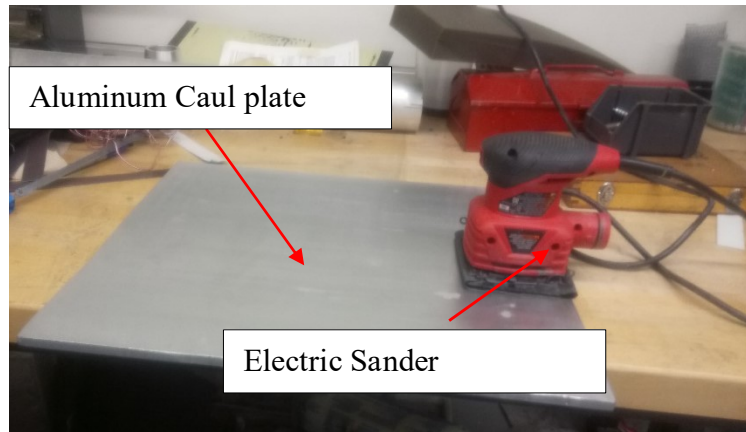


Figure 3-3 sandpaper the base tool and the caul plate

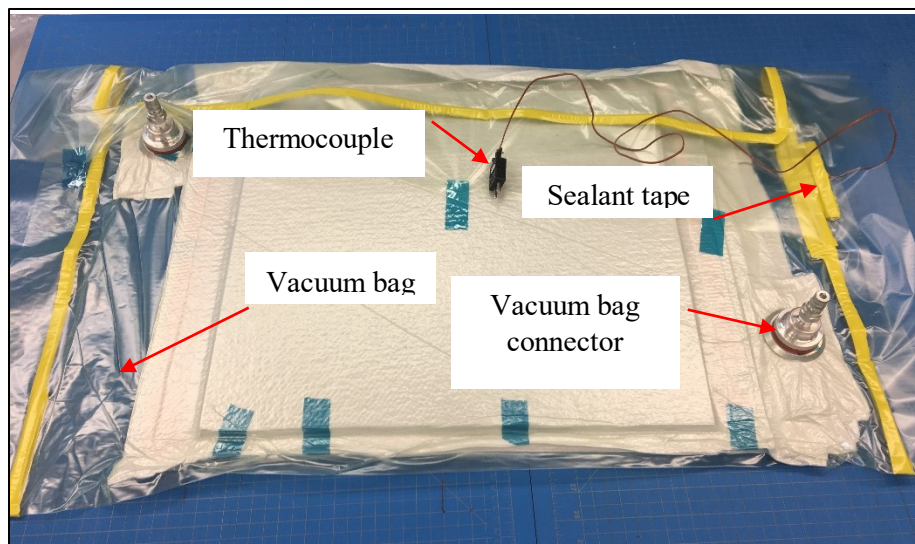


Figure 3-4 Vacuumed composite plate

A table circular power saw has been used to cut the plates (Figure 3-6(a)). Because the water is used for cooling the power saw, the samples must be dried before any mechanical tests. For this purpose, the specimens were firstly dried at room temperature for 24 hours. Afterwards, they were placed in an oven for two hours at the temperature of 80°C, as shown in (Figure 3-6(b)).

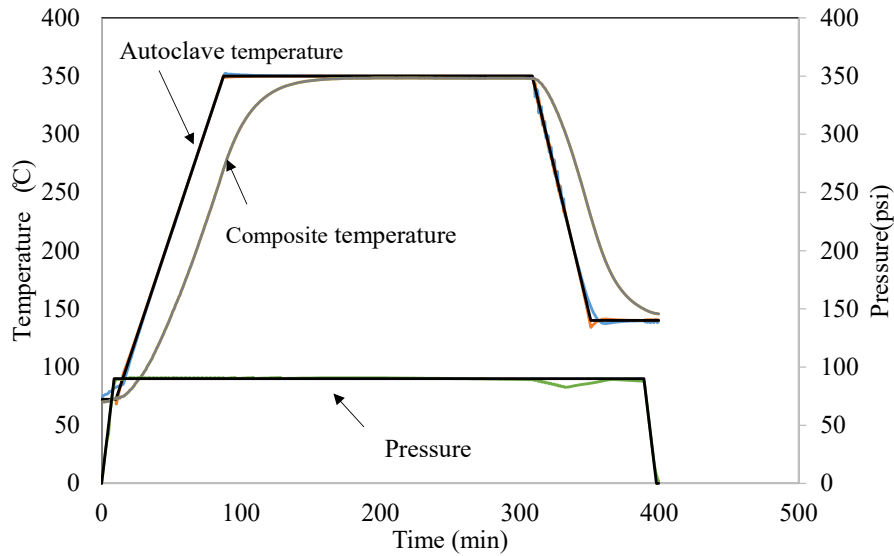
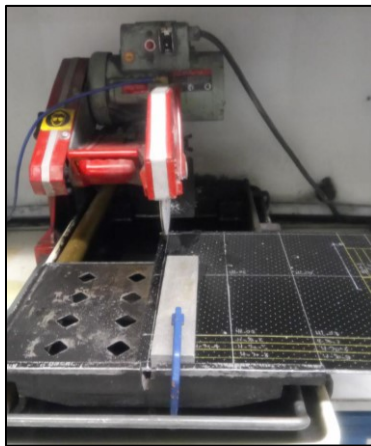


Figure 3-5 Curing Cycle of CYCOM 977-2 HTS 40



(a)



(b)

Figure 3-6 (a) Circular band saw machine (b) Drying the samples in the oven

3.3 Quality of the Cured Plates

Although no leakage was detected during the curing process, several tests were performed to ensure the quality of the cured plates was acceptable. The laminate quality is assessed to ensure (1) the plates have been well cured (2) The plates are flawless.

The Degree of Cure (DoC) is evaluated by Differential Scanning Calorimetry (DSC) test. A lower degree of cure causes a degradation in the material properties of the cured laminates. Although the DoC represents the curing quality of the whole plate, Ultrasonic C-scan tests were also performed on the plates to ensure that the plates do not contain any flaws and microscopic voids.

Finally, microscopic observation was performed on several spots of the plates to ensure that the fibres have been distributed uniformly and provided a homogenic fibre volume fraction

3.3.1 Differential Scanning Calorimetry Test

Using expired materials with low tackiness causes significant difficulties during the layup fabrication, especially with the AFP robot arm. The fibre tows may not stick to the mould properly, and the plies poorly stack together. Because Bombardier Company has provided the composite preregs, no recording history of the material storage was available. For instance, the time that materials have been out of the fridge may have exceeded the shelf life of the materials. Thus, the DSC test must be conducted on the prepreg materials to ensure the quality of the material is acceptable.

In addition, the DSC test should be performed on the cured sample and uncured prepreg to evaluate the DoC of the cured plates. The DoC is calculated by dividing the cured samples' generated heat into the uncured sample's generated heat. More details on the DSC test can be found in Ref. [48]

The DSC tests were conducted using the MDSC TA Q200 machine (Figure 3-7). Figure 3-8 shows the result of the curing cycle of the uncured prepreg sheet and tows. It can be seen that the exothermic heat for the prepreg tow and the prepreg sheet are 18.5 J/g and 16.1 J/g, respectively. Figure 3-9 shows the DSC result for the cured sample with defects (AFP-G). It is shown that the glass transition temperature of the sample is 160 °C. The DoC of the laminate is around 97% ($\text{DoC} = (0.75/18.5) \text{ J/g} \times 100$) which indicates the plate has been well cured.

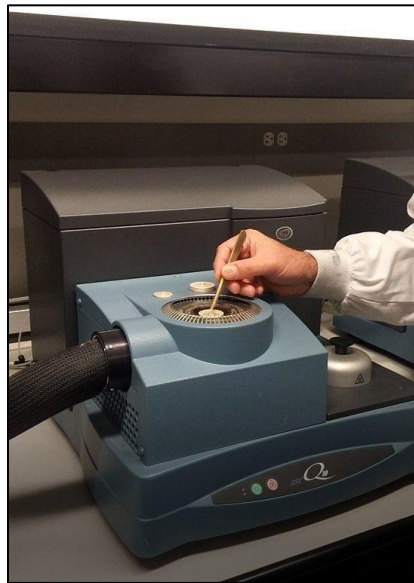


Figure 3-7 MDSC TA Q200 DSC machine

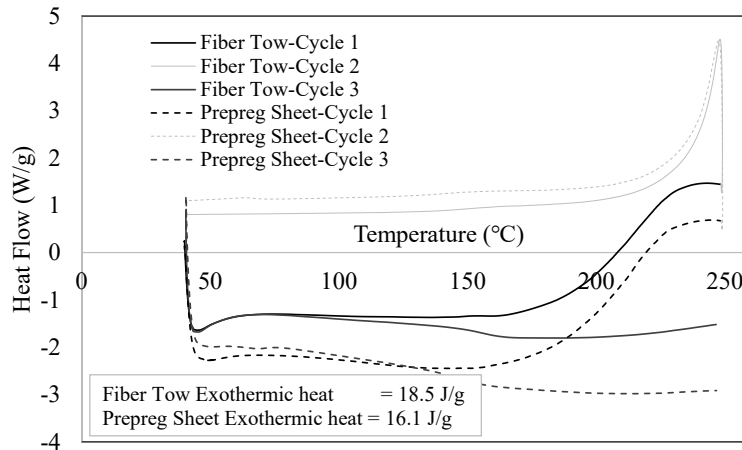


Figure 3-8 Heat flow versus temperature for the uncured selected material

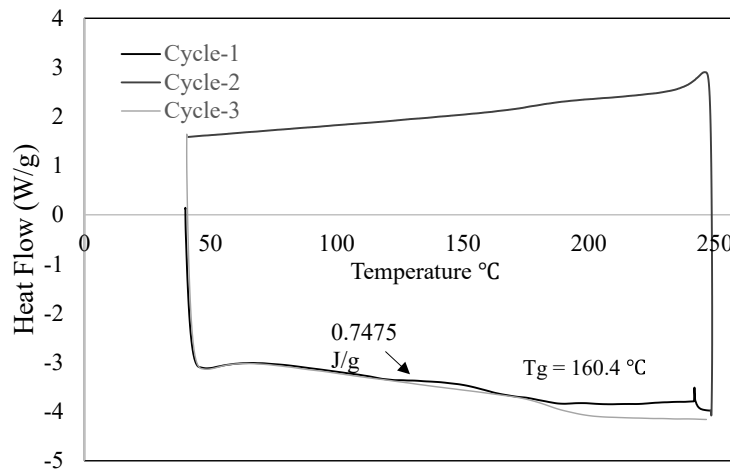


Figure 3-9 Heat flow versus temperature of the cured sample (AFP-G sample)

3.3.2 Ultrasonic C-Scan tests

Ultrasonic C-scan tests were conducted on the cured composite plates to ensure that the plates have been cured with no major flaws inside the plates. The scanning was done with the samples immersed in distilled water. They were positioned between two 5 MHz transducers with a resolution of 0.04 inches (1.01 mm). Figure 3-10 shows the result of the C-scan for plates manufactured by AFP and HL techniques. It can be seen that the plates contain no micro voids. Note that, different colour shows the signal amplitude at the scanned zones.

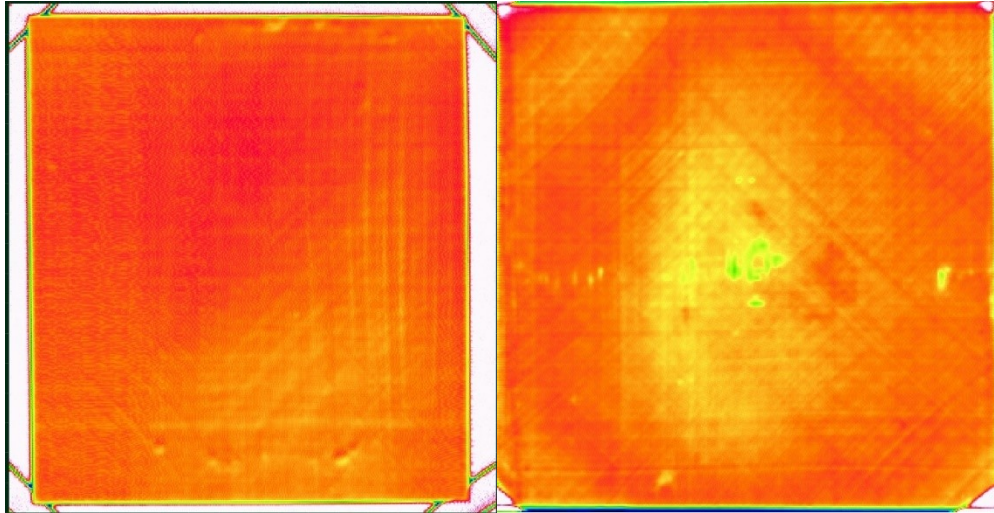


Figure 3-10 (a) manufactured by AFP AFP-G (b) manufactured by HL technique (baseline)

3.3.3 Microscopic Observation of the Cured Samples

Microscopic observation was performed on the cured intact plates. For this purpose, composite samples with the dimension of $25 \times 25 \text{ mm}^2$ have been cut and dried. The samples were then placed in the sample holders, and the holders were filled with epoxy resin. In this study, epoxy (D.E.R.324) + the curing agent (D.E.H. 24) were used by a weighting ratio of 89/11. First, the samples were cured in the environment temperature in 24 hours and then 1 hour in 100°C . Figure 3-11 shows the fixed samples in the samples holders. The sample surfaces were then polished by a 3.0 nm rotating sandpaper using a polishing machine, as shown in Figure 3-12.

Microscopic observation was performed on the samples. Figure 3-13 shows a microscopy image of the intact laminate. It can be seen that the fibres have been uniformly distributed in the resin epoxy. However, the Fibre Volume Fraction (FVF) has been dropped in the gap zone by around 50%



Figure 3-11 Immersed samples in the resin epoxy



Figure 3-12 Polishing machine

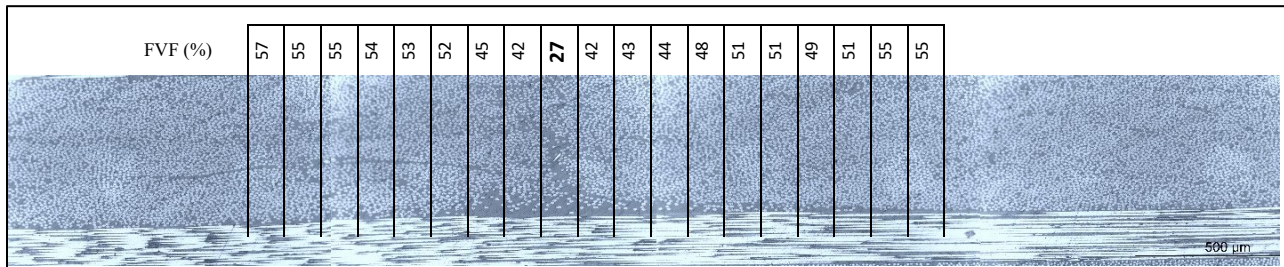


Figure 3-13 Microscopy image of the intact laminate

3.4 Experimental Procedure

Effect of widespread induced defects (WID) on the impact resistance and damage threshold of the composite plates are investigated by performing the Low-Velocity Impact (LVI) test based on ASTM D7136 standard with the boundary condition shown in Figure 3-14. For this purpose, CEAST 9340 Instron machine is used to perform the experimental impact tests. This machine is a state-of-the-art machine with advanced data acquisition that can record the data with a sampling frequency of 4000 kHz. Three levels of Impact Energy (IE) were chosen for the impact tests at room temperature; 5 J, 10 J, and 15 J. A standard hemispherical impactor was selected for the impact test. The impactor has a weight and head diameter of 3.215 kg and 16 mm, respectively.

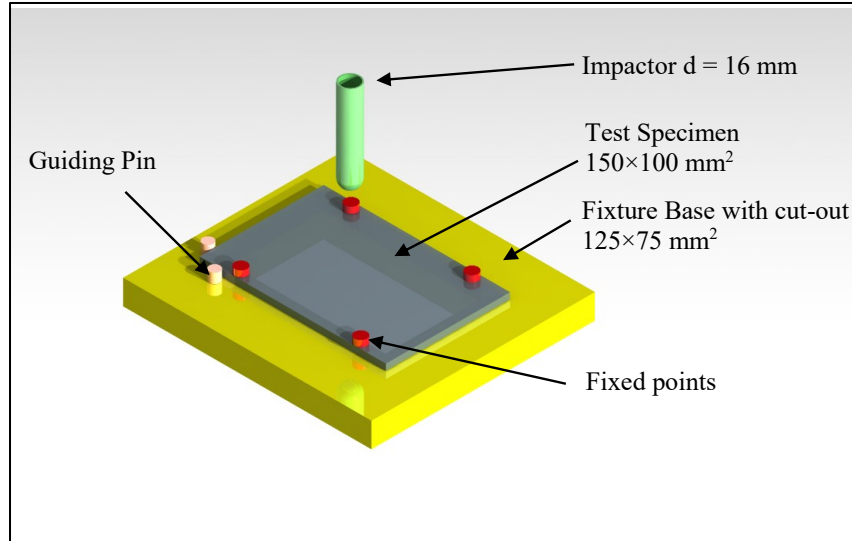


Figure 3-14 LVI test; Fixture and boundary condition

3.5 Semi-Analytical Approach

In this section, a semi-analytical approach is proposed to consider the effect of the widespread induced defect and delamination propagation on the impact response of the composite plate. The proposed model is based on the 2DOF mass-spring model [49] with modifications on the bending stiffness and the delamination threshold of the samples obtained from the experimental tests. The mass-spring model is defined by Eq. (1). Figure 3-15 shows a schematic view of the 2DOF mass-spring model with the proper boundary conditions

$$\begin{aligned} M_i \ddot{x}_i + P &= 0 \\ M_p \ddot{x}_p + K_b x_p - P &= 0 \end{aligned} \quad (1)$$

where M_i and M_p are the impactor mass and effective mass of the plate, respectively. K_b and P are the bending stiffness of the plate, and P is the contact force between the impactor and the plate. Indexes i and p refer to the impactor and the plate. The effective mass of the plate is a function of the boundary conditions. In this research, it is assumed that the M_p is equal to a quarter of the real plate mass, which is used for the plates with clamped boundary conditions [50]. However, the effect of this parameter on the impact response is negligible when the impactor mass is larger than twice the mass of the plate [51].

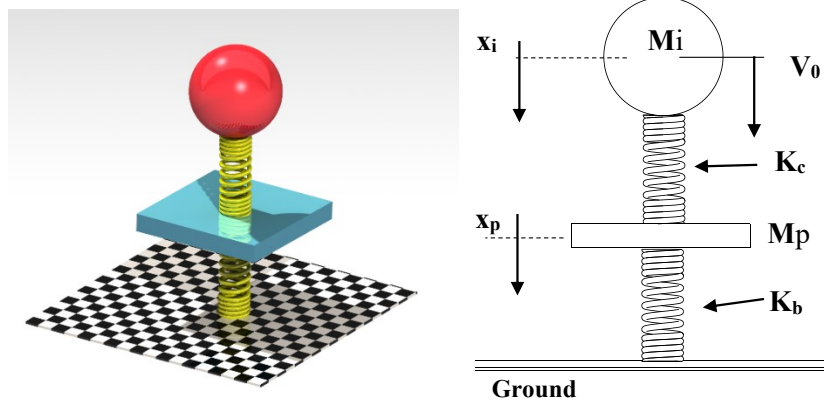


Figure 3-15: Two-Degree of freedom of Mass-Spring model

The contact force (P) is determined by using the Hertz law (Eq. (2)), and the contact stiffness K_1 is defined by Eq. (3).

$$P = K_1(x_1 - x_2)^{\frac{3}{2}} \quad (2)$$

$$K_1 = \frac{4}{3} Q R_i^{\frac{1}{2}} \quad (3)$$

R_i is the radius of the impactor, and the parameter Q can be determined by Eq. (4).

$$\frac{1}{Q} = \frac{1}{Q_{zp}} + \frac{1}{Q_{zi}} \quad \text{where } Q_{zp} = \frac{E_z}{1 - \nu_p^2}; \quad Q_{zi} = \frac{E_i}{1 - \nu_i^2} \quad (4)$$

where the parameter E_z is the effective out-of-plane stiffness of the laminate. In order to consider the effect of manufacturing induced defects on the bending stiffness reduction of the structure, parameter α is defined as a multiplier coefficient, as shown in Eq. (5).

$$K_b = (1 - \alpha)K_b^0; \quad ; \alpha = \left(1 - \frac{Q_{p2}h_2^3}{Q_{p1}h_1^3}\right) \quad (5)$$

where K_b^0 is the bending stiffness of the specimen with no defect, Q and h are the effective in-plane stiffness and thickness of the plates, and subscripts 1 and 2 indicated the plate with no defect and the plate with the defect, respectively. It can be seen that the Q_2 and h_2 are unknown functions that are a function of many unknown parameters, such as the pattern of the defect and the stacking sequence. The parameter Q_{p2} be evaluated by the implication of the Rule of Mixture on the material properties in the presence of the gap by considering the average gap percentage of the specimen. The parameter h_2 can also be determined by calculating the average thickness of the plate. However, due to the lack of data, Figure 3-16 can be used for Carbon/Epoxy laminates, with an average gap percentage up to 8% [32].

K_b^0 is also a function of the material properties and boundary conditions. Therefore, this value cannot be determined theoretically for the plate with the complex boundary condition. However, it can be evaluated from the FE model of the baseline sample [52] or the load-deflection of the impact test. The load-deflection graph is extracted with the Quasi-static assumption, an acceptable assumption for a low level of impact energy of larger mass impact response [53]. Note that, for a plate centrally loaded with simply-supported and clamped boundary conditions, K_b^0 can be evaluated by theoretical formula, as shown in Ref. [54]. In this research study, the slope of the tangent line of the force-displacement curve of the baseline sample for 5 J is considered as K_b^0 .

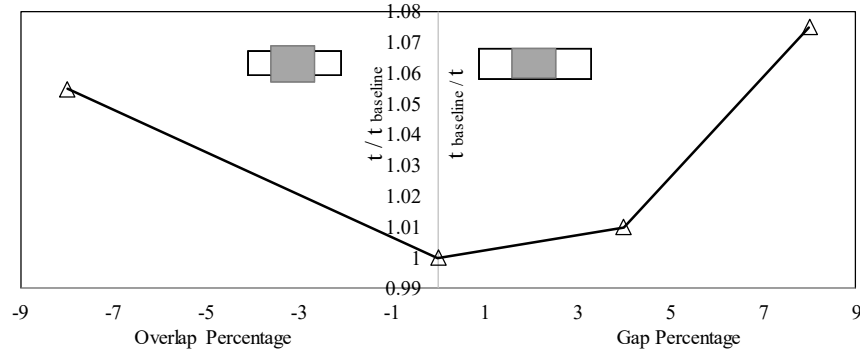


Figure 3-16 Effect of fibre tow gaps on the thickness change of Quasi-isotropic composite laminates

(Reproduced Figure from Automated Composites Manufacturing (ACM4), Fourth International Symposium, Montreal, Canada, 2019. Lancaster, PA: DEStech Publications, Inc.)

The effect of the delamination propagation on the impact response of the structure can be considered through Eq.(6) that is similar to Ref. [52]. For this purpose, K_b is assumed to be constant until the contact force reaches the delamination threshold load of the structure. Then, K_b decreases with an exponential law as follows:

$$K_b = \begin{cases} K_b & P \leq P_{cr} \\ K_b e^{-c(x_2-x_p)} & P \geq P_{cr} \end{cases} \quad (6)$$

P_{cr} is the delamination threshold load of the composite plate. The parameter of c is also chosen to fit the experimental results. This parameter can be evaluated theoretically for the plates with simple boundary conditions [51]. However, impact test is required to find the P_{cr}^0 of the baseline samples. Note that this value is not a function of the impact load for the complex boundary conditions. Thus, a single impact test is enough for finding this parameter. More details are provided in the result section. In this study, the Critical load (P_{cr}) for the specimens is defined by Eq. (7).

$$P_{cr} = P_{cr}^0 \frac{ILSS_2}{ILSS_1} \quad (7)$$

where ILSS is the representative of the interlaminar shear strength of the structure that can be determined by performing short-beam shear test or by performing an FE analysis for the desired sample. Note that the reason for reducing the P_{cr} for the structures with the defects comes from the experimental observations on the impact response of the samples with defects. The value of ILSS for the samples with gaps can also be evaluated experimentally or numerically by embedding the defects in the structures. The results of Ref. [55] on the effect of manufacturing defects on the reduction of ILSS can also be used as a rule of thumb for the quasi-isotropic Carbon/Epoxy Laminates. In this study, the ratio of the $ILSS_2/ILSS_1$ was determined by performing a short-beam shear test based on ASTM D2344 standard. It was found out that while the interlaminar shear strength of the baseline is equal to 94.9MPa, this value is reduced by 13%.

3.6 Results and Discussion

Microscopic observation was performed on the gap area to investigate the effect of the curing process on the final forming of the pre-set gaps.

Figure 3-17 shows the cross section-view microscopic observation of the pristine sample manufactured by AFP, and it was clear that no void and porosity were found in the laminates. It is also interesting that the pre-set gaps are formed in different ways for inner and outer layers. While free intentional spaces cause thickness scaling for the outer layers (Figure 3-17(a)), they are transformed into the resin pocket for interlayers (Figure 3-17(b)). However, the dimension of the pre-set gaps is reduced, and part of that is filled with fibres. For example, it can also be seen that for interlayers with the fibre angle of -45° , and the resin pocket includes inter and intra-resin-rich areas. Although the inter resin pocket's width remains as the dimension of the pre-set gap (2.0 mm), the intra-resin pocket's width within the layer is reduced to less than 0.5 mm.

It is worth noting that the fabrication process can affect the average Fibre Volume Fraction (V_f) of the cured plates. Thus, microscopic images were captured from different locations of both plates. Then the image processing was performed on the microscopic images to find the average value of the V_f . No significant difference was found between the values of the V_f for AFP-G and baseline plates.

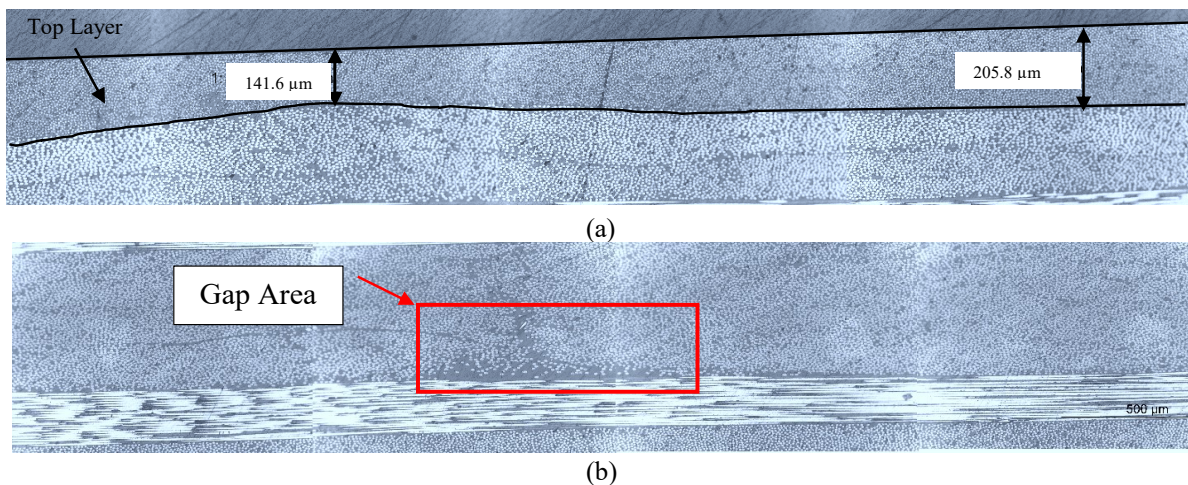


Figure 3-17 Gap area after the curing process for (a) interlayers (b) outer layers

An average thickness reduction was also found for the samples with intentional gaps. Figure 3-18 shows that around 8% of thickness reduction can be expected for the samples with 8% of widespread gap space, which reduces the surface density of the samples with defects.

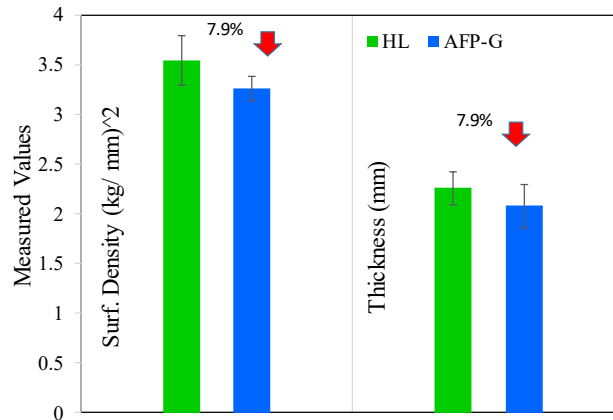


Figure 3-18 Thickness reduction of the composite plates with widespread induced fibre tow gaps

Figure 3-19(a). shows the impact responses and corresponding projected delamination areas for baseline samples and samples with defects for three different Impact Energy levels (IE). It can be seen that WID affects both the impact response and the delamination pattern of the impacted samples.

In terms of impact response, the maximum impact force has been reduced for the AFP-G samples. Figure 3-20 illustrates a comparison of the peak forces (F_p) for both AFP-G and baseline samples. It shows that 2.0 mm WID (8% gap percentage) decreases the peak force by 12%-16%. Thus, it seems that with increasing the IE, the effect of WID is more significant.

It is also worth noting that the induced gaps can affect the delamination threshold load (F_d). However, it contrasts to the earlier impact results on the regular composite plates with no defects that show F_d is a constant parameter for a laminate, independent of the impact energies [33, 56]. This value is about 2650 N for baseline samples with impact energies of 10 J and 15 J, consistent with the independence of the delamination threshold impact load from the impact energies. Nevertheless, this value changes from 1833 N to 2248 N for AFP-G samples with IE equals 10 J and 15 J, respectively. Thus, the F_d reduction for samples with gaps is probably because the resin pockets can accelerate the delamination initiation under impact loading. However, the amount of change is possibly dependent on the location of the gaps.

Ultrasonic C-Scan tests were also performed on the damaged samples to map the projected delamination area. Furthermore, a MATLAB code was developed for measuring the maximum length and the area of the projected delamination from the obtained frequency results. The criteria for mapping the delamination area are based on the measured frequency at the scanned areas. If the amount of the measured frequency decreases by at least 50%, the delamination has occurred at that location. Figure 3-19.b. shows the results of the C-scan test for the impacted samples. It is noticeable that the fibre tow gap changes the shape of the projected delamination area. For instance, the angle between the longest delamination and zero direction is almost zero for baseline samples for all IEs. However, this angle changes for AFP-G samples. The maximum difference can be observed for IE = 5 J, in which the longest diagonal length locates between zero and forty-five degrees. This observation also shows that the maximum diagonal delaminated area is in the

direction of the fibre, for any ply angle [50] is not necessarily correct for the samples with fibre tow gaps. In other words, the maximum delamination area for thin composite plates occurs between two last plies for the plates under the low-velocity impact loading, and the longest diagonal locates in the fibre direction of the bottom ply (e.g., see Ref. [33, 57–60]). That means the longest diagonal of delamination would be along the zero degrees direction for the studied samples with the stacking sequence of $[0_2/45_2/90_2/-45_2]_s$, which is consistent for baseline samples. However, an angle deviation can be found for AFP-G samples due to the existence of the defects. Furthermore, widespread gaps can also increase the longest diagonal length and projected delamination area.

Figure 3-21 compares the measured parameters from the C-scan results for both baseline and AFP-G samples. Results reveal that the samples with defects experience more internal damage for all IEs. For example, the delaminated area for the baseline sample with IE = 15 J is 133 mm^2 . However, this value is increased by 54% for the AFP-G sample with the same amount of IE and reaches 205 mm^2 . An increase in the longest diagonal delamination length with the range of 12%-33% is also expected for AFP-G samples. This effect is more severe at higher levels of IEs, similar to the impact resistance results. Although induced defects change the pattern and dimension of the internal damage, it was found that it has no significant effect on the visible damages. It was found out that the fibre split occurred at the bottom layer of the composite plates (zero layers) with lengths of 25 mm and 36 mm for the composite plates with IE = 10 J and 15 J, respectively. However, no significant difference was found between the AFP-G and baseline samples. Note that no visible damage was found for the samples with IE = 5 J.

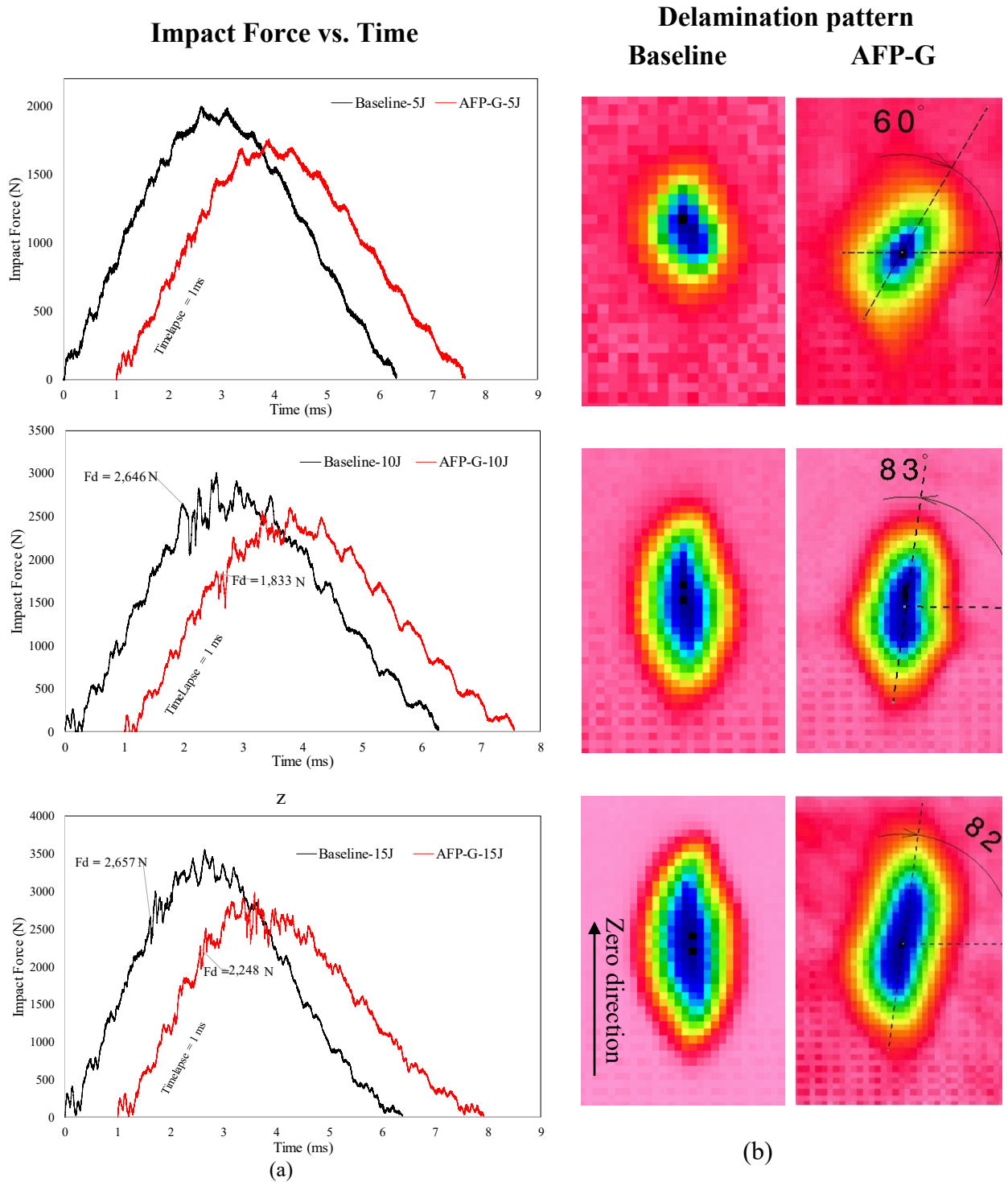


Figure 3-19 Comparison of the (a) Impact responses and (b) projected delamination patterns for AFP-G and baseline samples at different levels of impact energy

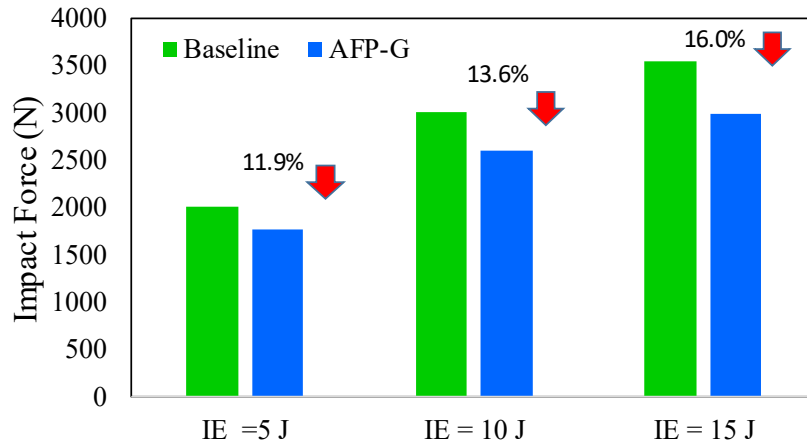


Figure 3-20 A comparison of the maximum impact force between the samples with widespread gaps and baseline samples for different impact energy levels.

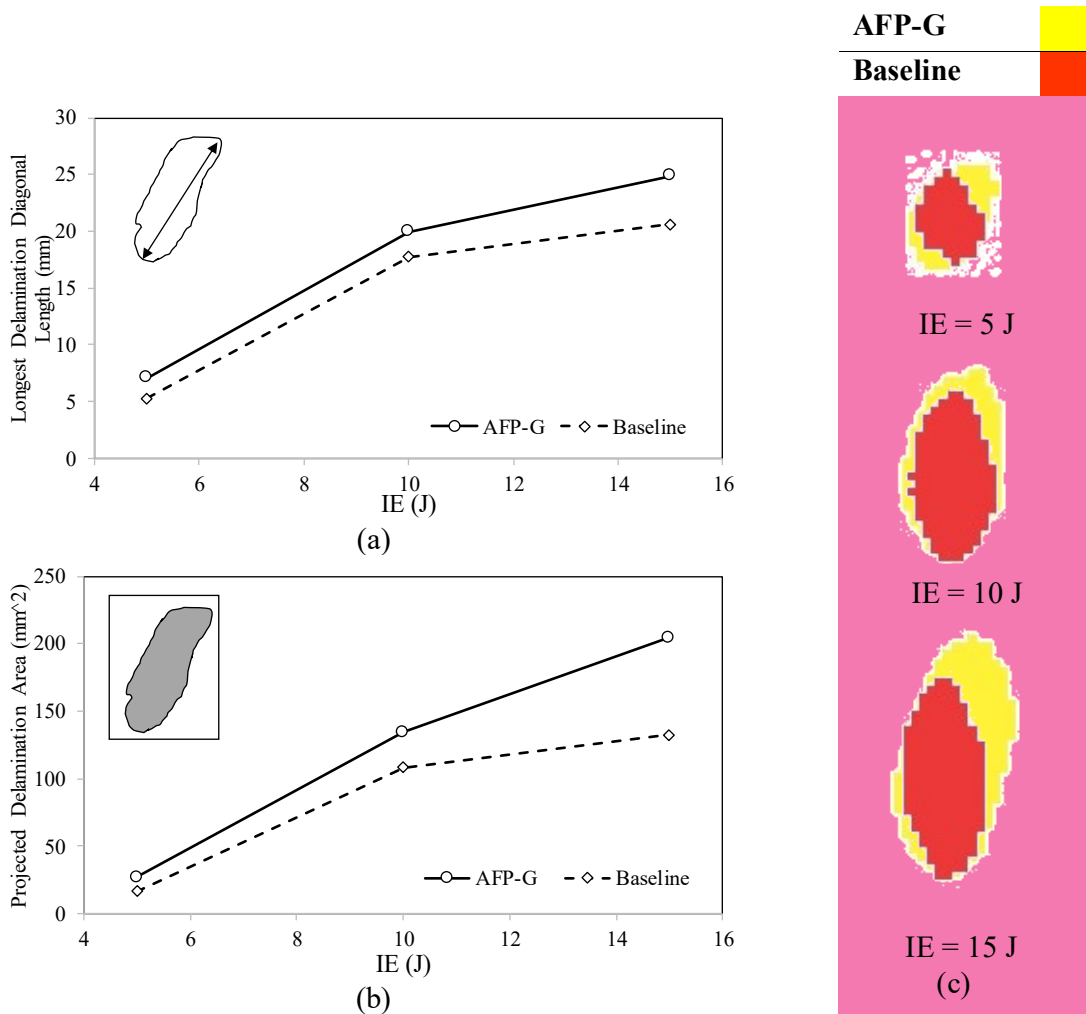


Figure 3-21 A comparison between the projected delamination of AFP-G with baseline at different levels of impact energy (a) Longest delamination diagonal length (b) Projected delamination area (c) Projected delamination shape

Effect of induced defect on the impact depth was shown in Figure 3-22 for different levels of IE's. It is interesting that a reduction of 20-30% can be expected for AFP-G samples, which causes the local indentations less visible. However, by comparing the trend of both baseline and AFP-G for three levels of IE's, it seems that the impact depth reduction is the result of the change in the flexural stiffness of the structures in the presence of WID. In other words, the sample with the gaps is less stiff than the baseline sample because of the flexural stiffness reduction. Thus, local indentation would be less for these samples for the sample level of IE.

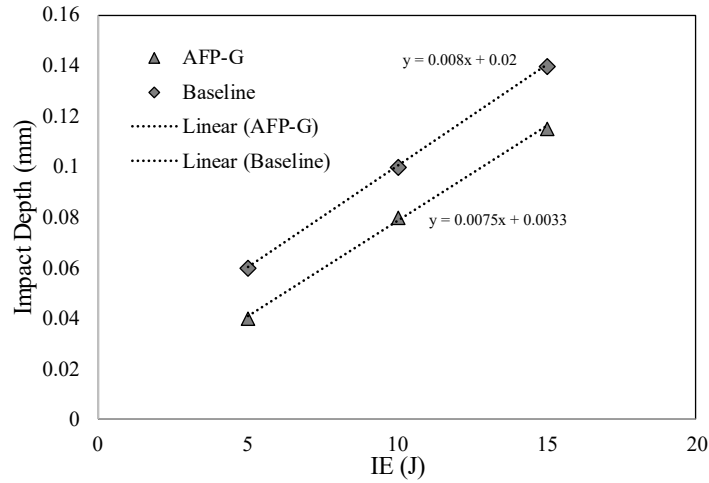


Figure 3-22 Impact depth versus impact energies for baseline and AFP-G samples

By integrating the force history $F(t)$, the impactor acceleration $a(t)$, velocity $v(t)$, displacement $\delta(t)$, and Impact Energy (IE) can be found, respectively [61, 62].

$$v(t) = v_i + \int_0^t a(t)dt = v_i - \frac{1}{m_e} \int_0^t F(t)dt$$

$$\delta(t) = \int_0^t v(t)dt = v_i t - \frac{1}{m_e} \int_0^t \left(\int_0^t F(t)dt \right) dt \quad (8)$$

$$E(t) = \frac{m_e(v_i^2 - v(t)^2)}{2} = \int_0^\delta F(\delta)d\delta$$

where v_i and m_e are the impact velocity and the mass of the impactor, respectively. Note that the Impact Energy (IE) obtained from the force-time curve is representative of the total energy supplied by the impactor system, which is different than the Absorbed Energy (AE). It can be understood from the energy equation that as time increases, at the time of the peak in F-t curve,

the IE reaches almost 50% of the peak value of maximum Impact Energy in the IE-time curve. This time value also dictates the inflection point in the IE-time curve.

As time progresses, IE continues to increase at a rate slower than before, and the IE-time curve will reach its peak at the time when the F-t curve becomes asymptotic to t-axis, and thereafter it remains flat. However, the amount of the absorbed energy by the plate is a function of the relative rigidities of the impactor and the plate and the permanent damages of the plate. Furthermore, the elasticity of the plate makes the plate return to the initial position via the release of strain energy. However, the dissipated energy, such as the plastic energy or fracture energies that caused permanent damage in the plate causes a reduction in the released strain energy value. More details about the relationship between the defined energies can be found in Ref. [62]. It is also worth noting that extra facilities such as high-speed cameras [63] are required to measure dissipated energy and absorbed energy. Numerical damage analysis [64] is also another way to measure these parameters.

Figure 3-23(a) shows the graphs of force versus displacement from Eq. (8). Using linear regression on the linear region of the diagram of the force-displacement for the IE = 5 J, it can be realized that the bending stiffness of the plate is reduced by 17%. A comparison between the results obtained by the proposed semi-analytical model and experimental work can also be found in Figure 3-23. The result shows that the proposed model can capture the force-displacement of the composite plates with defects for IE = 5 J. However, the method predicts less bending stiffness for higher impact energies. The reason is that the quasi-static assumption is no longer valid for a high level of impact energies. Thus, it can be said that the proposed model can predict the impact response of the composite plates with an acceptable error for the plates under low-velocity impact loads. Figure 3-23(b) shows the graphs of the impact energy versus time at different levels of IEs. It is clear that there is no significant difference between the results of the AFP-G and baseline samples. However, the time that the IE reaches the maximum value is larger for the samples with the defects.

Microscopic observations were also performed on damaged samples with defects. Figure 3-24 shows the multiple delamination pattern and matrix cracks in the middle section for AFP-G samples with IE = 10 J and 15 J. The interaction between the delamination and gap area can also be observed at different spots of the cross-section view of the damaged samples.

Figure 3-25 shows two different gap zones in which delamination initiated from there. That would probably be one reason that the shape and dimension of the projected delamination of the samples with gaps are different from those for baseline samples.

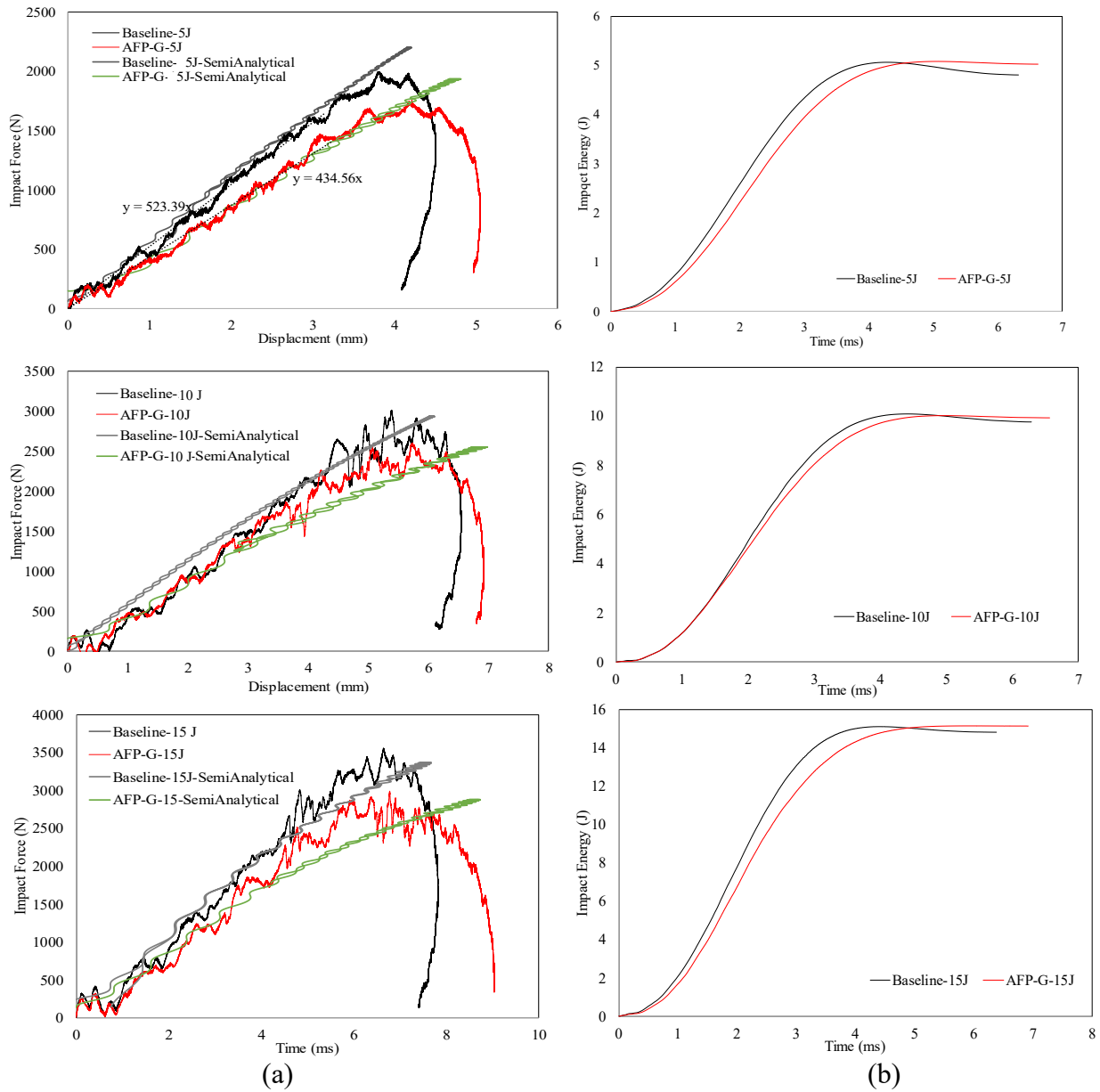


Figure 3-23 (a) Force versus impactor Displacement (b) Impact Energy versus time for different levels of IEs

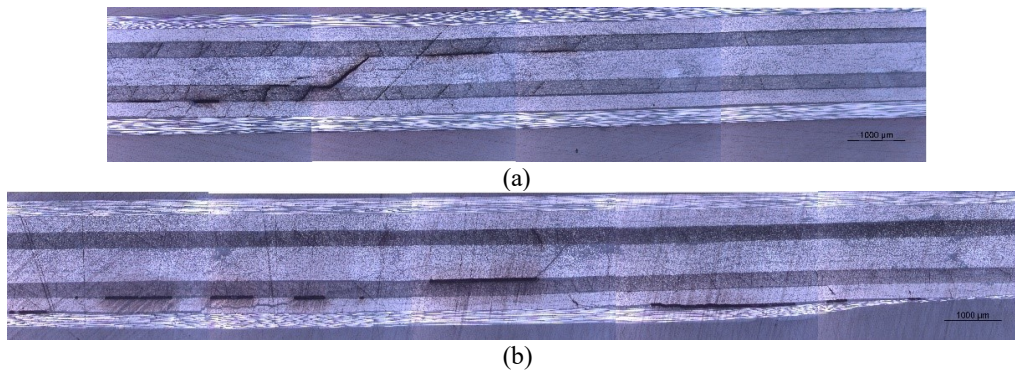


Figure 3-24 Delamination pattern and matrix cracking in the middle section of the samples for impact energy (a) 10 J (b) 15 J

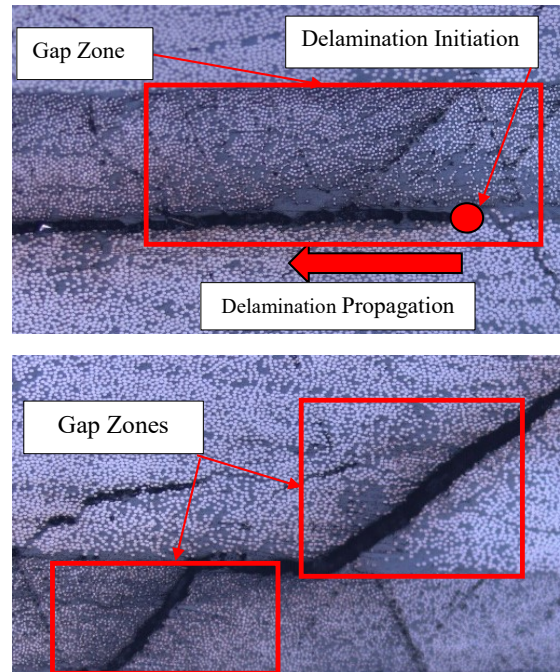


Figure 3-25 Delamination initiation in the composite plates under impact loading at gap area (Resin-rich area)

3.7 Concluding Remarks

In this chapter, the effect of fibre tow gaps on the low-velocity impact response of thin Carbon/Epoxy plates and corresponding delamination patterns were experimentally investigated. For this purpose, Carbon/Epoxy quasi-isotropic plates were manufactured by the Automated Fibre Placement technique with embedding 2.0 mm periodic gaps between fibre courses which result in a composite plate with an 8% gap. Furthermore, a semi-analytical approach was also developed to account for the effect of the manufacturing induced defect on the impact response of the composite plates.

Microscopic observations of the intact cured plates showed that the free spaces (gap) are filled with the resin and create the resin-rich area for interlayers, which affects the local fibre volume fractions at gap areas. However, the preset width of the gap is shrunk due to fibre movement during the curing process. On the other hand, the post-cure effect on the gap area turns into a local thickness reduction for outer layers. Furthermore, the thickness of the samples was reduced due to the intentional pre-set gaps, which may decrease the bending rigidity of the structure. In this study, an average of 8% reduction of the sample thickness was found, which is equal to the intentional gap percentage. However, more studies are required to obtain a relationship between the gap percentage and thickness reduction.

The effect of manufacturing defects on the impact response of the samples was investigated by performing drop weight impact tests. By comparing the results with the baseline samples (no defects), it can be understood that widespread gaps with 8% of volume percentage can decrease the maximum impact force of composite plates up to about 17% for impact energies less than 15 J. It is also interesting that delamination threshold load (F_d) of the composite plates with defects varies for different levels of impact energy which probably shows that the defect areas can

accelerate the delamination initiation and propagation. By looking at the amount of F_d for the baseline samples and also earlier studies, one can say that F_d is almost constant for a particular lay-up, and it is independent of the level of impact energy.

Furthermore, by comparing the experimental results and the results obtained by the proposed semi-analytical model, it was found out that the proposed model can predict the impact response of the composite plate with defects with a good agreement for the low level of the impact energy.

It was also found out that fibre tow gaps can also change the shape of the projected delamination pattern and increase the delamination area up to 50%. Microscopic images show that the gap areas are prone to be a source of delamination initiation. That is probably the reason that the delamination threshold force for the sample with defects is smaller than that of the baseline samples, and also why a larger delamination area was observed for these samples.

The contribution of both thickness reduction and local material inhomogeneities on the impact resistance of the composite plates cannot be interpreted by experimental observations alone. However, it seems that the reduced thickness is more significant on the elastic behaviour of the composite plate under impact loading. On the other hand, induced material inhomogeneity can change the pattern of delamination.

CHAPTER 4

Flexural Response of Defective Composite Beams

This work has been published in:

Ghayour M, Ganesan R, Hojjati M. "Flexural response of composite beams made by Automated Fibre Placement process: Effect of fibre tow gaps". *Compos Part B Eng* 2020; 201: 108368.

<https://doi.org/10.1016/j.compositesb.2020.108368>

4. Flexural Response of Defective Composite Beams

In this chapter, the flexural response of defective beams is studied using experimental work and numerical simulations. It was shown in Chapter 3 that the induced gap reduces the flexural response and the delamination pattern of the impacted plates under LVI. However, due to the complexity of the stress state of the impacted plates, it is difficult to interpret the interaction mechanism of the gap and impact damages. In addition, the scenario of homogenic gap distribution helps to evaluate the impact response of the plate at the structural level. Thus, further experimental tests are required to address the gap-damage interaction at the material level. This chapter extends our current knowledge on the gap-damage interaction for the structures under the out-of-plane loading.

For this purpose, standard-size beams and short beams have been selected for the experimental studies. The experimental tests include three-point bending tests on (1) standard beams for measuring the flexural stiffness and strength of the defective beams (2) short beams for measuring the interlaminar shear strength (ILSS) of the laminates. Using the beams for investigating the gap effects on the damage behaviour of the composite laminates moderates the complexity of the experimental tests. The results of the flexural tests help interpret the flexural behaviour of the plates under LVI. The short beams results enhance our knowledge in the gap-delamination interaction. The result reveals the reason for the delamination threshold reduction of the defective laminates under LVI.

Furthermore, Finite Element simulations are used for stress analysis and damage assessment of the beams under out-of-plane load. In this chapter, the standard FE method is used due to the limited gap areas. An enhanced computational model is developed in chapter 4 for damage assessment and failure analysis of large defective laminates with arbitrary gap distributions. Results include the graphs of stress distribution (in-plane and through the thickness) and failure modes of the defective beams. In addition, the combined effect of thickness reduction and resin pocket on the flexural strength/ILSS reduction of the beams is numerically investigated.

Results show that the thickness reduction and resin pockets that are two consequent effects of the induced gaps should be considered in the stress analysis of the laminated under out-of-plane loading. Furthermore, FE results show that induced gaps interact dissimilarly in delamination initiation and delamination propagation of the beams under out-of-plane loads. While the gap zones are prone to initiate delamination, the stress relaxation in the gap areas acts as delamination stoppers. The results are in accordance with the impact results presented in chapter 3.

Summary

AFP induced defects can be a source of both intralaminar and interlaminar damages, which reduce the mechanical performance of the final products. Although the effect of these defects on the performance of the composite structure, especially the in-plane behaviour, can be found in the literature, there is still a lack of knowledge in studying the mechanical performance of the composite structures with manufacturing induced defects. In this chapter, the effect of automated manufacturing induced gaps on the mechanical response and failure of the Quasi-isotropic Carbon/Epoxy thin beams under out-of-plane loading is investigated. For this purpose, three-point bending tests are carried out on both short and standard beams to measure the interlaminar shear strength and flexural stiffness/strength of the composite beams with the gaps. The results are then compared with the results of the baseline sample (the one with no defect). Furthermore, Finite Element simulations are used to examine the stress distribution and damage initiation and propagation of the composite beams under out-of-plane loading in the gaps. It is shown that the material scaling at the inhomogeneity area, which is widely used in the literature for Finite Element simulation of the composite structure with the gaps, is not sufficient for all scenarios of the loading and thickness scaling might also be applied to the models.

4.1 Introduction

Automated Fibre Placement (AFP) is a new robot technology that has brought many benefits to the manufacturing of composite structures, especially in the aircraft industry. However, structures manufactured by AFP techniques are prone to have several types of micro-induced defects during the fibre deposition process. These include gap and overlap between the fibre tows, tow wrinkling, missing or twisted tow, upfolding, bridging, and crowning [19]. However, gap is one of the most probable types of defects that may occur between two adjacent fibre tows during the automated fibre deposition, especially for multi-curve structures [7]. This defect may bring local material inhomogeneity and geometrical discontinuities that affect the mechanical performance of the composite structures. It can also accelerate the process of damage initiation and catastrophic failure, which decreases the durability of the composite structures.

Experimental studies show that the effect of gaps on the tensile strength of composite laminates is negligible [28, 35]. However, a reduction of compressive strength between 5-27% can be expected for the composite plate under compressive loading [28, 36–38]. The wide range of effectiveness comes from the fact that different scenarios of embedding the gaps into the structures can be defined. For instance, an experimental study on the quasi-isotropic laminates with a 2.0 mm intentional gap and overlap between the tapes has been performed in Ref. [65], and it was shown that the compressive strengths of the composite beams could be reduced by around 7% and 15%, respectively. However, the existence of the stress concentration due to having an open hole makes this effect negligible to consider [31]. An experimental in-plane fatigue test has also been performed on a unidirectional laminate with a single intentional gap with the dimensions of 0.125×0.25 square inch in Ref. [41]. Results reveal that the effect of gaps becomes more severe with increasing the maximum applied stress. However, this effect is negligible for the low level of fatigue stress.

A comprehensive study on the different patterns of the gaps and overlaps can also be found in Ref. [34]. In this study, several composite plates with different sizes of defects from 1 *mm* to 10 *mm* were fabricated, and the effect of the defects on the thickness reduction, tensile and compressive strengths were examined by performing expensive experimental tests.

It is also important to note that, although the induced gaps result from machine malfunction for regular composite laminates, it is impossible to avoid these defects in the new concept of composite manufacturing with fibre steering. Designing the structure with the curvilinear fibre path changes the in-plane stress distribution and causes a considerable increase in the buckling capacity of the composite structures [30, 66–71]. However, the existence of the induced gaps is still a significant issue for these types of structures.

Although the effect of fibre tow gaps on the ultimate strengths of the composite plates under in-plane loading can be found in literature, there is still a lack of knowledge in the study of the effect of induced gaps for the composite structures under out-of-plane loading. Furthermore, many researchers have examined the effect of the induced gap on the mechanical response of the structure with the assumption that the induced gaps cause only local material inhomogeneities. However, local thickness reduction is the other consequence of the induced gaps that need to be considered in experimental and numerical investigations. For example, a local buckling might be expected in defected composite structures due to the local thickness reduction even though no material-level damage mechanism is activated. It can also reduce the stiffness of the structure that might be problematic for the structure designed using the maximum displacement criteria.

The main objective of the present chapter is to study the effect of fibre tow gaps induced in the thin quasi-isotropic Carbon/Epoxy beams on the ultimate strength and on the elastic behaviour of the beams under transverse loading. For this purpose, standard flexural and short-beam shear tests are carried out to observe the effect of the manufacturing-induced gaps on the flexural behaviour and interlaminar shear strength of the composite beams. The results are further compared with the results obtained from the “baseline” samples. The baseline samples refer to those samples with the same stacking sequence and material properties but no defects. These samples have been manufactured by the hand-layup technique.

Furthermore, Finite Element (FE) method is used to investigate the effect of the presence of the gap on the flexural response of the beams under transverse loading for both short and standard beams. It is also shown that the material scaling, which is found in the literature to have been used for simulation of the gap areas, is not adequate to simulate the mechanical behaviour of the composite structures under transverse loading. Thus, both material scaling and thickness scaling is proposed to capture the elastic behaviour and failure of the composite structures with the defects.

4.2 Experimental Investigation

In this study, a ZX103L Kawasaki fibre placement machine with the six-axis articulated robot arm provided by Automated Dynamics Inc., shown in Figure 1(a), was used to fabricate the samples with the periodical gaps between fibre courses. The fibre course is the parallel fibre tows within each robot head pass during the fibre deposition. The number of tows per course may vary for the different AFP robots. In this study, the robot places four fibre tows at a time in a course, and the width of each course is equal to 25.4 *mm* (1.0 inches). In this study, a gap width of 2.0 *mm* was chosen to be embedded between the fibre courses, which is the maximum acceptable gap width in

practical applications. The process of embedding the gaps between fibre courses was proceeded by adjusting the AFP software to consider the course's width to be 2.0 mm longer than the actual width. The gaps have been embedded between all the fibre courses in all the plies, and a 5 mm ply-staggering was applied to avoid overlapping the gaps between the adjacent plies. This scenario of pre-setting the gaps causes 8% of the free spaces (Gap percentage) in the whole laminate during the fibre deposition and before the curing process (Figure 4-1(b)). The hand-layup technique was also chosen for fabricating the composite plate with no defects. These samples are considered as the “baseline samples “(that have no defects). This technique was selected for fabricating the baseline samples to eliminate all the possible defects (See Ref. [19]) that might occur during the fibre deposition by the AFP technique.

Two composite plates with the dimensions of 480×430 mm² were fabricated with both AFP and Hand-layup techniques and have been vacuumed and cured in an autoclave according to the manufacturer manual. It was shown in Ref. [72] that putting a caul plate on top of the composite plate during the curing process has a significant effect on the final quality of the plate. Thus, an Aluminum hard tool (caul plate) was used to reduce the out-of-plane fibre waviness caused by free spaces between the fibre tows. The composite plates are then cut with a circular diamond power saw into the desired samples for both flexural and Short Beam Shear (SBS) tests, as shown in Table 3-1. Furthermore, the visual inspection was performed on all samples to make sure that the samples do not have any edge delamination that might occur during the cutting process.

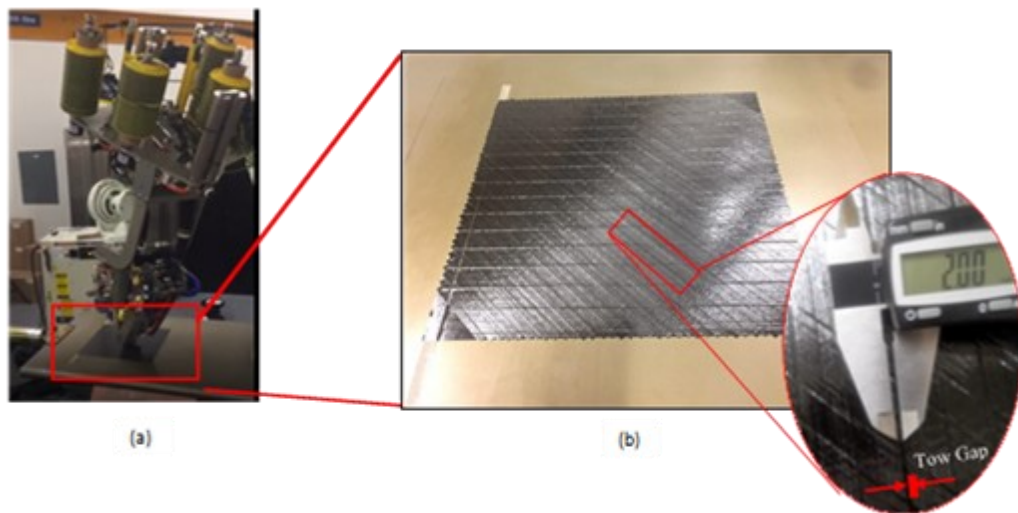


Figure 4-1 Automated Fibre Placement process (a) Fibre deposition by a 6-axis articulated robot arm (b) Fibre tow gap between the fibre courses

Table 4-1. Properties of the test samples

<i>Type of the Test</i>	<i>Sample Dimensions</i>	<i>Stacking Sequence</i>	<i>Material</i>
Short Beam Shear (SBS)	15 × 5 × 2.1 mm ³	[0 ₂ /45 ₂ /90 ₂ /-45 ₂] _s	HTS 40 12K /977-2
Three-point bending	100 × 13 × 2.1 mm ³	[0 ₂ /45 ₂ /90 ₂ /-45 ₂] _s [90 ₂ /-45 ₂ /0 ₂ /45 ₂] _s	

The effect of the distributed gaps on the interlaminar shear strength and also on the out-of-plane flexural stiffness/strength of composite beams is investigated by performing a series of three-point bending tests on the standard and short beams, respectively based on ASTM D7264 [73] and ASTM D2344 [74] standards. Figure 4-2 shows the dimensions and applied boundary conditions for flexural and SBS test setup. It can be seen that the standard beams have dimensions of $100 \times 13 \text{ mm}^2$ with a span length of 80 mm (Figure 4-2(a)). The span-to-thickness ratio of the beams is around 40:1, which is larger than the ASTM recommended ratio. The reason for choosing this ratio is to reduce the effect of the shear deformation (See Note 8, ASTM D7264). The dimensions of the short beams are $15 \times 5 \text{ mm}^2$, with a span length of 11 mm , which corresponds to the span-to-thickness ratio of around 5:1. Furthermore, two 5.0 mm diameter rollers simulate the simply-supported boundary conditions, and the cross-head load is applied by a 10.0 mm diameter roller for the flexural test. The same boundary condition but with a cross-head roller with a diameter of 5.0 mm was used for SBS tests (Figure 4-2(b)). An MTS universal testing machine with a maximum load capacity of 5 kN was used for recording the data of load-displacement for both series of tests. The device can record 50 data per second with the displacement and load precisions of 0.01 mm and 0.1 N , respectively. A minimum of three samples per category was subjected to loading with a loading rate of 1.0 mm/min to achieve consistency in the results.

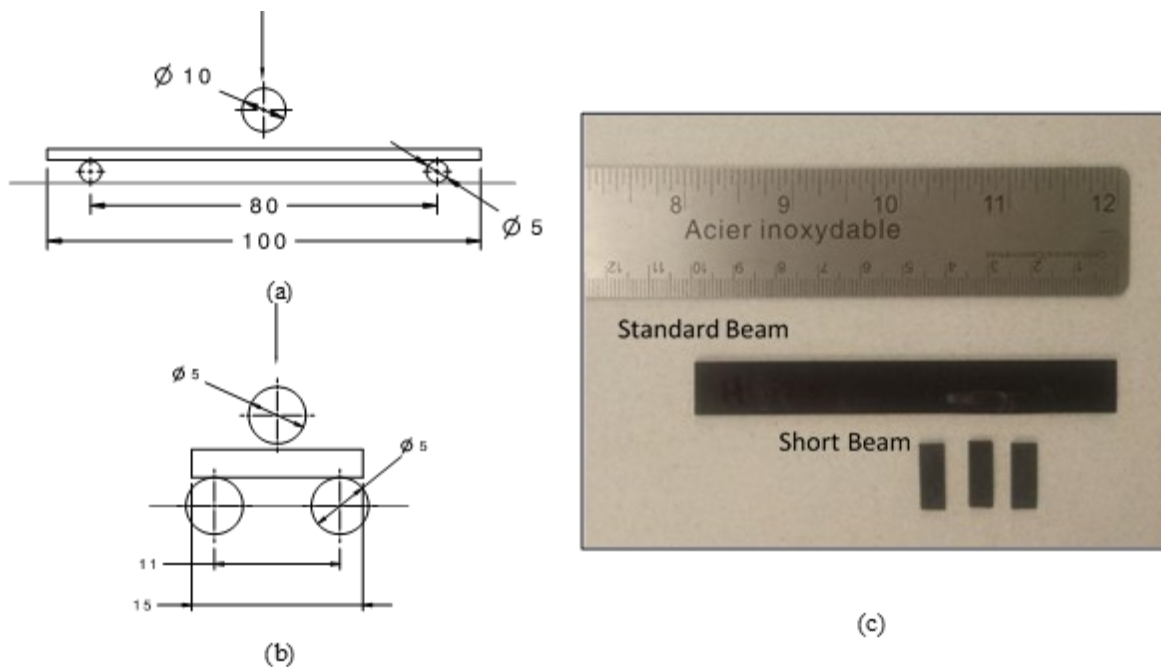


Figure 4-2 Dimensions and boundary conditions of the specimens for the (a) three-point bending test and (b) short-beam shear test (All dimensions are in mm)

4.3 Numerical Simulation

Embedding the free spaces between the fibre tows have two consequent effects on the cured samples. During the curing process, the resin phase changes to the liquid and fills the gap area. But at the same time, fibre filaments in the vicinity of the free spaces are free to move around. This process results in the resin-rich areas on the scale of hundred microns and also local thickness reduction in the final product.

In this study, numerical simulation was carried out to investigate the effect of material scaling and thickness scaling on the flexural response and damage initiation and propagation in the beams.

For this purpose, a 3D model was created using ABAQUS/Explicit software. The constitutive law with damage parameters was implemented in the model by developing a user-material subroutine (VUMAT). The solid element C3D8R was used for meshing the composite solid parts of the FE models to avoid the shear locking problem. This element is an 8-node brick element with a linear shape function and one integration point at the center of the element. The FE model has one element per ply (16 solid elements through the thickness), and the ply orientation was defined by applying material orientation on each ply individually. Furthermore, the interface between the plies and between the composite and epoxy materials was simulated by 8-node three-dimensional cohesive elements (COH3D8) with a thickness of 0.01 *mm*. Aluminium rollers were discretized using rigid body elements. The contact behaviour between the rollers and the composite beam was simulated using the ABAQUS general contact algorithm with the Coulomb friction model [75]. The friction coefficient is the required parameter for calculating the contact force, and it depends on the surface quality of both surfaces in contact. A value of 0.3 is adopted for the metal-laminate contact [64, 76, 77]. The Constitutive Law for composite ply used in this study is based on the Ref. [78], in which shear damage parameters are treated as independent of the matrix damage parameters. The damage parameters are applied directly to the Young's Modulus (E_{ii}) and shear modulus (G_{ij}) of the material, as shown in Eq. (9) in which $[S]_{ijkl}$ is the compliance matrix of the composite material, and d_{ij} is the corresponding damage parameter. Note that the gap area was considered as epoxy resin and was meshed separately with the corresponding material properties. Table 4-2 shows the material properties of the composite material and epoxy resin. Figure 4-3 shows an isometric view of the FE models of both short beam and standard beam.

$$[S]_{ijkl} = \begin{bmatrix} \frac{1}{E_1(1-d_f)} & -\frac{\nu_{12}}{E_1} & -\frac{\nu_{13}}{E_1} & 0 & 0 & 0 \\ & \frac{1}{E_2(1-d_m)} & -\frac{\nu_{23}}{E_2} & 0 & 0 & 0 \\ & & \frac{1}{E_3(1-d_m)} & 0 & 0 & 0 \\ & & & \frac{1}{G_{12}(1-d_{12})} & 0 & 0 \\ & \text{Symmetric} & & & \frac{1}{G_{13}(1-d_{13})} & 0 \\ & & & & & \frac{1}{G_{23}(1-d_{23})} \end{bmatrix} \quad (9)$$

Table 4-2 Material properties of Cycom 977-2/ HTS 40 unidirectional ply [79, 80]

Composite Elastic Properties	$E_1 = 153000 \text{ MPa}$, $E_2 = E_3 = 10300 \text{ MPa}$; $\nu_{12} = \nu_{13} = 0.3$; $\nu_{23} = 0.4$; $G_{12}^0 = 6000 \text{ MPa}$, $G_{13}^0 = 6000 \text{ MPa}$, $G_{23}^0 = 3700 \text{ MPa}$
Composite Damage Parameters Hashin Parameter (MPa) In-plane Fracture Toughness (N/mm)	$X_T = 2537$, $X_C = 1580$; $Y_T = 82$, $Y_C = 236$, $S_{12} = S_{13} = 90$, $S_{23} = 40$ $G_{IC}^T = 91.6$, $G_{IC}^C = 79.9$, $G_{2C}^T = 0.22$, $G_{2C}^C = 0.2$, $G_s = 0.2$ $\gamma_{12}^f (\%) = \gamma_{13}^f (\%) = 17\%$, $(\gamma_{23}^f)^* = ((\gamma_{12}^f)/2)$
Epoxy Properties¹	$E = 3500 \text{ MPa}$, $\nu = 0.35$, Plastic Poisson's Ratio (ν_p) = 0.30, Tensile Strength = 81.4 MPa, Compressive Strength* = 160 MPa Failure Strain in Tension = 2.5% [79] $G_c = 0.478 \text{ N/mm}$ Tensile Yield Strength = 50 MPa, Compressive Yield Strength = 100 MPa Tensile and Compressive Hardening Modulus $H_t = H_c = 1500 \text{ MPa}$
Interface properties Stiffness (MPa/mm) Strength (MPa) Fracture Toughness (N/mm)	$K_n = K_s = K_t = 10^6$ $N = 62.3$, $S = T = 92.3$ $G_{IC} = 0.28$, $G_{IIC} = G_{IIIC} = 0.79$

¹ Manufacture datasheet

* Assumption

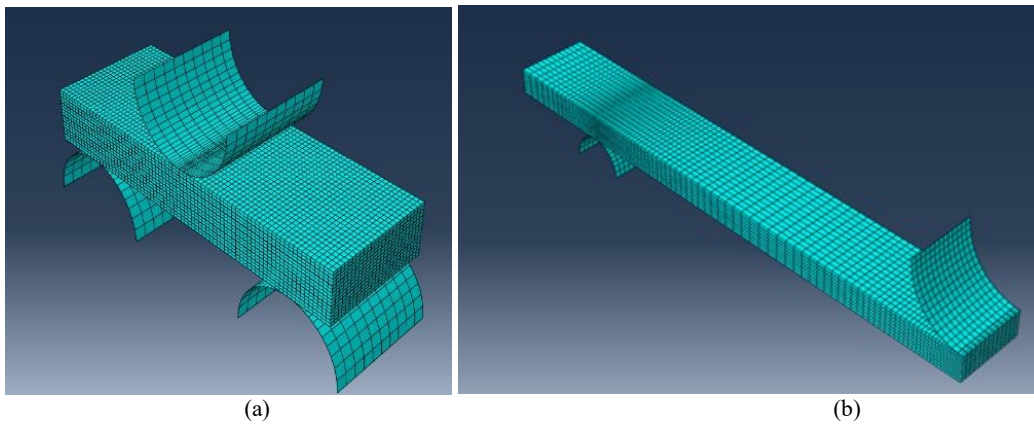


Figure 4-3 Isometric view of the FE models for (a) Short beam shear test (b) Flexural test

4.3.1 Material Damage Model

4.3.1.1 Composite Damage Model

The stress-based 3D Hashin failure criteria [81] are used for damage onset prediction for both tension and compression modes of the failure. Table 4-3 shows the failure criteria for fibre and matrix failure modes.

Table 4-3 Hashin Failure Criteria

Failure Mode	Failure Criteria
Fibre Tensile ($\sigma_{11} > 0$)	$F_{ft} = \left(\frac{\sigma_{11}}{X_T}\right)^2 + \alpha \left(\frac{1}{S_{12}^2}\right) (\sigma_{12}^2 + \sigma_{13}^2) = 1$ (10)
Fibre Compression ($\sigma_{11} < 0$)	$F_{fc} = \frac{\langle -\sigma_{11} \rangle}{X_c} = 1$

Matrix Tensile ($\sigma_{22} + \sigma_{33} > 0$)	$F_{mt} = \frac{1}{Y_T^2} (\sigma_{22} + \sigma_{33})^2 + \left(\frac{1}{S_{23}^2} \right) (\sigma_{23}^2 - \sigma_{22}\sigma_{33})$ $+ \left(\frac{1}{S_{12}^2} \right) (\sigma_{12}^2 + \sigma_{13}^2) = 1$
Matrix Compression ($\sigma_{22} + \sigma_{33} < 0$)	$F_{mc} = \frac{1}{Y_c} \left[\left(\frac{Y_c}{2S_{23}} \right)^2 - 1 \right] (\sigma_{22} + \sigma_{33})$ $+ \frac{1}{4S_{23}^2} (\sigma_{22} + \sigma_{33})^2$ $+ \frac{1}{S_{23}^2} (\sigma_{23}^2 - \sigma_{22}\sigma_{33})$ $+ \frac{1}{S_{12}^2} (\sigma_{12}^2 + \sigma_{13}^2) = 1$

where X_T and X_c are tensile and compressive strengths in the fibre direction, Y_T and Y_C are tensile, and compressive strengths transverse to the fibre direction, and S_{12} and S_{23} are longitudinal and transverse shear strengths. The coefficient α determines the contribution of the shear stress to the tensile damage initiation in the fibre direction, which is assumed to be equal to 1.0, as suggested in Ref. [81].

A linear softening damage model [82] was also assumed for damage propagation of the composite materials in tensile and compressive loading conditions. Eq. (11) shows the definition of the damage parameters in fibre and matrix directions. δ indicates the displacement and superscripts 0 and f denote the initial and final state, respectively. The corresponding damage parameters for fibre and matrix directions can be found in Table 4-4.

$$d_j^i = \frac{\delta_{eq}^{fi}(\delta_{eq} - \delta_{eq}^0)}{\delta_{eq}(\delta_{eq}^f - \delta_{eq}^0)}; i = t, c; j = f, m \quad (11)$$

4.1 Nonlinear Shear Model

Experimental results show that the composite laminates have a non-linear shear behaviour [78, 83, 84] in each shear plane direction. In this research, a semi-empirical model [80] is used for simulating the non-linear shear behaviour of composite ply. The non-linear stress-strain relation is expressed by Eq. (12):

$$\tau_{ij} = S_{ij} \left(1 - \exp \left(- \frac{G_{ij}^0}{S_{ij}} \gamma_{ij} \right) \right) \quad i, j = 1, 2, 3, \quad i \neq j \quad (12)$$

τ_{ij} , G_{ij}^0 , γ_{ij} and S_{ij} are the shear stress, linear elastic shear modulus, shear strain, and shear strength in the i - j shear plane of the material, respectively.

Chapter 4

The shear damage behaviour is simulated by the definition of a shear damage parameter, as well. The nonlinear shear damage initiation for a given shear plane can be expressed by a stress-based criterion given as follow:

$$F_{ij}^{Shear} = \frac{|\tau_{ij}|}{S_{ij}} = 1 \quad ; \quad i, j = 1, 2, 3, \quad i \neq j \quad (13)$$

In order to define the damage evolution parameter (d_{ij}), shear strain is decomposed into two parts, that are elastic strain (γ^e) and inelastic strain (γ^{in}). The inelastic strain is defined as:

$$\gamma_{ij}^{in} = \gamma_{ij} - \gamma_{ij}^e = \gamma_{ij} - \frac{\tau_{ij}}{G_{ij}^0} \quad (14)$$

The damage evolution parameter for the shear plane i - j is also expressed by a strain-based criterion which is given by:

$$\begin{aligned} d_{ij} &= 1 - \frac{\gamma_{ij,0} - \gamma_{ij,0}^{in}}{\gamma_{ij} - \gamma_{ij,0}^{in}} [1 + \lambda^2(2\lambda - 3)]; \quad i, j = 1, 2, 3, \quad i \neq j \\ \lambda &= \frac{\gamma_{ij} - \gamma_{ij,0} - 2\gamma_{ij,0}^{in}}{\gamma_{ij,0} - \gamma_{ij,0}^{in} - \gamma_{ij}^f} \\ \gamma_{ij}^f &= \frac{2G_s}{S_{ij}l^*} \end{aligned} \quad (15)$$

where $\gamma_{ij,0}$ and $\gamma_{ij,0}^{in}$ denote (total) shear strain and inelastic shear strain at the shear damage initiation. γ_{ij}^f is the shear strain at complete failure and l^* is the characteristics length of the element. Figure 4-4 shows the non-linear shear behaviour of the composite ply and the corresponding damage parameter at the shear plane 1-2.

Table 4-4 Damage evolution parameters for composite ply [82]

Damage Mode	Damage Evolution Parameters	(16)
Fibre Tensile ($\sigma_{11} > 0$)	$\delta_{eq}^{ft} = l^* \sqrt{\epsilon_{11}^2 + \alpha(\epsilon_{12}^2 + \epsilon_{13}^2)}$ $\delta_{eq,0}^{ft} = \frac{\delta_{eq}^{ft}}{F_{ft}^{0.5}}, \delta_{eq,f}^{ft} = \frac{2G_{IT}}{\sigma_{eq,0}^{ft}}$ $\sigma_{eq}^{ft} = \frac{l^*}{\delta_{eq}^{ft}} [\sigma_{11}\epsilon_{11} + \alpha(\sigma_{12}\epsilon_{12} + \sigma_{13}\epsilon_{13})]$	
Fibre Compression ($\sigma_{11} < 0$)	$\delta_{eq}^{fc} = l^* \sqrt{\epsilon_{11}^2}$ $\delta_{eq,0}^{fc} = \frac{\delta_{eq}^{fc}}{F_{fc}^{0.5}}, \delta_{eq,f}^{fc} = \frac{2G_{IC}}{\sigma_{eq,0}^{fc}}$ $\sigma_{eq}^{fc} = \frac{l^*}{\delta_{eq}^{fc}} [\sigma_{11}\epsilon_{11}]$	
Matrix Tensile ($\sigma_{22} + \sigma_{33} > 0$)	$\delta_{eq}^{mt} = l^* (\sqrt{\epsilon_{22}^2 + \epsilon_{33}^2 + \alpha(\epsilon_{12}^2 + \epsilon_{13}^2 + \epsilon_{23}^2)})$ $\delta_{eq,0}^{mt} = \frac{\delta_{eq}^{mt}}{F_{mt}^{0.5}}, \delta_{eq,f}^{mt} = \frac{2G_{IIT}}{\sigma_{eq,0}^{mt}}$ $\sigma_{eq}^{mt} = \frac{l^*}{\delta_{eq}^{mt}} [\sigma_{22}\epsilon_{22} + \sigma_{33}\epsilon_{33} + (\sigma_{12}\epsilon_{12} + \sigma_{13}\epsilon_{13} + \sigma_{12}\epsilon_{12} + \sigma_{23}\epsilon_{23})]$	
Matrix Compression ($\sigma_{22} + \sigma_{33} < 0$)	$\delta_{eq}^{mc} = l^* (\sqrt{\epsilon_{22}^2 + \epsilon_{33}^2 + \alpha(\epsilon_{12}^2 + \epsilon_{13}^2 + \epsilon_{23}^2)})$ $\delta_{eq,0}^{mc} = \frac{\delta_{eq}^{mc}}{F_{mc}^{0.5}}, \delta_{eq,f}^{mc} = \frac{2G_{IIC}}{\sigma_{eq,0}^{mc}}$ $\sigma_{eq}^{mc} = \frac{l^*}{\delta_{eq}^{mc}} [\sigma_{22}\epsilon_{22} + \sigma_{33}\epsilon_{33} + (\sigma_{12}\epsilon_{12} + \sigma_{13}\epsilon_{13} + \sigma_{12}\epsilon_{12} + \sigma_{23}\epsilon_{23})]$	

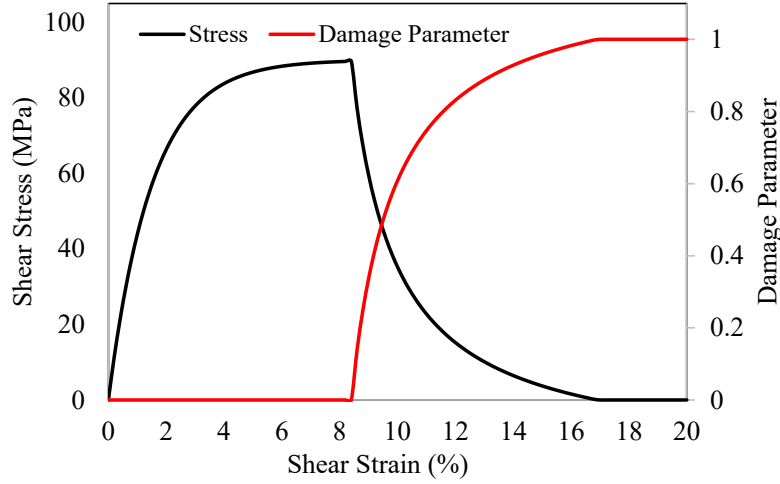


Figure 4-4 Non-linear shear stress and shear damage parameter versus shear strain

4.1.1 Epoxy Material Model

Mechanical behaviour of the epoxy at the gap area is modelled with an elasto-plastic model. Recent studies [40, 85] show that the current built-in ABAQUS plastic models, such as Mohr-Coulomb elasto-plastic model and Drucker-Prager model, are unable to simulate the behaviour of epoxy material under general state of loading conditions [86]. For this purpose, a user material was developed to simulate the elasto-plastic behaviour of the epoxy material. A 3D isotropic model simulates the linear behaviour of the epoxy until it meets the yield criterion proposed in Ref. [87]. The yield criterion of the epoxy can be defined by a paraboloidal model [88] as follow:

$$\phi(\sigma) = 6J_2 + 2I_1(\sigma_C - \sigma_T) - 2\sigma_T\sigma_C = 0 \quad (17)$$

where $\phi(\sigma)$ is the yield function, and σ is the stress tensor of the epoxy material. The parameter I_1 is the first invariant of the stress tensor, and J_2 is the second invariant of the deviatoric stress tensor and σ_T and σ_C are absolute values of tensile and compressive yield stresses. The yield function (ϕ) has a negative value at the elastic regime of the structures at it is equal to zero when the material reaches the yield point. Figure 4-5a shows the graphical view of the yield surface for the present epoxy material system.

The flow rule and integration return mapping algorithm were developed using the method proposed in Ref. [89]. For this purpose, a non-associated flow rule is selected as follow:

$$g = \sigma_{von}^2 + \zeta p \quad (18)$$

where σ_{von} is the von Mises equivalent stress, ν_p is the plastic Poisson's ratio, which is determined from the standard tension test and, $p=1/3 I_1$ is the hydrostatic pressure. The parameter ζ is a function of the plastic Poisson's ratio and can be found as follow:

$$\zeta = \frac{9}{2} \frac{1 - 2\nu_p}{1 + \nu_p} \quad (19)$$

Chapter 4

The trial stress is evaluated for the plasticity of the model by the following equation:

$$\sigma_{n+1}^{tr} = \sigma_n + D: \Delta \epsilon^{tr} \quad (20)$$

where D is the fourth-order isotropic elasticity tensor and σ_{n+1}^{tr} is the trial stress tensor at time $n+1$. The plastic strain increment is defined by Eq. (21) by using the flow rule presented in Eq. (18):

$$\Delta \epsilon^p = \Delta \gamma \left(3\mathbf{S} + \frac{2}{9} \zeta I_1 \mathbf{I} \right) \quad (21)$$

\mathbf{S} is the deviatoric stress tensor, \mathbf{I} is the identity matrix, and $\Delta \gamma$ is the plastic multiplier. Thus, the relation between stress and $\Delta \gamma$ can be written as:

$$\sigma = \frac{S_{tr}}{1 + 6 G \Delta \gamma} + \frac{\frac{1}{3} I_1^{tr} \mathbf{I}}{1 + 2K\zeta \Delta \gamma} \quad (22)$$

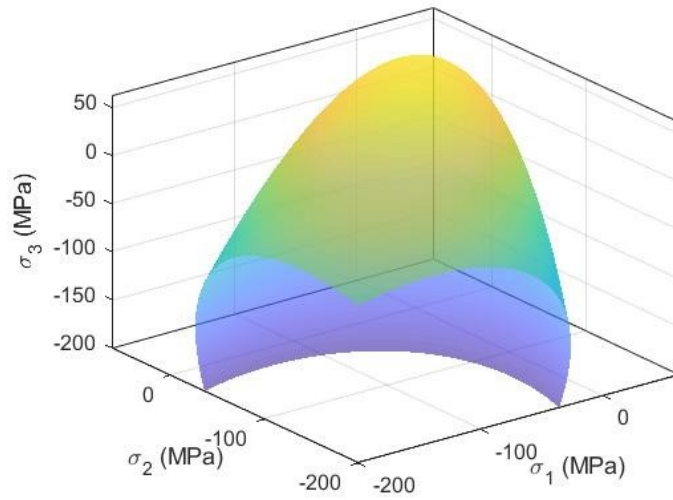
Besides, hardening is assumed to affect both σ_c and σ_t and it is considered to be a function of the equivalent plastic strain, as shown in Eq. (23) as follow:

$$\sigma_t = \sigma_t(\epsilon_e^p); \quad \sigma_c = \sigma_c(\epsilon_e^p) \quad (23)$$

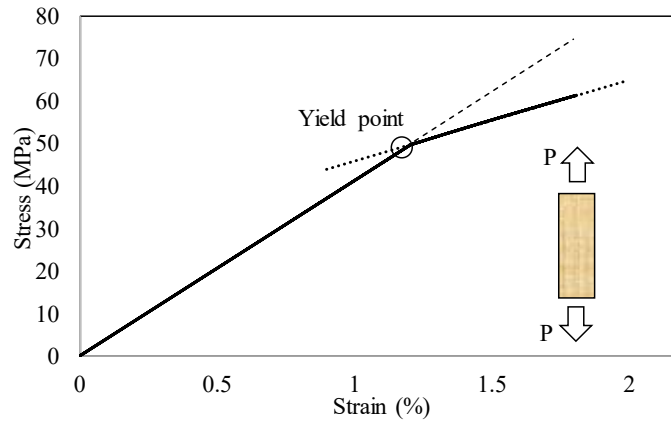
and the equivalent plastic strain can be calculated by the following formula:

$$\Delta \epsilon_e^p = \sqrt{\frac{1}{1 + 2\nu_p^2}} \Delta \epsilon^p: \Delta \epsilon^p \quad (24)$$

Note that I_1 and \mathbf{S} in Eq. (22) are expressed in terms of trial stress. That means the yield function (ϕ) in Eq. (17) is just a function of the plastic multiplier ($\Delta \gamma$). Thus, if ($\phi(\sigma^{tr}, \epsilon_e^p) > 1.0$), the plastic strain is increased by increasing the $\Delta \gamma$ until the yield function reaches the value of zero. In order to find the plastic multiplier at every time step, a Return Mapping Algorithm (RMA) is developed, and the Newton-Raphson iterative algorithm is utilized for the solving of the RMA. Note that, in this study, the hardening moduli are constants and are not the function of the effective plastic strain and are assumed to be constant due to a lack of experimental data for the selected epoxy material. More details on the numerical integration and formulae derivation can be found in Ref. [89]. Figure 4-5b shows the stress-strain graph for the selected epoxy material under the uniaxial loading condition.



(a)



(b)

Figure 4-5 (a) A graphical view of the yield surface of the epoxy resin material (b) Stress-strain curve of the epoxy resin under uniaxial loading condition

4.1.2 Damage Law for Cohesive Elements

The delamination between the composite plies is simulated by defining the cohesive zone elements between the composite plies. These elements were found to be an effective way to capture the propagation of the damage between the composite layers. For this purpose, a bilinear traction-separation law is defined for three failure modes of the delamination, Mode I, II, and III, to predict the delamination onset and propagation (Figure 4-6). It can be seen that the elastic behaviour of the interface element is described by a linear relationship between the traction-displacement for different fracture modes as follow:

$$t_i = k_i \delta_i ; \quad i = n, s, t \tag{25}$$

Chapter 4

where t_i , k_i and δ_i are traction stress, penalty stiffness, and relative displacement at normal (n), shear (s), and tear (t) modes of the fracture.

In practical applications, delamination is likely to occur under mixed-mode loading. In this study, the delamination initiation is predicted by a mixed-mode quadratic stress failure criterion proposed in Ref. [90] defined by:

$$\left(\frac{t_n}{N}\right)^2 + \left(\frac{t_s}{S}\right)^2 + \left(\frac{t_t}{T}\right)^2 = 1 \quad (26)$$

where t_n , t_s and t_t represent the interface stresses, and N , S , and T are the normal and shear strengths at the cohesive plane. Furthermore, the softening behaviour is defined by the following:

$$d = \frac{\delta_m^f(\delta_m - \delta_m^0)}{\delta_m(\delta_m^f - \delta_m^0)} \quad (27)$$

where δ_m is the mixed-mode displacement which is given by:

$$\delta_m = \sqrt{(\delta_n^2 + \delta_s^2 + \delta_t^2)} \quad (28)$$

δ_m^0 and δ_m^f are mixed-mode displacements at damage initiation and complete failure, respectively. δ_m^f is also defined by using the energy-based Benzeggagh–Kenane (BK) fracture criterion [91], which is given by [92]:

$$\begin{cases} \left[\frac{2}{K\delta_m^0} \left[G_{IC} + (G_{IIC} - G_{IC}) \left(\frac{\beta}{1 + \beta^2} \right)^\eta \right] \right. & \delta_n > 0 \\ \left. \sqrt{(\delta_s^f)^2 + (\delta_t^f)^2} \right. & \delta_n \leq 0 \end{cases} \quad (29)$$

where parameter $\beta = \left(\frac{\delta_s + \delta_t}{\delta_n} \right)$ and η is the cohesive property coefficient. This parameter is dependent on the material properties and needs to be determined experimentally. However, it was shown in Ref. [80] that $\eta = 1.45$ can be used for the present Carbon/Epoxy system.

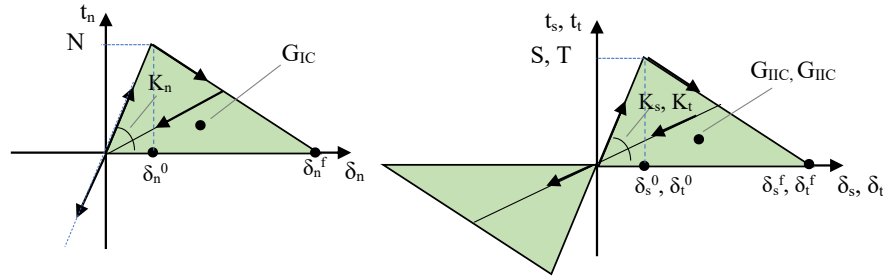


Figure 4-6 Traction-displacement relationship for cohesive surface under mixed fracture modes

4.2 Results and Discussion

The effect of induced gaps on the quality of the cured plate was investigated by measuring the thickness of the samples and the microscopic observation of the cross-section of the intact samples. Figure 3-16(a) shows that the average thickness for both baseline and AFP-G with the corresponding standard deviation. The thickness of the samples has been measured at different locations of the beams with a Vernier Caliper with a precision of 0.01 mm . It is shown that the average thickness of the baseline samples is 2.1 mm . However, embedding 8% of the gap in the composite plate during fibre deposition may decrease the final thickness of the plates by around 7%. This value is consistent with the result provided in Refs. [32, 55]. Note that there is no linear relation between the average gap percentage and thickness reduction. Figure 3-16b shows the gap-overlap percentage versus the thickness reduction for the Carbon/Epoxy quasi-isotropic laminates for gap/overlap percentage of up to 8%. This change might have a significant effect on the flexural behaviour of the samples. Figure 4-8 shows the cross-section view of the AFP-G samples at the gap area. It can be seen that the thickness of the -45° plies has been reduced in the gap area by around 7%.

The other effect of the existence of the induced gaps on the quality of the composite samples can be found in Figure 4-9. The pre-set gap affects the uniformity of the Fibre Volume Fraction (FVF) in the gap area. For instance, FVF drops by 50% at the -45° lamina and reaches 27% at the centre of the gap area. It is also worth noting that the width of the resin-rich area (pre-set gap area) is reduced due to fibres' movement during the curing process. However, the effective domain of the FVF reduction seems to remain around 2.0 mm , which is equal to the width of the embedded intentional gap. In other words, it is apparent in the close view of the gap section that the resin pocket induced by gap includes both interlaminar and intralaminar resin-rich pockets. The interlaminar resin pocket's width is about $1750 \mu\text{m}$ which is almost the dimension of the pre-set gap (2.0 mm). It was shown in Ref. [93] that the inter-laminar resin pocket can accelerate the delamination initiation in the structure. Thus, the authors believe that the assumption of a 2.0 mm gap in the numerical study is acceptable.

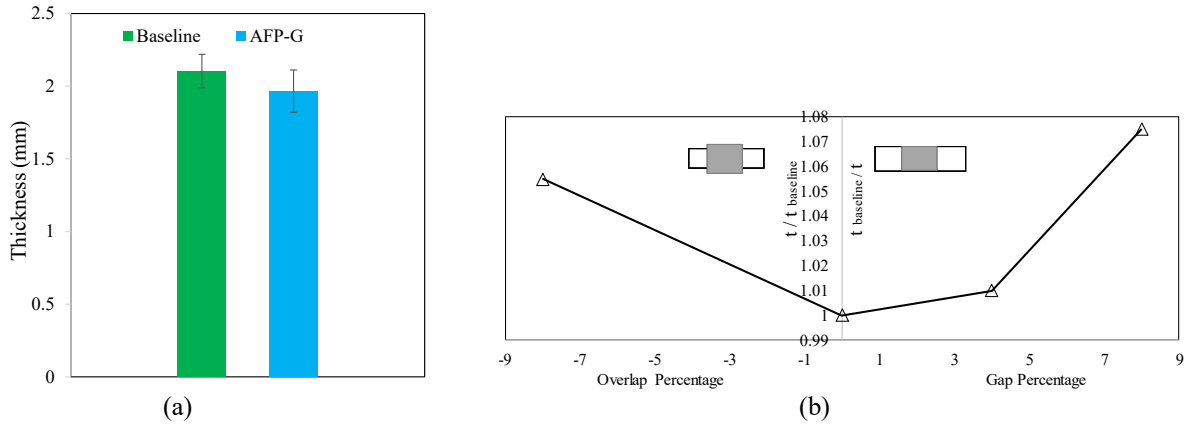


Figure 4-7 Effect of fibre tow gaps on thickness reduction of Carbon/Epoxy composite laminate (a) in the present study (b) (Reproduced Figure from Ref. [32] from *Automated Composites Manufacturing (ACM4), Proceedings of the Fourth International Symposium of ACM, Montreal, Canada, 2019*. Lancaster, PA: DEStech Publications, Inc.)

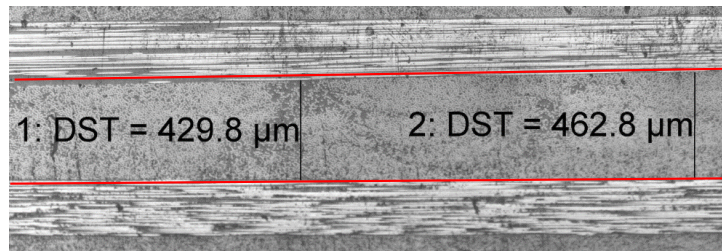


Figure 4-8 Local thickness reduction at the gap area

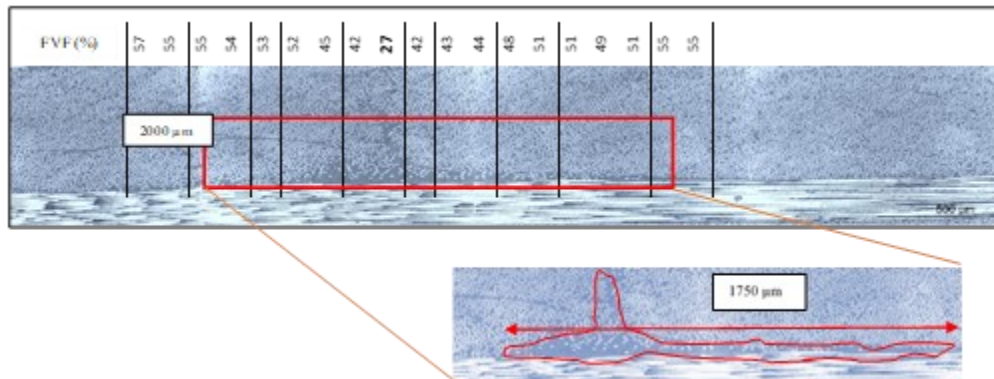


Figure 4-9 Distribution of the Fibre Volume Fraction and fibre distributions at the gap zone in 45° lamina

4.2.2 Short Beam Shear Test

The effects of both material and thickness scaling on the damage mechanism and also failure of the short beam are studied by performing the numerical simulation. For this purpose, three FE models were developed to be studied on (1) the baseline short beam with no gap (Baseline sample), (2) The short beam with the embedded gap with no thickness scaling (FE-G-A) (3) The short beam with both gap and thickness scaling (FE-G-B) as shown in Table 4-5. Note that the thickness scaling in the FE-G-B model is corresponding to the results illustrated in Figure 3-16.a. Furthermore, the location of the pre-set gap may affect the final result for short beam shear tests. In this study, a 2.0 mm gap is located at the centre of the beams in -45° lamina. This beam is consistent with one of the experimental SBS test samples. Besides, this scenario can be considered the worst scenario of the failure because the highest shear stress and, consequently, the delamination initiation occurs at the centre of the short beams. The gap volume of AFP-G samples is assumed to be filled with epoxy resin. This assumption has been successfully used in Refs.[30, 40] to simulate the in-plane mechanical response of the composite plates with the gaps.

Table 4-5 General characteristics of the FE models of the short beam

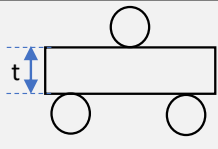
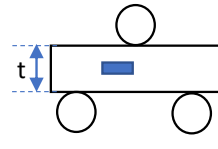
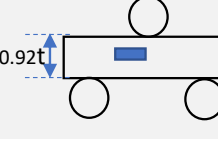
Model	Description	Thickness (mm)	Preset Gap	Schematic View of SBS Model
FE-Baseline	No Gap	2.1	No	
FE-G-A	Gap- No Thickness Reduction	2.1	Yes	
FE-G-B	Gap- With Thickness Reduction	1.95	Yes	

Figure 4-10a and Figure 4-10b show the load graphs versus out-of-plane displacement for short beam baseline and AFP-G samples, respectively. It is clear that the loading capacity of the short beams can be reduced by around 15% in the presence of the gap. However, no change in the final failure mode of both groups of the beams was found in the experimental studies. The beams failed due to the delamination between 45° and 90° plies at the lower sides of the beams, as shown in Figure 4-10c. Figure 4-10d illustrates a cross-section view of the failed beam obtained from the numerical simulation, which shows a good agreement with the experimental observation.

Figure 4-11 shows the results for the interlaminar shear strength of the short beams from both experimental and numerical investigations. Comparing the experimental results of the baseline and AFP-G samples, it can be understood that fibre tow gaps reduce the interlaminar shear strength of the composite laminates by about 13%. Note that the Interlaminar Shear Strength is evaluated by

Chapter 4

$\sigma_{sbs} = \frac{3 P_m}{4 b t}$ where b and t are the width and thickness of the short beam. A reference thickness equals to 2.1 mm was considered for both baseline and AFP-G samples. It is also worth noting that because of the small dimensions of the short beams, there is a possibility of not having a gap area in the tested samples. In other words, all of the tested samples are not necessarily representative of the samples with the resin-rich area. In order to overcome this issue, more than 15 samples were tested experimentally, and the average value was calculated for the four samples with the induced defect by using microscopic observation. It is important to note that a reduction in ILSS can be observed for the short beams extracted from the AFP-G plate, even if no resin-rich area was observed in the beam. This reduction is the consequence of the thickness consolidation due to inducing the gaps into the composite plate. Thus, the average results of the 15 samples are the average ILSS of the plate with the induced gaps. However, the authors believe that it is more beneficial to report the results of the beams with the material defects inside the beams, which can be considered the worst-case scenario.

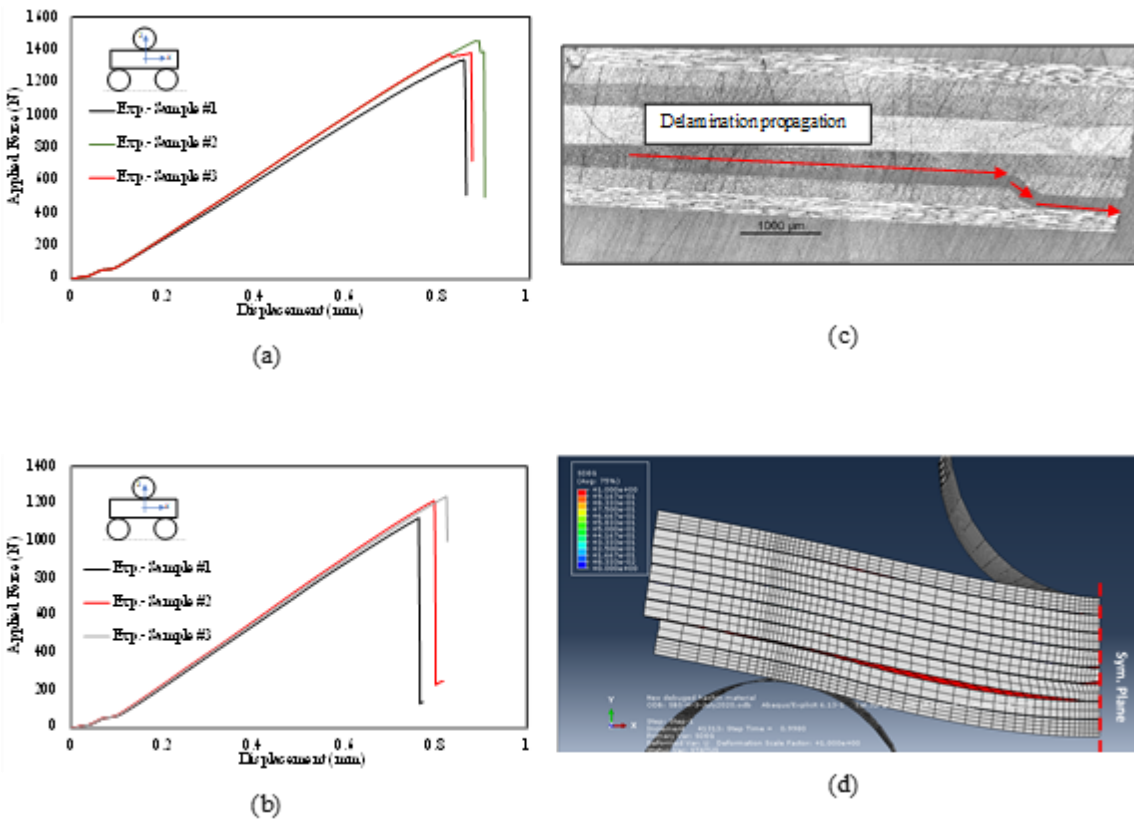


Figure 4-10 Applied force versus. Out-of-plane displacement of short beams for (a) Baseline (b) AFP-G samples. The final failure of the short beams under flexural loading: (c) Experimental observation (d) Numerical simulation

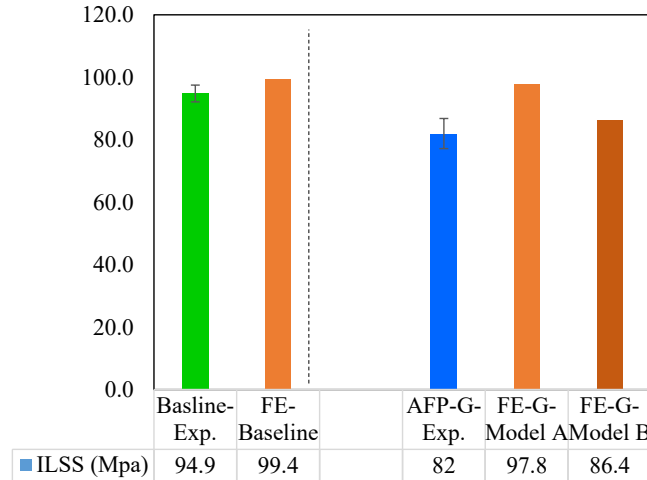


Figure 4-11 Comparison of ILSS between the experimental and numerical results

It can also be seen that the numerical results are in good agreement with the experimental ones. By looking at the results of FE-G-A and FE-G-B samples, it is evident that the material scaling (embedding the gap in the FE model) without thickness scaling fails to predict the interlaminar shear strength of the composite beams with the induced defect. In other words, both material and thickness scalings are required to predict this behaviour under transverse loading. Although the thickness reduction has a major effect on the ILSS reduction, material inhomogeneity (material scaling) caused by gap can affect the stress distribution and delamination initiation. Figure 4-12 shows the contour of the transverse stress and the delamination pattern between the layers with the gap. It is shown that the shear stress is reduced in the gap. This reduction has a consequent effect on the delamination initiation between the plies with the fibre tow gaps. A numerical comparison between the shear stresses of the baseline sample and AFP-G sample in section *A* can be found in Figure 4-13. It is clear that there is a jump in the shear stress of the AFP-G sample, where τ_{13} is reduced by around 30%. Figure 4-14 shows the nondimensional interlaminar shear stress at section *B*, where *L* denotes the length of the short beam. It is shown that the location of the maximum interlaminar shear stress shifts from point *A* to point *B* at the intersection of the epoxy and composite materials. In other words, gap area causes stress relaxation at the defect zone and suspends the delamination initiation in that area. Besides, the microscopic observation was performed on the damaged specimen, and it reveals the same behaviour where the delamination starts from the intersection of the gap-composite interface (Figure 4-15). It also proves the same statement declared in Ref. [33, 93], where the experimental results show that the tow gaps change the delamination pattern of the impacted composite plate.

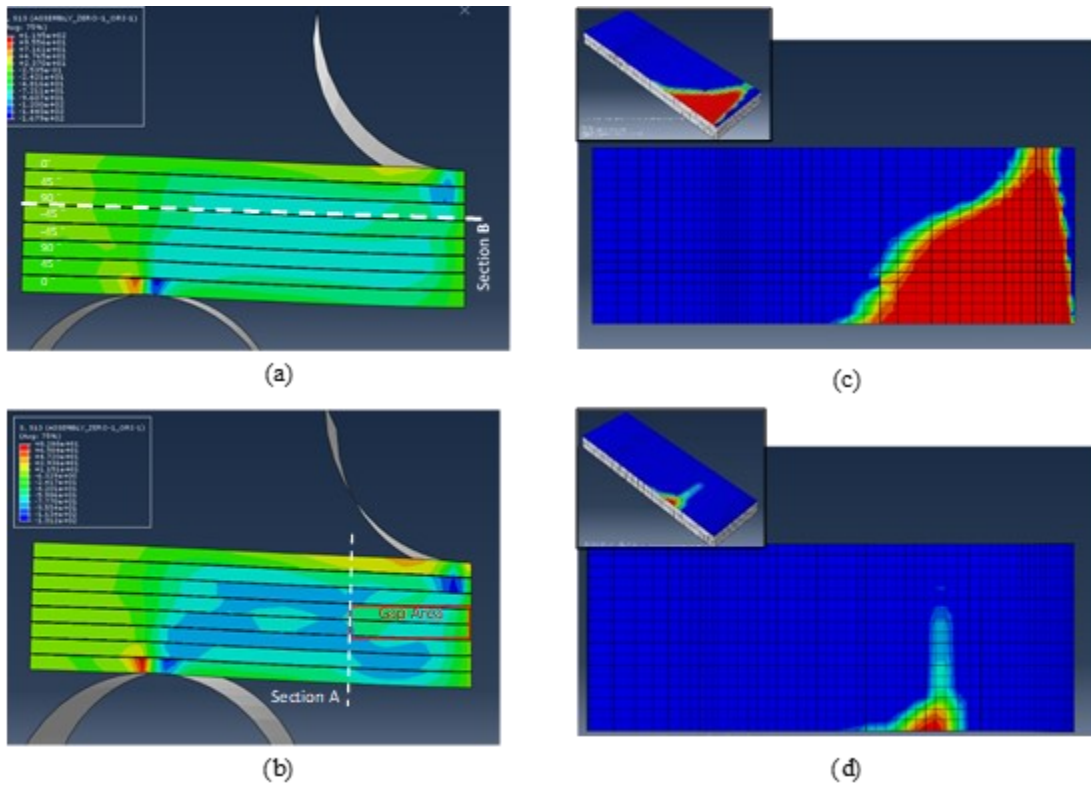


Figure 4-12 Effect of fibre tow gap on the shear stress contour and the delamination of the short beam under transverse loading. Shear stress (τ_{13}) for (a) baseline (b) AFP-G samples right before the failure. Delamination pattern at section *B* for (c) baseline (d) AFP-G samples

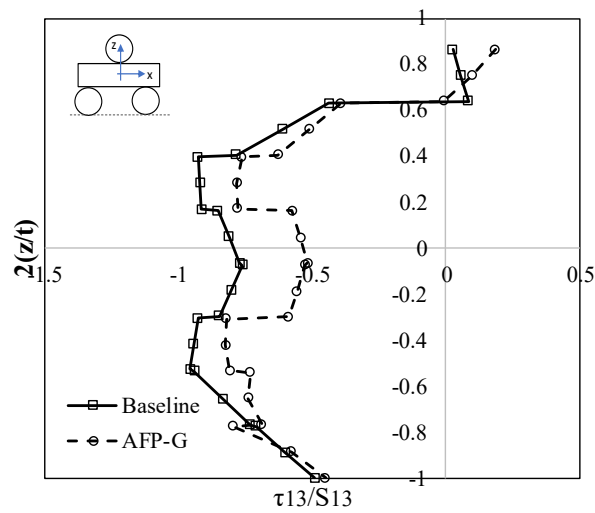


Figure 4-13 Effect of tow gap on the through-the-thickness shear stress at section *A*

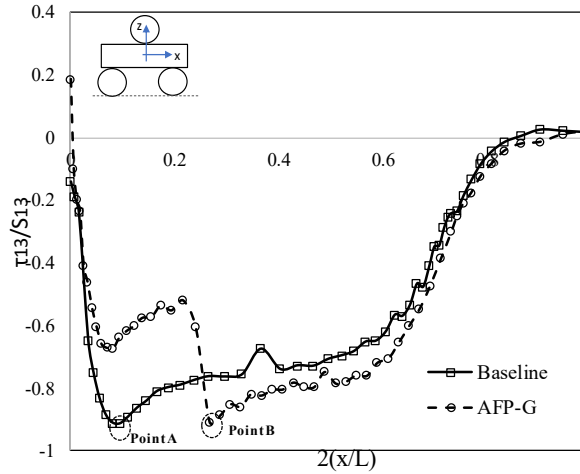


Figure 4-14 Effect of the tow gap on the interlaminar shear stress of the short beams in section *B*

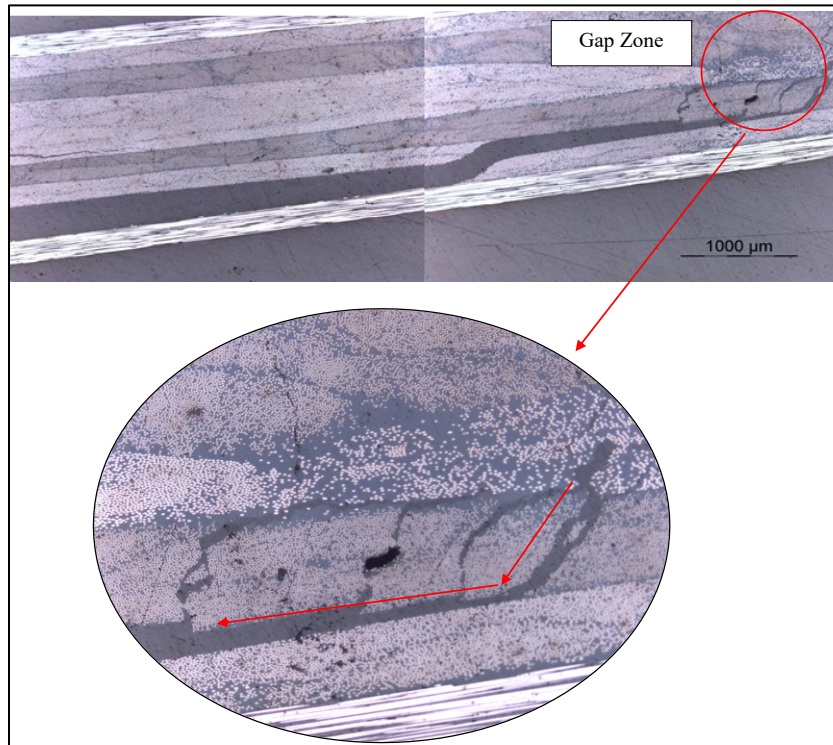


Figure 4-15 Delamination initiation from the gap area

4.3 Flexural Test

Figure 4-16(a) and Figure 4-16(b) show the out-of-plane load versus displacement for baseline and AFP-G samples. It is shown that gaps can reduce the loading capacity of the composite beams by around 35%. It is also shown that the presented numerical models can predict the out-of-plane behaviour of the beams with a good agreement. The failure modes of the beam under the three-

point bending condition obtained from experimental observation and numerical study were also shown in Figure 4-16(c) and Figure 4-16(d), respectively.

Note that both baseline and AFP-G beams were failed in compression, which occurred at the top zero degree plies (at loading nose). That means the induced gap does not probably have a direct effect on the failure of the beam, where the fibre breakage is the failure mode. However, the consequent thickness reduction causes a significant decrease in flexural stiffness and strength of the beam.

Table 4-6 shows the flexural stiffness and strength of both baseline and AFP-G samples. While the flexural stiffness of the baseline beam is around 75 GPa, there is about a 35% reduction in the flexural stiffness of the samples with gaps (AFP-G). Almost the same amount of reduction can be expected for the flexural strength of the beams. In this case, flexural stiffnesses are about 1200 MPa and 840 MPa for the baseline and AFP-G samples, respectively. Note that the flexural stiffness and strength were determined using Eq. (30) and Eq. (31). P_m is the maximum applied load, L is the span length, b , and h are the width and thickness of the specimens, respectively, and m is the slope of the secant of the force-displacement curve.

It is worth noting that the reduction in flexural stiffness and strength should be categorized as reducing the structural property and not the material property. It means that both groups of the beams (baseline and beams with gaps) have the same material properties at the micro-level. However, an elastic/strength reduction can be expected in the composite beams due to the existence of the manufacturing induced gaps. Besides, one of the critical aspects of this study can be addressed here by interpreting the reduction of both flexural stiffness and strength. In other words, although the existence of the resin-rich pockets (material defects) in composite beams can affect the flexural strength of the beams to a larger extent than the stiffness, the manufacturing induced gaps have an impact on both stiffness and strength. Thus, the “presence of the gap” can be interpreted as “the presence of the resin-rich pockets” (AND/OR) “the local thickness reduction”.

It is important to note that a fraction of this reduction comes from the assumption of using the reference thickness for both baseline and AFP-G samples. For example, by substituting the actual thickness of the AFP-G sample in Eq. (30) and Eq. (31), the flexural stiffness of the samples would be around 65 MPa. It means only a 12% reduction in flexural stiffness results from the thickness reduction and material properties reduction due to a resin-rich area. The reason for using the reference thickness instead of the actual one is that the gaps can be induced at a partial zone of composite laminates in the actual practice. Thus, it is more practical to consider the effect of the manufacturing gap as local material degradation rather than local thickness reduction. The same explanation can be expressed for the decrease in the flexural strength of the standard beams with the gaps. Therefore, it is safe to say that the obtained results can be considered either as the conservative results for the samples with the local defect or an average result for the composite laminates with an average GP equals to 8%.

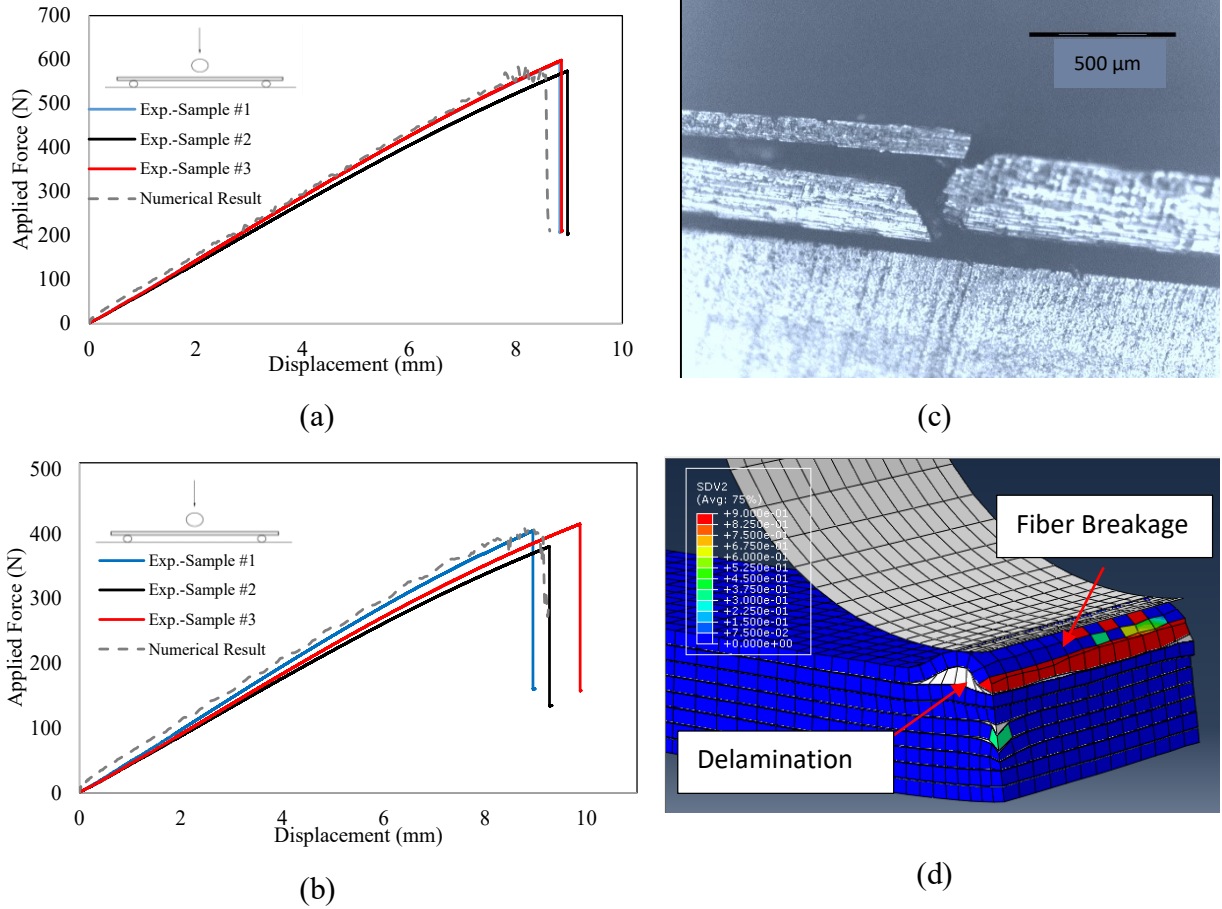


Figure 4-16 Applied force versus out-of-plane displacement for (a) Baseline (b) AFP-G samples. Comparison of the failure of the beams under out-of-plane loading between (c) Experimental observation and (d) Numerical study

Table 4-6 Experimental results of the flexural tests for both baseline and AFP-G samples

	Baseline	AFP-G	Difference (%)
Flexural stiffness (GPa)	74.08 Std. Dev. = 1.7	47.98 Std. Dev. = 1.88	35
Flexural strength (MPa)	1232 Std. Dev. = 20	836.6 Std. Dev. = 26	32

$$\text{Flexural strength} \quad \sigma_m = \frac{3P_m L}{2bh^2} \quad (30)$$

$$\text{Flexural stiffness} \quad E_F^{Secant} = \frac{L^3 m}{4bh^3} \quad (31)$$

Effect of the induced gap on the intralaminar damage of the composite laminate is another interesting subject that needs more attention. Although matrix cracking is not a catastrophic failure,

it reduces the in-plane stiffness of the composite material and might accelerate the delamination initiation and cause a catastrophic failure.

On the one hand, Matrix Cracks (MC) reduce stress due to free surface area and cause stress perturbation at the MC zone [94, 95], similar to the effect of gaps area at the composite laminates. That means forming a matrix crack is unlikely to occur in the vicinity of the area of the gaps. However, on the other hand, thickness reduction due to the gaps might affect the stress contour of the laminates under loading.

In order to investigate the effect of the tow-gaps on the MC growth and an interlaminar failure, three-point bending tests were performed on the beams with the stacking sequence of $[90_2/-45_2/0_2/45_2]_s$ as shown in Figure 4-17(a). These beams have less flexural rigidity than one with the beam with the stacking sequence of $[0_2/45_2/90_2/-45_2]_s$. Thus, they can bear a higher level of transverse displacement before the final failure. For example, the ratio of the transverse displacement at the failure to the thickness of the beam is about 25 for the baseline sample (Figure 4-17b). It is also worth noting that the failure mode of these beams is multiple delaminations between the plies, as shown in Figure 4-17c.

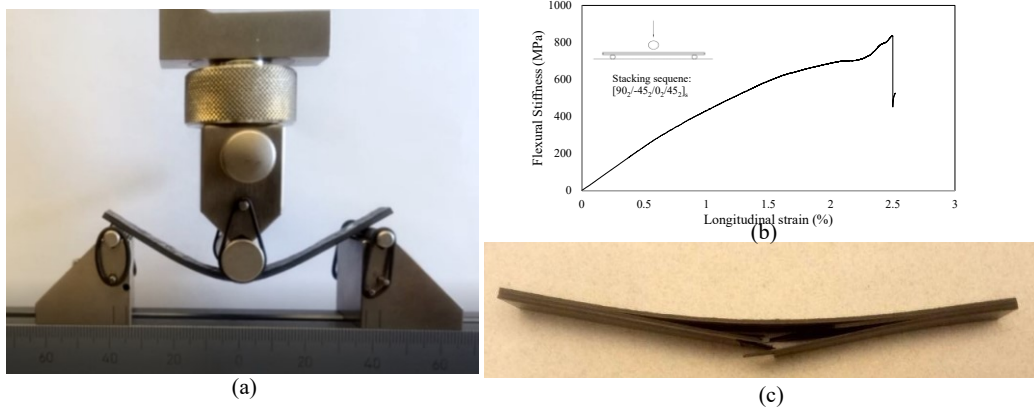


Figure 4-17 (a) Experimental setup (b) load-displacement curve for $[90_2/-45_2/0_2/45_2]_s$ (c) damaged beam after the failure

In order to investigate the effect of induced gap on the pattern of the crack density, the number of matrix cracks at the bottom layers (90° plies) was determined at different cross-head loads. These layers are under tension load perpendicular to the fibre direction. Thus, matrix cracks propagate from the spot with the highest level of stress, which in this case, is placed in the middle of the beam in the x -direction.

Figure 4-18 shows the graph of the crack density versus the longitudinal strain of the bottom surface at the centre of the beams. The longitudinal strain (ϵ_{xx}) was calculated based on the Euler-Bernoulli beam theory. It is evident that the MC initiate at lower strain for the AFP-G sample. However, there is no significant difference between the MC propagation for both samples. That probably shows that gap defects do not have any significant effect on the matrix crack propagation.

Furthermore, no evidence on the interaction of MC and gap defects was also found by microscopic observation. However, more experimental studies are required to confirm this statement. However, the study of this effect is not a part of the scope of the present research, and standard tensile tests are needed to characterize the interaction of the matrix cracks for different stacking sequences.

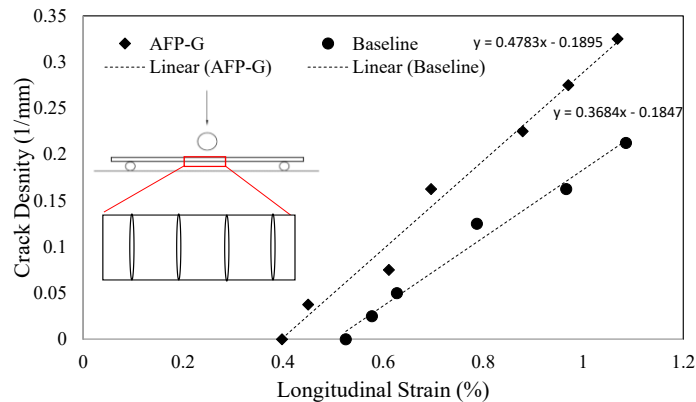


Figure 4-18 Comparison of the crack density of 90° plies versus longitudinal strain for AFP-G and baseline samples with the stacking sequence of $[90_2/-45_2/0_2/45_2]_s$ under flexural loading

FE simulation was used to investigate the interaction of the gap areas with the delamination initiations under the out-of-plane loading before the failure. Figure 4-19(a) shows that the delamination initiation likely occurs at the gap and composite ply interface, which is similar to the results shown in Figure 4-12. Furthermore, it can also be seen that the gap areas reach the yield criteria and experience a non-reversible plastic strain (Figure 4-19(b)). That means the beam might have local residual stress at the defect areas, which might affect the mechanical behaviour of the composite beams, such as fatigue life after the unloading process. However, the study of these effects is out of the scope of this research study.

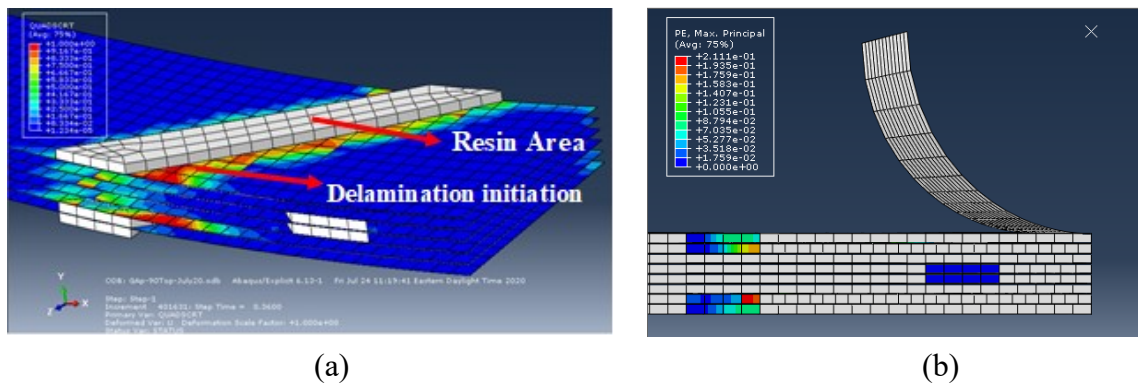


Figure 4-19 (a) Delamination initiation in the standard beam under transverse loading (b) Contour of the plastic strain at the gap area at the cross-head displacement of 15 mm

4.4 Concluding Remarks

In this chapter, a comparative study was performed to investigate the effect of fibre tow gaps on the failure of the thin composite beams under transverse loading experimentally and numerically. For this purpose, both three-point bending and short beam shear tests were selected to measure the flexural stiffness and strength of the standard beams and the interlaminar shear strength of the short beams in the presence of the manufacturing induced gaps. A quasi-isotropic composite plate with periodic gaps between the fibre courses was fabricated by the Automated Fibre Placement

technique. This plate is representative of the samples with the manufacturing gap, and the results were compared with that of the samples with no defects (baseline samples), which have been manufactured by hand-layup technique. Results show that the flexural stiffness of the beam is reduced by around 35% due to thickness reduction and material degradation caused by fibre tow gaps. The same percentage of reduction can also be expected for the flexural stiffness of the quasi-isotropic beams. Interlaminar shear strength is also decreased by about 13%.

The effect of the fibre tow gaps on the matrix cracks propagation for the beam under transverse load was studied by performing a three-point bending test on the beams with the stacking sequence of $[90_2/-45_2/0_2/45_2]_s$. It was shown that the matrix cracks onset at lower longitudinal strain for the beams with defects. However, no significant difference was found between the matrix cracks propagation in AFP-G and baseline samples. Therefore, it probably shows that the effect of the gaps on the matrix crack propagation can be neglected for practical purposes. However, more studies are required to confirm this statement.

Furthermore, elastic-damage and elastoplastic models were developed for composite ply and epoxy material, respectively, to study the interaction of the gap areas and interlaminar damage. It was shown that the gap area could influence the location of delamination initiation and also delamination patterns due to stress relaxation in the gap area. Stress relaxation can change the failure property of the composite laminates. For example, it can change the failure mode of the composite laminates at different types of loading conditions and prevent the laminate from catastrophic failure. It was also shown that the residual stress at the gap areas is likely to occur due to plastic deformation of the epoxy. This feature might affect the mechanical performance of the structure, such as high and low cycle fatigue performance and damage tolerance of the composite laminates. However, more experimental studies are required.

It was also shown that thickness scaling might be as essential as material scaling for the FE simulation of the composite laminates with defects, especially for those under out-of-plane loading such as impact loading conditions.

CHAPTER 5

Induced Defect Layer Method

This work has been published in:

Ghayour M, Hojjati M, Ganesan R. "Induced defect layer method to characterize the effect of fibre tow gaps for the laminates manufactured by automated fibre placement technique."

<https://doi.org/10.1177/00219983211031649> 2021; 002199832110316.

5. Induced Defect Layer Method

In this chapter, a robust computational model is developed for failure analysis and damage assessment of the composite structures manufactured by the AFP technique. It was shown in chapter 4 that the FE stress analysis is helpful for stress analysis and for interpreting the gap-damage interaction of the composite beams. However, the effectiveness of the standard FE method is restricted to laminates with a limited number of gaps. In other words, FE methods that have been widely used for the stress analysis of the defective laminates are useful tools for virtual testing of composite laminates. Thus, the lack of a robust numerical method was found in the literature for stress, and damage analysis of the composite samples has been experimentally tested in chapter 3.

Composite structures manufactured by the AFP technique, are most likely contained arbitrary/random distributed gaps. Furthermore, the composite failure criteria can not evaluate the failure and damage of the composite laminates at gap zones. Thus, a numerical model should capture the gap zones pattern on the structural level and incorporate them at the material level. Induced Defect Layer Method (IDL) is a robust meso-macro scales method developed in this chapter to overcome this issue.

IDL is based on the concept of the Continuum Damage Mechanics (CDM) that uses the Generalized Method of Cells (GMC) technique on a novel Representative Unit Cell (RUC). In this method, a geometrical parameter is used for quantifying the gap percentage in material points. This parameter is calculated for every FE elements by applying a mapping algorithm on composite laminates. Thus, arbitrary FE elements can be applied for stress analysis of defective laminates. In other words, IDL is a mesh-independent method, and distributed defects are not required to be meshed individually.

Because the induced gap is categorized as a mesoscale defect (not a micro defect), the RUC's sub-cells include *Composite* and *Resin* instead of fibre and resin. In this method, strain tensor and gap parameter are imported to the RUC. The damage parameters of the selected material point in then calculated, and stress homogenization is evaluated for the RUC using the GMC technique. The damage parameters that are evaluated by IDL include fibre failure, matrix cracks, and matrix plasticity and failure. Note that the resin plasticity/failure is calculated for the material points that are mapped over the induced gaps.

IDL has been developed by the FORTRAN programming language. It can be integrated into ABAQUS software as a user material subroutine for explicit analysis of composite structures. It can also be individually used for parametric study of the composite materials with induced gaps.

Results include the failure envelope and graphs of stress-strain for a single material point. It is shown that the IDL can be used for failure analysis of defective structures with any arbitrary gap distribution. The IDL results have been compared with several experimental studies, and it is shown that it is a robust method for failure and damage analysis of composite laminates manufactured by the AFP technique.

Summary

The effect of induced gaps on the mechanical response of the composite laminates has been investigated experimentally in the literature. However, there is still no efficient numerical/analytical method for damage assessment of composite structures with distributed induced gaps manufactured by the AFP technique. The present chapter aims to develop the Induced Defect Layer Method (IDLMM), a new robust meso-macro model for damage analysis of the composite laminates with gaps. In this method, a geometrical parameter, Gap Percentage (GP), is implemented to incorporate the effect of induced gaps in the elastic, inelastic, and softening behaviour at the material points. Thus, while the plasticity and failure of the resin pockets in conjunction with intralaminar composite damages can be evaluated by this method, the defective areas are not required to be defined as resin elements in the Finite Element (FE) models. It can also be applied for any arbitrary distributions of the defects in the multi-layer composite structures, making it a powerful tool for continuum damage analysis of large composite structures. Results indicate that the proposed method can consider the gap effect in both elastic and inelastic behaviour of the composite laminate with defects. It also provides good agreement with the experimental results.

5.1 Introduction

Automated Fibre Placement (AFP) is a new technology used to fabricate large and complex composite structures in the aerospace industry. The ability of the fibre tow steering with high precision and speed and the flexibility of having different modular lay-up heads for both thermoset and thermoplastic material systems are two benefits of this new advanced technique. However, due to replacing the prepreg sheets with fibre tows, several new types of manufacturing defects [19, 21, 26] can occur during the fibre deposition by AFP technique that needs to be considered for analyzing the structural integrity of the composite structures.

Fibre tow gap is one of the most observed types of manufacturing-induced defects that occurs between two adjacent tows [7]. Local material inhomogeneity and out-of-plane misalignment are two main consequences of the gap in the composite structures [96–98]. However, the level of inhomogeneity and also misalignment is a function of many parameters, such as the dimension of the gaps, stacking sequence, ply staggering, and structure's curvature [46, 99]. The size of the gap may vary by the width of the single fibre tow, geometry, and complexity of the composite structures, material systems, and curing process. Although the maximum width of the gap can be assumed as the width of a single fibre tow, the allowable width of this defect should not exceed 3.0 mm in practical applications. However, the application of the desired structure might even restrict this allowance further.

One of the main challenges with the gap is that this defect is a structural-level defect. In other words, different structures with the same material system and fabrication process might experience different levels of manufacturing induced defects. Thus, it requires extensive works to investigate the effect of gap on the mechanical performance of the composite structures. Furthermore, the consequent gap effect is mode-dependent in terms of applied loads. Therefore, it might have a different impact on the mechanical performance of the structures for different scenarios of loading conditions. The experimental studies can be categorized by the works performed on tensile [28,

34, 35], compressive [28, 34, 36–38, 100], flexural [101], and impact [33, 93] loadings, and also fatigue loading [41] cases of the defective composite laminates.

Experimental studies indicate that the defective composite laminates are more vulnerable to compressive loading than the tensile loading for composite laminates with the same pattern of embedding gaps in the composite plies. For instance, it was shown in Refs. [28, 35] that the effect of gaps on the tensile strength of the composite laminate is negligible. However, an experimental study [34] on the tensile loading of the quasi-isotropic laminates with relatively large width of the gaps (1/2 inch) shows that both stiffness and strength of the structure can be reduced by 60% and 40%, respectively. The research also indicates that a reduction of 45% can be expected for stiffness and strength of the composite samples under compressive loading but with a gap width of ¼ inch. However, for the gap size, less than 3.0 mm, a reduction of compressive strength between 5-27% can be expected for the composite plate under compressive loading [28, 36–38, 65]. It is important to note that the stiffness/strength reduction level is highly dependent on the size and distribution of the gaps in the composite plies. Thereby a considerable variation of the reduction in tensile and compressive strengths can be found in the literature.

Effect of fibre tow-drop gaps on damage resistance of variable stiffness composite plates was carried on in Ref. [33] with performing a series of impact tests with medium to high impact energy (15 J - 45 J). Results show that the influence of the gap is more relevant to the low level of impact energy. A study on the effect of gap on the low-velocity impact strength of thin quasi-isotropic composite plates with gaps was performed in Ref. [93]. It was shown that the periodic gaps between the fibre courses with an average width of 2.0 mm could affect the impact response, damage threshold load, and delamination pattern of the impacted plates. The flexural behaviour study [101] of the Carbon/Epoxy composite beams shows that the induced gap can initiate the delamination in the beams under out-of-plane shear loading. It can also decrease the interlaminar shear strength and flexural strength of the thin composite beams by 13% and 35%, respectively.

Numerical studies of composite structures with defects can also be found in the literature. However, the research contribution seems to be less compared to the experimental work. A 2D FE model was developed in Ref. [36] to account for the gap and overlap. The FE model was based on experimental observation and stress localization and redistribution at the defect zones. An FE model for estimating the stiffness and strength of the variable stiffness composite laminates was developed in Ref. [16], based on a progressive damage model with a LaRC expand failure criterion. The results show deviations from the experimental results. The same procedure for estimating the strength of the plates with a hole under tensile loading can be found in Ref. [40]. The developed model requires high mesh density at the defect area to obtain a satisfactory result. A FE model was developed in Ref. [43] for simulating the gaps based on the microscopic observation for both hard and soft tooling with thickness scaling at the defect zones of the structure. In conjunction with Continuum progressive damage model, a FE model was developed in Ref. [46], accounting for the effect of gap and overlap on the tensile and compressive strengths of composite laminates.

Although the mentioned FE models help characterize the gap effect, their effectiveness has been limited to the virtual testing of samples (Coupon tests) with limited pre-set gap areas. In other words, these methods implement the built-in FE packages to simulate the pre-set gap area as individual resin FE elements. Besides, the FE geometries are created based on microscopic observations of the defective areas of a selected specimen. Thus, the effectiveness of these methods

for simulating the continuous fibre-reinforced composite with widespread distribution of the gaps in the structural level is still uncertain and limited.

A Defect Layer Method for instability analysis of the variable stiffness structure was developed in Ref. [30] to overcome this problem. The homogenization process of this method is based on a series of offline FE simulations on a defined Unit-Cell. This method eliminates the mentioned drawbacks of the other methods by introducing a non-dimensional defect length in FE elements. But, the method implements an elastic homogenization technique that restricts the method to the linear elastic analysis of composite structures with defects. However, failure strength reduction [28, 34, 38] and accelerating damage initiation [34, 94] are the primary issues of the gaps in the structures rather than the local reduction of the elastic properties. Thus, up to the knowledge of the authors, there is still no practical method that can assess the structural integrity of the composite structures in the presence of the automated manufacturing induced gaps under general loading conditions.

The primary purpose of this study is to develop the IDLM method, a new enhanced meso-macro numerical model, to characterize the effect of fibre tow gaps on the elastic and inelastic behaviour of the material points for the laminates manufactured by the AFP technique. This method applies the Generalized Method of Cell (GMC) technique to the Representative Unit Cell (RUC) used in Ref. [30] to homogenize the defective zone. Then, the damage analysis is then performed on the sub-cells to evaluate the damage parameters in the composite and resin (sub-cell levels) individually. The key feature of the RUC is that the geometry of the RUC sub-cells varies by the dimension of the gap. The sub-cell dimensions are updated by implementing a geometrical parameter, Gap Percentage (GP). This parameter is transferred from the macro-level to the meso level of the structure. Then, the stress-strain behaviour of the material point can be evaluated by the homogenizing process on the sub-cells of the RUC. Hashin damage model [81] and elastoplastic failure model [102] are implemented in the IDLM method to calculate the damage parameters for the composite and resin, respectively. Finally, the stress states and intralaminar damage state of composite structures, including the distributed induced gaps, can be evaluated at the macro level by applying the Continuum Damage Mechanics (CDM) approach to the composite structure under general loading conditions.

5.2 Induced Defect Layer Method (IDLM)

Figure 5-1 shows the cross-section view of a quasi-isotropic Carbon/Epoxy laminate with induced gaps. The laminate has a stacking sequence of $[0_2/45_2/90_2/-45_2]_s$ with non-staggered gaps in the -45° plies. It can be seen that the gap can create a resin-pocket with a dimension of a hundred microns to a millimetre. Thus, the current theoretical and numerical micro-mechanical models [103–105] are not capable of performing the homogenization on the defective areas for multiscale damage analysis of the composite structure. On the other hand, the current FE approaches use FE packages with built-in damage models. These models assume that the gap areas are full resin, and its mechanical behaviour is simulated by elasto-plastic and failure models. However, it means that resin-pockets result in automated manufacturing should be meshed individually by applying different material properties than the composite system. Thus, although those models can be helpful for virtual testing of the samples with limited pre-set gap areas, it can be time-consuming and even impossible to be applied in damage analysis of large structures with random widespread gap defects.

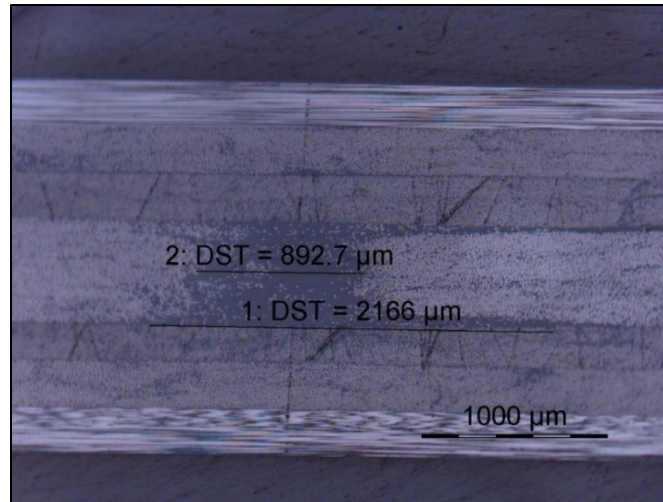


Figure 5-1 Cross-section view of a composite laminate with the induced gap

The IDLM method proposes a meso-scale analysis by mapping the gap area over the FE elements of the composite plies. Figure 5-2a shows a Carbon/Epoxy composite 45° ply with the induced gap fabricated by the AFP robot. It is then depicted in Figure 5-2b that the gap zones can be mapped over arbitrary FE meshes using an enhanced ply-by-ply mapping algorithm technique. Thus, the GP can be defined for all FE elements of every ply by dividing the gap area's portion mapped in the element to the element area (Figure 5-2c). Note that the present chapter does not deal with estimating the gap areas in the composite plies. This process can be performed during the quality control process, which is out of the scope of the study. It is also assumed that the gap distribution is uniform through the thickness of the ply. Therefore, a GP value equal to 0.0% means that the element includes composite material.

On the other hand, a GP of 100% means that the element is full of resin. However, depending on the mesh patterns and mesh sizes, there might be elements with a portion of resin and a portion of composite material ($0.0 < GP < 100\%$). The GP calculation is performed offline using the mesh data (mesh connectivity and nodal coordinates) and the geometry of the gaps. It is then stored as a database for FE analysis, and it is called one time at time-step equal to zero.

The next step is the definition of a proper RUC that is representative of the defective area. Despite the well-known RUCs with the fibre and resin sub-cells, the RUC of IDLM consists of three sub-cells of composite-resin-composite in which the lengths of the sub-cells are a function of GP of the selected element (Figure 5-3a). This RUC is defined based on the physical observations in which the gap can occur between the adjacent fibre tows, and the geometry of the RUC does not change through the fibre direction (Direction-1). Figure 5-3 shows the RUC at the local coordinate system defined for the homogenization of the defective areas.

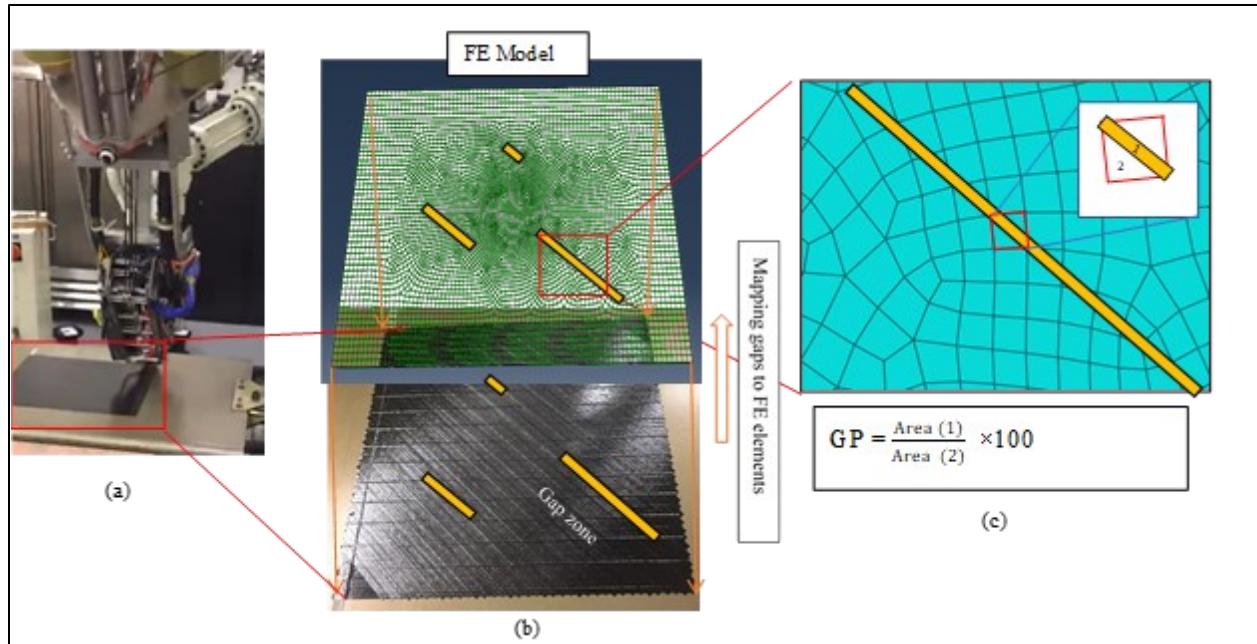


Figure 5-2 (a) Fabrication of a composite plate with AFP robot (b) ply-by-ply mapping induced gaps to FE meshes (c) Definition of Gap Percentage at macro FE model

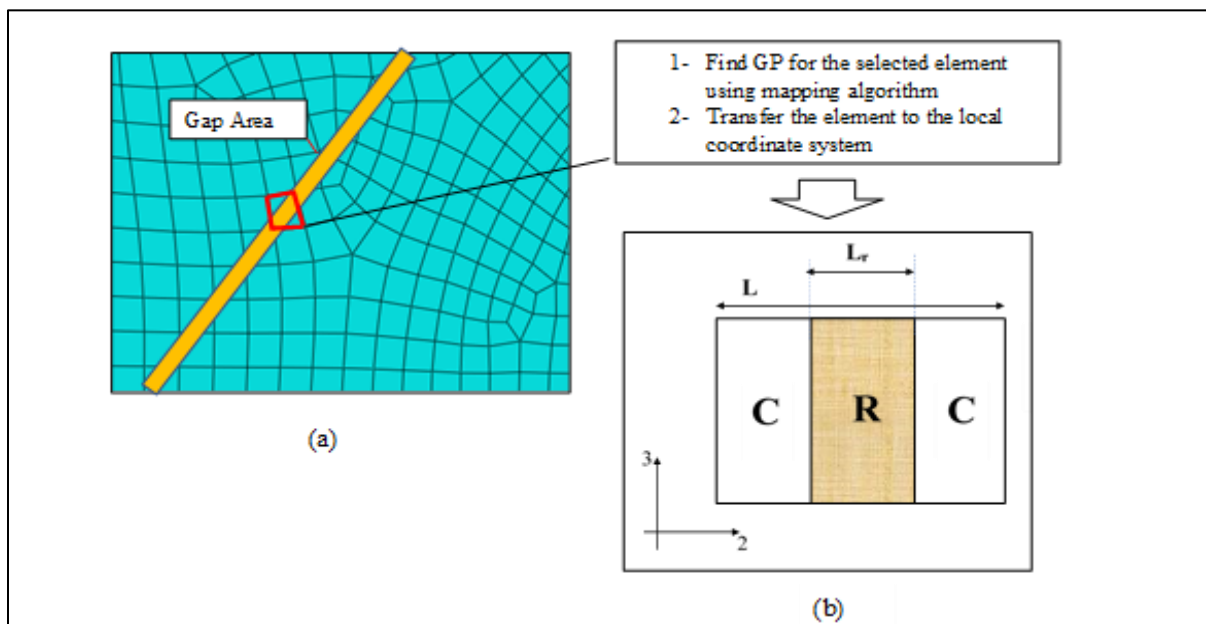


Figure 5-3 (a) macro meso gap percentage transfer from the selected element (b) Representative Unit Cell of the IDLM method (*C* and *R* stand for composite material and resin, respectively)

The Generalized Method of Cell (GMC) [106–108] was chosen in this study for calculating the stress-strain relationship of the selected RUC. This method is an updated version of the Method of Cell (MOC) [109], which consists of the imposition of the displacement and traction continuity conditions at the interfaces within the unit cell and at the interfaces between neighbouring unit cells, in conjunction with equilibrium conditions. This model is a middle ground between the

closed-form methods and FE Unit Cell approach for composite micromechanics analysis. Thus, in comparison with FE micro models, this model is more efficient in computational time. It is also more accurate than the current closed-form solutions. The basic assumption in GMC is that the displacement vector in every sub-cell is linear in terms of local coordinates located at the centre of the sub-cell. The readers are referred to Ref. [103] for more details. The other advantage of the proposed model is that the damage and failure of the RUC are evaluated by applying the Hashin damage model [81] and elasto-plastic failure model [89] to the individual sub-cells. Thus, the failure mode of the material point can be identified for different loading conditions.

5.2.1 Generalized Method of Cell

GMC is an updated version of the Method of Cell (MOC) [109], which consists of the imposition of the displacement and traction continuity conditions at the interfaces within the unit cell and at the interfaces between neighbouring unit cells, in conjunction with equilibrium conditions. This model is a middle ground between the typical closed-form methods and FE Unit Cell approach for composite micromechanics analysis. Thus, comparing with FE micro models, this model is more efficient in terms of computational time. It is also more accurate than the current closed-form solutions for the micro-study of the composite materials

The GMC analysis consists of four steps as follow:

- 1- The repeating unit-cell Figure 5-4(a) is identified from a periodic pattern of the composite structure (Figure 5-4(b)). Then, the RUC is divided into $N_p N_q N_r$ rectangular sub-cells. The sub-cells are labelled as (p, q, r) in which $p=1, N_p, q=1, N_q, r=1, N_r$ as shown in Figure 5-4(c). The Constitutive law for any sub-cell can be described as:

$$\sigma^{(\alpha\beta\gamma)} = \mathcal{C}^{(\alpha\beta\gamma)} \epsilon^{(\alpha\beta\gamma)} \quad (32)$$

- 2- The definition of the average macroscopic strain $\bar{\epsilon}$ and stress $\bar{\sigma}$ from the corresponding microscopic average $\bar{\epsilon}^{(\alpha\beta\gamma)}, \bar{\sigma}^{(\alpha\beta\gamma)}$ are as follows.

$$\bar{\epsilon} = \frac{1}{DHL} \sum_{p=1}^{N_p} \sum_{q=1}^{N_q} \sum_{r=1}^{N_r} \sum_{\alpha,\beta,\gamma=1}^2 d_\alpha^{(p)} h_\beta^{(q)} l_\gamma^{(r)} \bar{\epsilon}^{(\alpha\beta\gamma)} \quad (33)$$

$$\bar{\sigma} = \frac{1}{DHL} \sum_{p=1}^{N_p} \sum_{q=1}^{N_q} \sum_{r=1}^{N_r} \sum_{\alpha,\beta,\gamma=1}^2 d_\alpha^{(p)} h_\beta^{(q)} l_\gamma^{(r)} \bar{\sigma}^{(\alpha\beta\gamma)} \quad (34)$$

The basic assumption in GMC is that the displacement vector $u^{(\alpha\beta\gamma)}$ in every sub-cell is linear in terms of local coordinates $(\bar{y}_1^{(\alpha\beta\gamma)}, \bar{y}_2^{(\alpha\beta\gamma)}, \bar{y}_3^{(\alpha\beta\gamma)})$, located at the centre of the sub-cell.

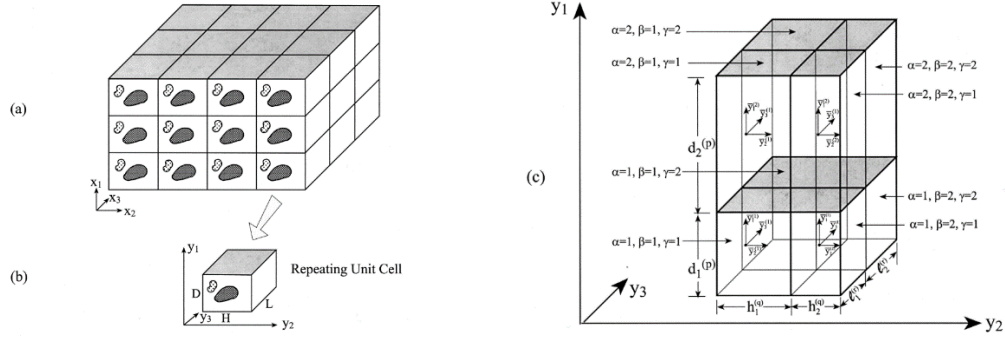


Figure 5-4 (a) A multiphase composite with periodic microstructure and (b) corresponding RUC (c) Discretized RUC with eight sub-cells labelled as $\alpha, \beta, \gamma = 1, 2$ [107]

- 3- Traction and displacement continuity are imposed at the interfaces between the constituents that fill the sub-cells and also between the repeating cells.
- 4- The overall constitutive equation (C^*) of the RUC is given in terms of the elastic stiffnesses of the sub-cells:

$$C^* = \frac{1}{DHL} \sum_{p=1}^{N_p} \sum_{q=1}^{N_q} \sum_{r=1}^{N_r} \sum_{\alpha, \beta, \gamma=1}^2 d_{\alpha}^{(p)} h_{\beta}^{(q)} l_{\gamma}^{(r)} C^{(\alpha\beta\gamma)} A^{(\alpha\beta\gamma)} \quad (35)$$

where, $A^{(\alpha\beta\gamma)}$ is the appropriate concentration tensor. Thus, the average stress-strain relationship of the RUC can be found as follow:

$$\bar{\sigma} = C^* \bar{\epsilon} \quad (36)$$

GMC can also be implemented for any arbitrary distribution of the fibres in the resin in the micromodel by defining the arbitrary number of the subcells in the micro unit cell. Thus, an efficient micro model with an arbitrary gap percentage can be achieved by this model. More details on the GMC can be found in Ref. [107]. It can be understood that the

5.2.2 Composite damage model

The constitutive law for composite ply considered here is that of Ref. [78]. The damage parameters are applied directly to the elastic modulus, as shown in Eq. (9). $[S_c]_{ijkl}$ is the compliance matrix of the composite material, and d^j is the corresponding damage parameter.

$$[S_c]_{ijkl} = \begin{bmatrix} \frac{1}{E_1(1-d_f)} & -\frac{\nu_{12}}{E_1} & -\frac{\nu_{13}}{E_1} & 0 & 0 & 0 \\ & \frac{1}{E_2(1-d_m)} & -\frac{\nu_{23}}{E_2} & 0 & 0 & 0 \\ & & \frac{1}{E_3(1-d_m)} & 0 & 0 & 0 \\ & & & \frac{1}{G_{12}(1-d_m)} & 0 & 0 \\ & \text{Symmetric} & & & \frac{1}{G_{13}(1-d_m)} & 0 \\ & & & & & \frac{1}{G_{23}(1-d_m)} \end{bmatrix} \quad (37)$$

where d_f and d_m are the composite damage parameters in longitudinal (fibre direction) and transverse direction, respectively. Composite damage onset is based on stress-based 3D Hashin failure criteria [81]. A linear softening damage model [82] was also considered for damage propagation in tensile and compressive loading conditions.

5.2.3 Epoxy Material Model

Mechanical behaviour of the epoxy in the resin sub-cell is modelled with an elasto-plastic failure model. For this purpose, a 3D isotropic model is used to simulate the linear behaviour of the epoxy, as shown in Eq. (38), until it reaches the yield condition.

$$[S_r]_{ijkl} = \begin{bmatrix} \frac{1}{E(1-d_r)} & -\frac{\nu}{E} & -\frac{\nu}{E} & 0 & 0 & 0 \\ & \frac{1}{E(1-d_r)} & -\frac{\nu}{E} & 0 & 0 & 0 \\ & & \frac{1}{E(1-d_r)} & 0 & 0 & 0 \\ & & & \frac{1}{G(1-d_r)} & 0 & 0 \\ & \text{Symmetric} & & & \frac{1}{G(1-d_r)} & 0 \\ & & & & & \frac{1}{G(1-d_r)} \end{bmatrix} \quad (38)$$

where, E and ν are Young's modulus and elastic Poisson's ratio of the resin. The parameter d_r is the damage parameter of the resin. It is equal to zero before the failure, and it is assumed to be equal to 0.99 after the failure occurs.

The yield criterion used in this study is based on the criteria proposed in Ref. [87], which has shown a good agreement with the experimental results of the resin epoxies under different mechanical loading conditions. It is defined by a paraboloidal model [88] as follow:

$$\phi(\sigma) = 6J_2 + 2I_1(\sigma_{yC} - \sigma_{yT}) - 2\sigma_{yT}\sigma_{yC} = 0 \quad (39)$$

where $\phi(\sigma)$ is the yield function, and σ is the stress tensor of the epoxy material. The parameters I_1 and J_2 are the first invariant of the stress tensor and the second invariant of the deviatoric stress tensor, respectively. σ_{yT} and σ_{yC} are absolute values of tensile and compressive yield stresses. A non-associated flow rule was also developed using the method proposed in Ref. [89] as follow:

$$g = \sigma_{von}^2 + \zeta p \quad (40)$$

$$\zeta = \frac{9}{2} \frac{1 - 2\nu_p}{1 + \nu_p} \quad (41)$$

where σ_{von} is the Von-Mises equivalent stress, and ν_p is the plastic Poisson's ratio, which is determined from the standard tension test. The trial stress tensor is evaluated for the plasticity of the model by the following equation:

$$\sigma_{n+1}^{tr} = \sigma_n + D : \Delta \epsilon^{tr} \quad (42)$$

where D is the fourth-order isotropic elasticity tensor and σ_{n+1}^{tr} is the trial stress tensor at time $n+1$. The plastic strain increment is defined by Eq. (21) by using the flow rule presented in Eq. (18):

$$\Delta \epsilon^p = \Delta \gamma \left(3\mathbf{S} + \frac{2}{9} \zeta I_1 \mathbf{I} \right) \quad (43)$$

\mathbf{S} is the deviatoric stress tensor, \mathbf{I} is the identity matrix, and $\Delta \gamma$ is the plastic multiplier. Thus, the relation between stress and $\Delta \gamma$ can be written as:

$$\sigma = \frac{S_{tr}}{1 + 6G\Delta\gamma} + \frac{\frac{1}{3} I_1^{tr} \mathbf{I}}{1 + 2K\zeta\Delta\gamma} \quad (44)$$

Besides, hardening is assumed to affect both σ_c and σ_t . It is assumed that the hardening parameters are constant due to a lack of experimental data for the selected epoxy material.

The failure condition is also evaluated by Eq.(17), in which the yield strength parameter is replaced by the strength of the resin in tension and compression. Figure 4-5 shows the stress-strain graph for the Cycom-977-2 epoxy material under the uniaxial (Figure 4-5a) and shear (Figure 4-5b)

loading condition. It can be seen that the developed elasto-plastic model can estimate the yield conditions and also the final failure of the epoxy resin under various loading conditions.

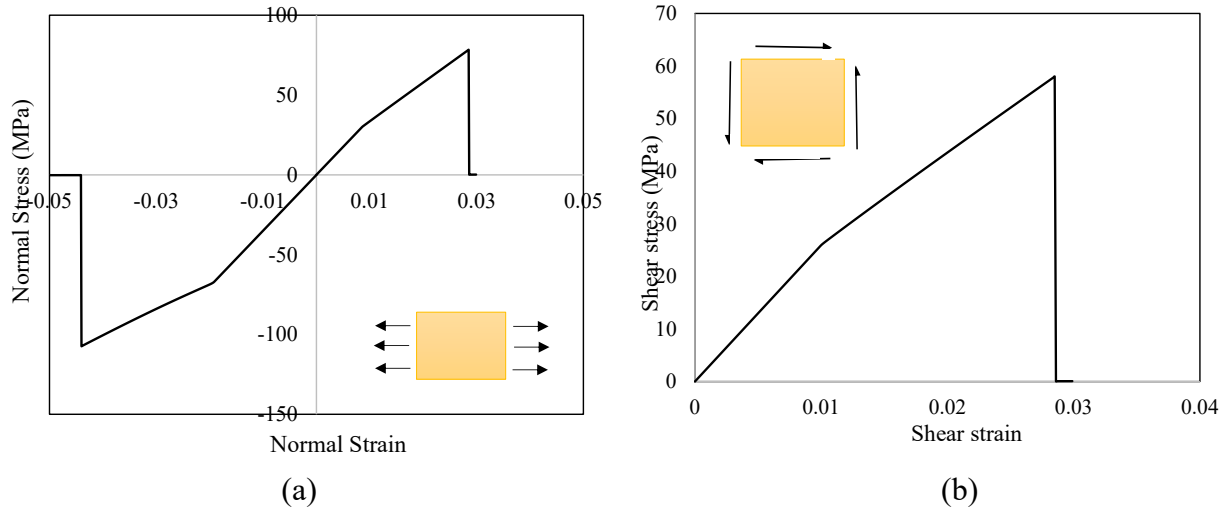


Figure 5-5. Stress-strain curves of the epoxy resin under (a) uniaxial (b) in-plane shear loading condition

5.3 Results and Discussion

In this section, effect of the manufacturing-induced gap on the stress-strain behaviour of the composite material at the meso level is discussed in section 5.3.1. For this purpose, the IDLM is applied on a single material point with a variable GP. Then, graphs of the stress-strain of the material point are extracted under different loading conditions to investigate the intensity of the elastic, damage initiation, and final failure of the material point to the GP variable. For this study, Cycom 977-2 HTS 40 was selected for the case study with the material properties presented in Table 4-2. Furthermore, multiscale analyses are performed on the structural level of the composite structures with distributed induced gaps. Results are then compared with the experimental results for the samples under in-plane and out-of-plane loadings.

5.3.1 Single Material Point

Figure 5-6 shows the effect of GP on the non-dimensional elastic modulus of the selected material. The stiffnesses have been non-dimensionalised with the corresponding stiffness of the no defective composite ($GP = 0.0$). It can be seen that the developed model can estimate the incorporation of the GP on the linear elastic behaviour of the composite materials with gaps.

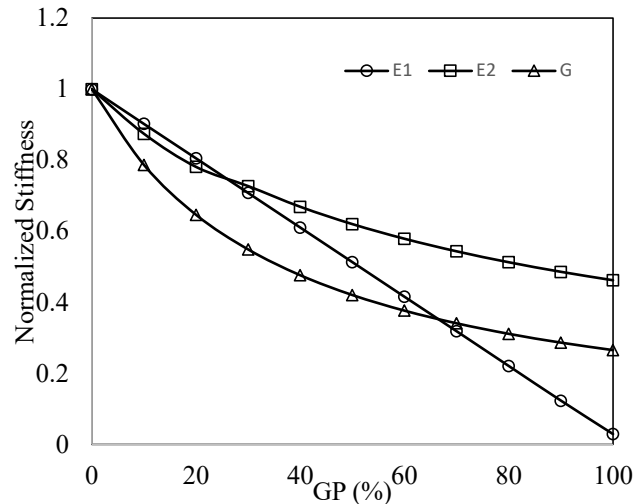
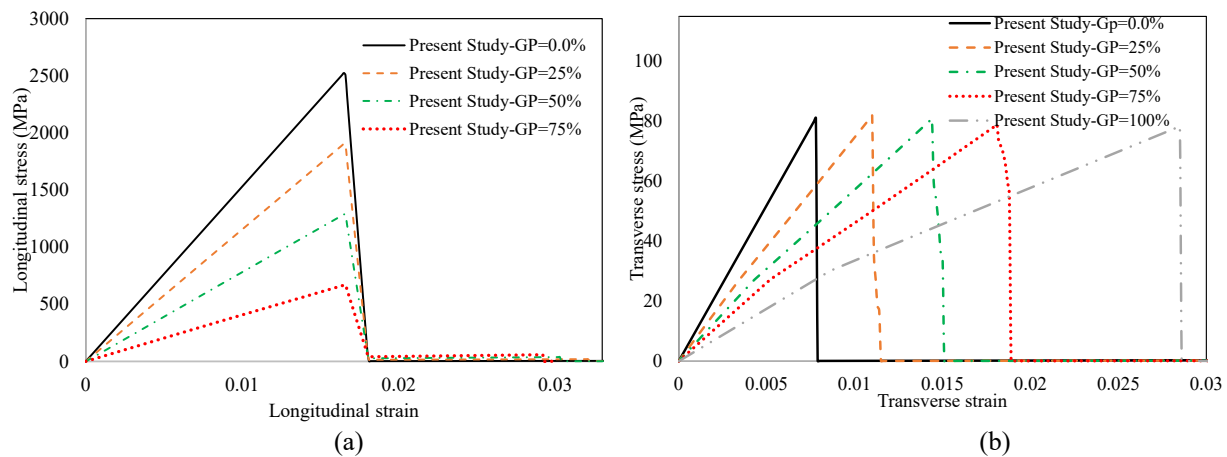


Figure 5-6 Effect of GP on the stiffness reduction of Cycom 977-2/ HTS 40 unidirectional ply

Effect of GP on the stress-strain behaviour of the composite material point with the defect can be found in Figure 5-7. Figure 5-7a shows the longitudinal stress-strain curve of a single material point for different gap percentages. Results show that the GP can significantly reduce the failure strength of the material points in the fibre direction. However, its effect on the failure strain is negligible. On the contrary, GP can increase the failure strain of the material points by more than 300% in the transverse direction (direction-2). However, it has less effect on transverse strength. That is because the longitudinal strength is more dependent on fibre properties than resin. Thus, the gap defect increases the stress level on the composite sub-cells after the resin failure. On the other hand, the transverse strength is largely a function of the resin properties. That is why the GP has a negligible effect on the transverse strength of the material point with defects under uniaxial loading. It is important to note that the integrity of the IDLM RUC in the transverse direction (direction-2) is affected by both resin and composite sub-cells. In other words, either failure of composite sub-cell (C) or resin sub-cell failure (R) results in the RUC failure in direction-2. Figure 5-7c also illustrates the in-plane shear stress-strain behaviour of the material point for different levels of GP. Interestingly, the gap can affect both shear stiffness and strength. It can also be seen from Figure 5-7 (b) and Figure 5-7 (c) that the plasticity behaviour of the resin can significantly affect the tangent of the stress-strain curve at higher GPs (GP > 50%).



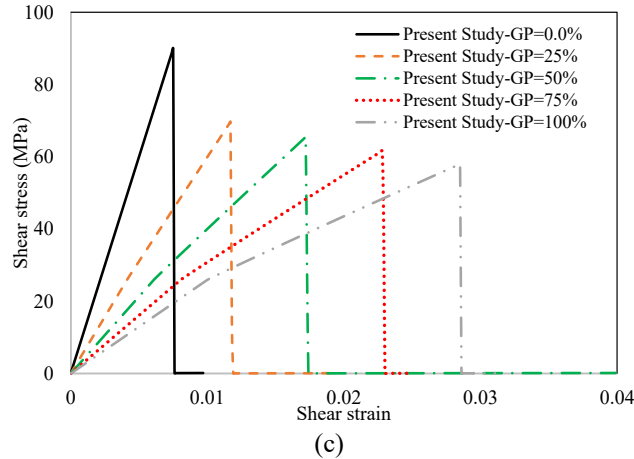


Figure 5-7 Effect of GP (a) on the stress-strain behaviour in longitudinal direction and(b) transverse direction, and (c) on in-plane shear stress-strain

Figure 5-8 and Figure 5-9 provide helpful information on the effect of GP on the failure envelope of the defective material point. These graphs clearly show how the gap's existence can affect the failure of the material point at different in-plane loading conditions. Figure 5-9 shows the failure envelope for the in-plane stresses in the fibre direction ($\sigma_{11} - \sigma_{12}$) for different GPs. It can be seen that the presence of gap can significantly shrink the failure envelope area. Comparing the tensile strength on the material point with no defects (i.e., with GP = 0.0%) with the material point, including the gap (GP > 0%), it can be said that the effect of the gap is more dominant at a lower level of shear stress. Furthermore, the failure stress at a lower level of shear stress is almost a linear function of the GP's value at that point. It is worth noting that the material failure criterion in the fibre direction is based on fibre failure.

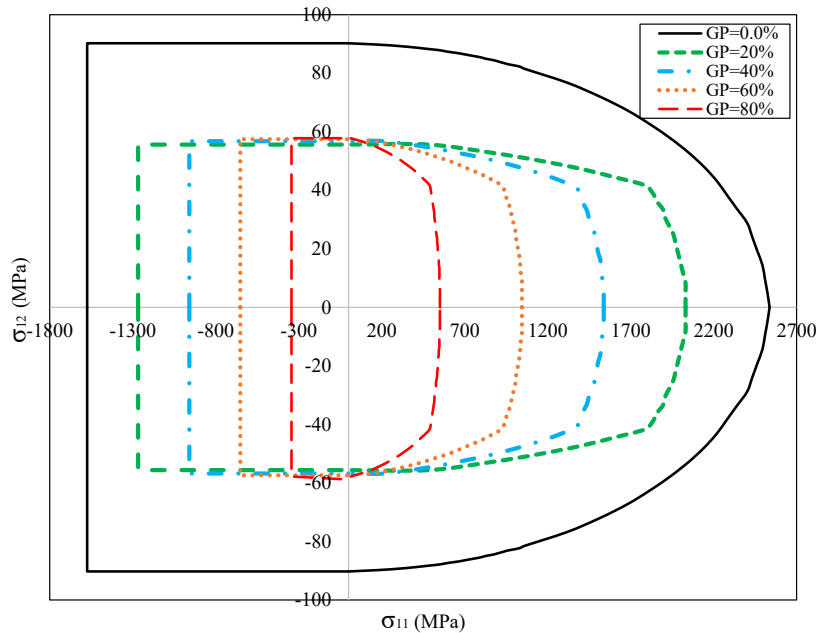


Figure 5-8 Effect of GP on the failure envelope for in-plane stresses in the fibre direction

Effect of gap on the failure envelope of the material point for in-plane transverse loading conditions can be found in Figure 5-9. Results indicate that the gap does not change the shape of the failure envelope. It can also be seen that there is a binary drop from GP = 0% to GP = 20%. The reason for the dropping is that the damage mechanism of a no-defect composite (GP = 0) can be different from the defective composite (GP > 0%). In other words, while matrix cracks can cause failure in no-defect composite, the failure of the defective composite can be either matrix cracks or resin failure at the gap area. This difference is more highlighted in the compressive adding condition, where the compressive strength of the resin is relatively smaller than the composite in the transverse direction. Furthermore, it is also interesting that the gap percentage can decrease the failure stress of the material point for any loading conditions. However, the amount of GP does not significantly affect the failure strength of the material point. Besides, the compression failure of the material point, including the pure resin (GP = 100%), is less than that of with $0.0 < GP < 100$. Note that the failure envelope in the transverse direction is highly dependent on the ratio of the transverse failure of the selected composite material to the failure of the resin system. This is because both failures can cause failure in the transverse direction. For example, the transverse compressive failure strength of the resin is less than that of the selected composite material. Thus, the compressive failure strength of the IDLM RUC is based on resin failure. On the other hand, transverse composite failure is the failure mode of the RUC at transverse tensile loading.

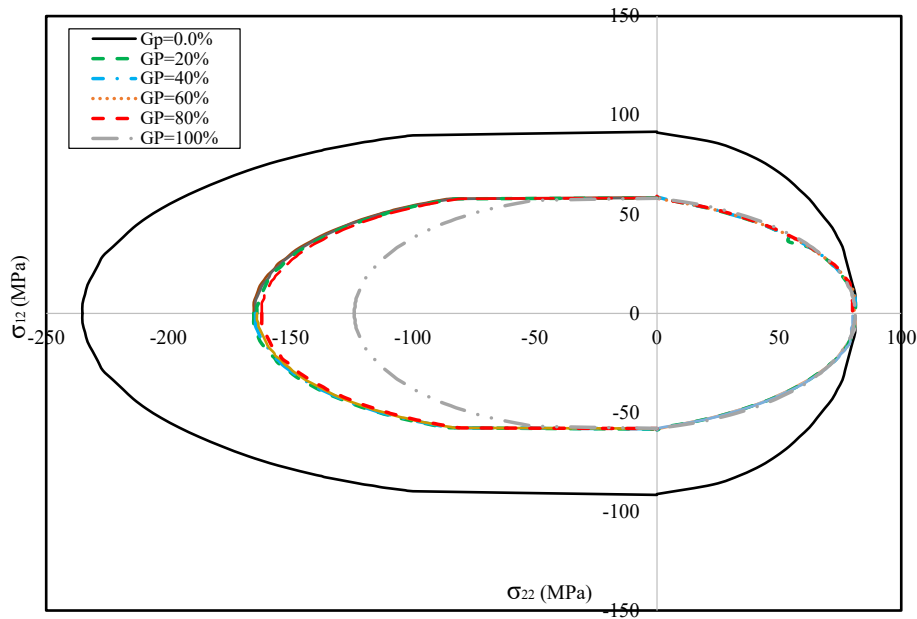


Figure 5-9 Effect of GP on the failure envelope for in-plane transverse stress (direction 2)

5.3.2 Multiscale Analysis of Defective Composite Laminates

It was mentioned earlier that one of the benefits of the proposed numerical model is the ability for damage analysis of the large composite structures without requiring the re-mesh of the FE composite model. For this purpose, the multiscale analysis was carried out by developing a 3D model using ABAQUS/Explicit software. The constitutive law with damage parameters was implemented in the model by developing a user material subroutine (VUMAT). The solid 8node

brick element C3D8R was used for meshing the composite solid parts of the FE models to avoid the shear locking problem.

A FE model of a laminate with the dimensions of $80 \times 12 \text{ mm}^2$ and with the stacking sequence of $[0/90_2]_s$ was selected for the study. Furthermore, an arbitrary periodic gap pattern with a gap width of 3.0 mm was embedded in all plies with the pattern shown in Figure 5-10. The FE model has meshed with three different approximate global mesh sizes of 0.5 mm , 1.0 mm , and 2.0 mm , respectively, to examine the mesh sensitivity of the proposed IDLM method.

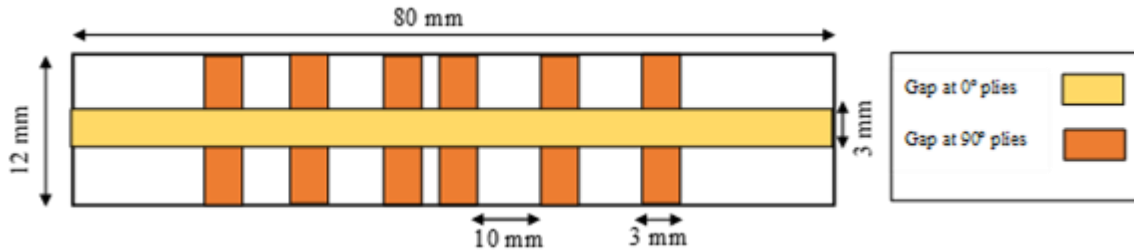


Figure 5-10 Top view of the numerical model with gaps

Figure 5-11 shows the contour of GP for 0° and 90° plies for different mesh sizes. The contour of GP has been evaluated based on a developed mapping algorithm. The developed code can map the predefined gap pattern on arbitrary FE mesh for multi-layer composite laminates. It is shown that the developed code can evaluate the GP for any arbitrary pattern of the FE mesh.

Figure 5-12 shows the stress-strain graphs of the numerical FE model for baseline (sample with no gap) and defective samples under tensile loading. It is demonstrated that the proposed model can capture the effect of gap on the elastic behaviour and damage of the composite laminates without distinguishing the composite and resin in FE meshes. Regarding the effect of mesh size, it can be said that the IDLM method can alleviate FE mesh dependency by defining the GP parameters at material points.

In order to verify the proposed IDLM method, the results of the method were compared with the experimental results given in Ref. [110]. The test is a compression test on a 24 plies Carbon/Epoxy laminate with the stacking sequence $[45/0/-45/90]_{3s}$. The sample is a rectangular plate with dimensions of $80.8 \times 12.7 \times 3.8 \text{ mm}^3$. Note that the reason for choosing the compression test is that the defective composite laminates are more sensitive to compression than tension.

A 3 mm gap was embedded in the middle of the plies. The compressive strength of three different samples, including baseline, G-zero (gap in zero layers), and G-zero-ninety (gap in zero and ninety plies), were compared with the experimental results (See Ref. [110] for more information about the experimental procedure). Figure 5-13 shows the comparative results of the compressive strength for both experimental and present studies. It is clear that a 3 mm gap can reduce the compressive strength of the sample by 11-15%. It is also shown that the IDLM method can capture the effect of the gap on the macro-level of the structures under in-plane loading conditions with a satisfactory agreement.

The effect of manufacturing defects on the stress distribution in the zero-degree layers is shown in Figure 5-14 for the G-zero-Ninety sample. It can be seen that the existence of the gap does not

only affect the final failure of the structure. It can also cause local stress relaxation in the composite plies due to the presence of the relatively large resin pocket, which might lead to damage initiation at certain loading conditions [101].

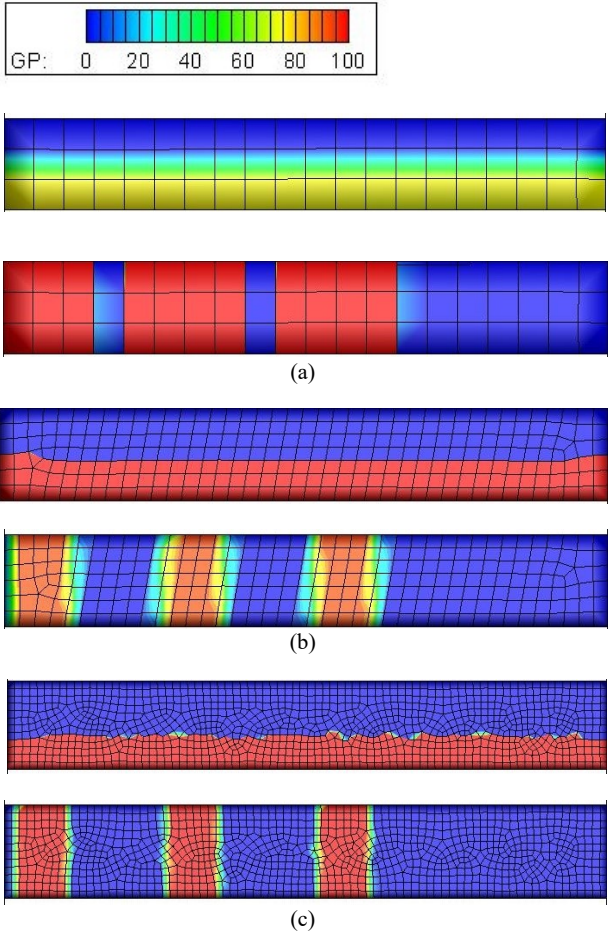


Figure 5-11 Contour of GP for different mesh sizes for zero and 90° plies for (a) 2.0 mm (b) 1.0 mm (c) 0.5 mm of the approximate global mesh size (only a quarter of the samples have been shown)

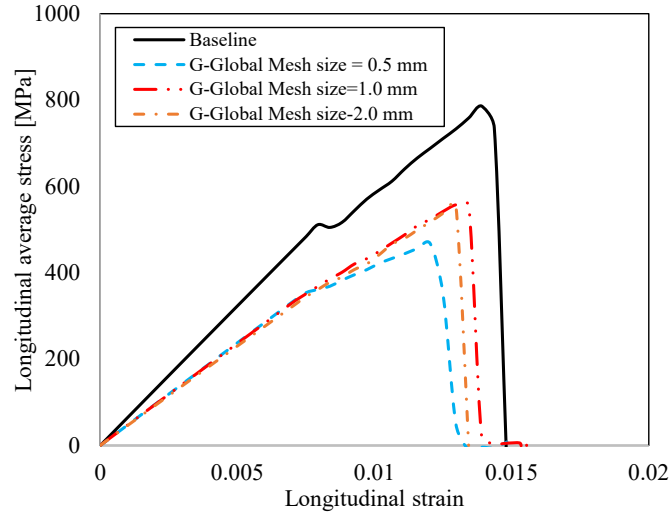


Figure 5-12 Effect of mesh size and gap on the tensile response of the FE numerical model presented in Figure 5-10

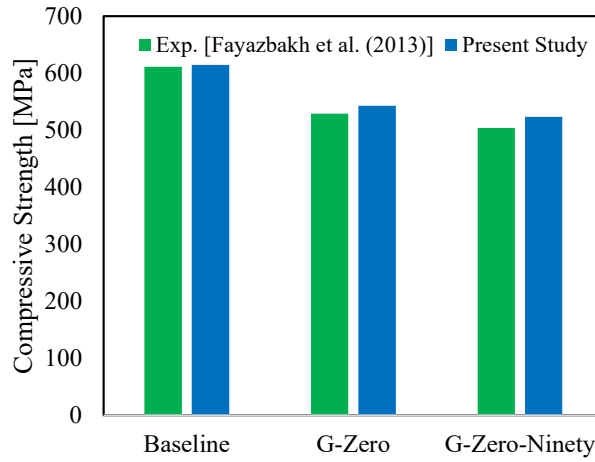


Figure 5-13 Comparison of the Compressive strength of the defective composite laminate; present study versus the experiment

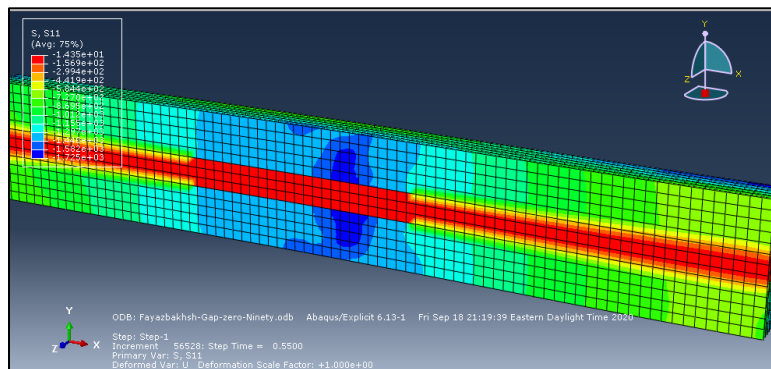


Figure 5-14 Effect of gap on the in-plane stress distribution (σ_{11}) at zero-degree plies for G-Zero-Ninety case before the failure

The performance of the IDLM method for the structures under out-of-plane loading was examined by comparing the obtained results with the experimental results presented in Ref.[101]. Figure 5-15 compares the results with the experimental results for composite beams with a distributed gap under flexural loading. Results show that the proposed method evaluates the flexural load-displacement of the composite beams with a satisfactory agreement.

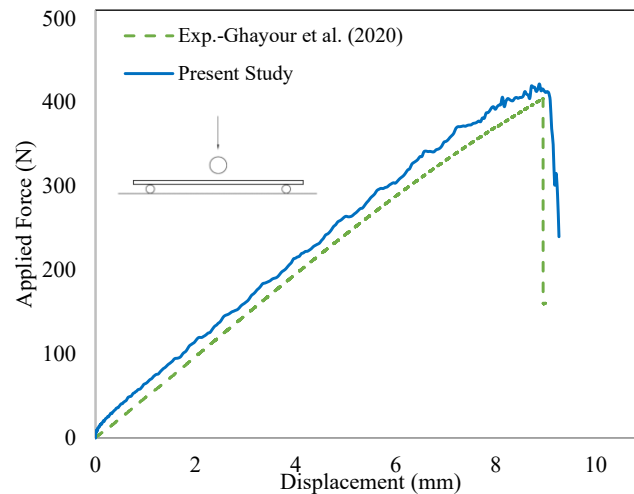


Figure 5-15 Comparison of the flexural load versus displacement of the defective composite beams; present study versus the experiment

It is important to note that the tow gap defects are not necessarily induced in the whole length of the fibre tows in real applications. These defects might have a finite length with triangular or square shapes. However, these samples were chosen for verification studies because the models with continuous gaps have been the subject of several experimental studies [34, 38, 93, 101]. Furthermore, having a random gap pattern in experimental specimens makes it difficult to interoperate the relationship between the gap patterns and the mechanical degradation of composite structures. Figure 5-16(a) shows partially random distributed gaps in 90° plies and its corresponding maximum principal stress for a cross-ply composite laminated under tensile loading. Comparing the results with the results of non-defective laminate with the same stacking sequence (Figure 5-16(b)), it can be said that the proposed model can capture any arbitrary shape of gap pattern and its effect on the stress distribution and mechanical performance of the structures.

In order to evaluate the performance of the IDLM method on different gap sizes, a verification study was performed to compare the results with the experimental results presented in Ref. [34]. For this purpose, sixteen layers quasi-isotropic laminate with induced defects were simulated under tensile and compressive loading. The stacking sequence and the material are $[45/0/-45/90]_{2s}$ and T800S/3900 [32], respectively, and four different gap sizes with the dimensions of 1.65 mm, 3.17 mm, 6.35mm, and 12.7 mm were induced in the zero and ninety plies with a staggering of 10 mm.

Figure 5-17 (a) shows a comparison of non-dimensional tensile strength with the experimental results [34], and it demonstrates a good agreement. The matrix cracks pattern around gap zones and the fibre breakage location at zero plies are shown in Figure 5-17(b).

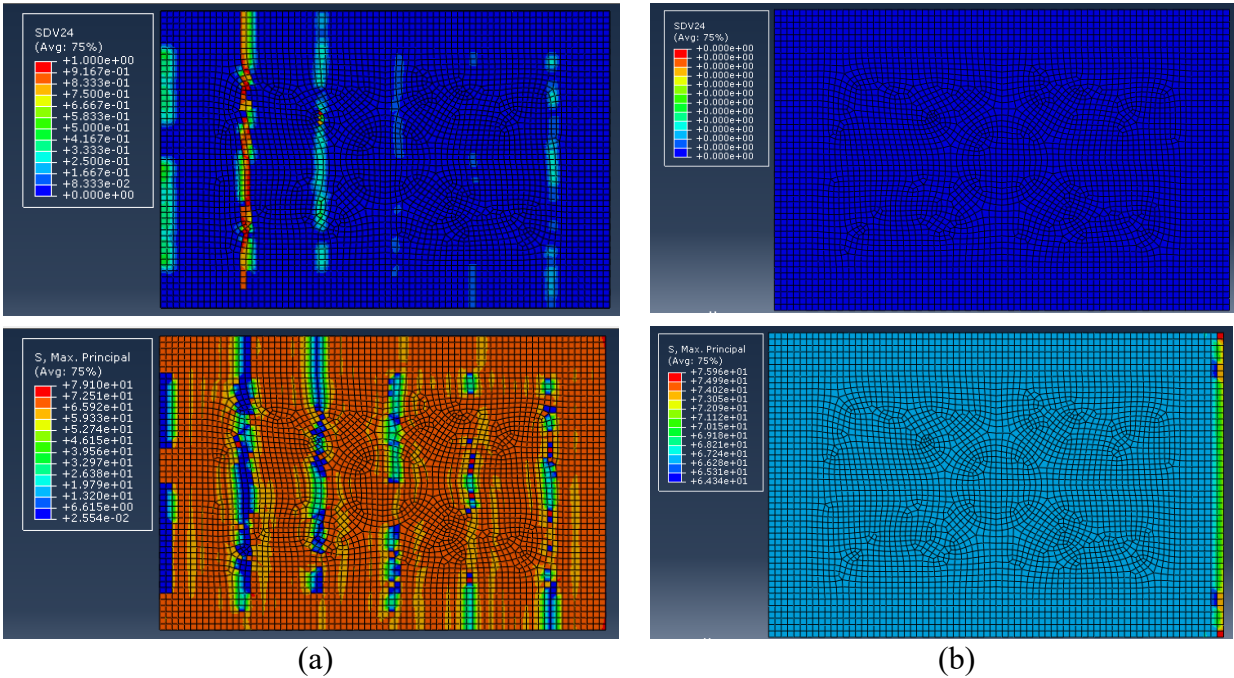


Figure 5-16 Distributed partial gaps and the corresponding max principal stress for 90° ply (a) with AFP tow gaps (b) without gaps

The same result but for the compressive loading condition is shown in Figure 5-18(a). While the results are in good agreement with the experiments for small gap sizes, the presented method estimated a higher compressive strength for the samples with gap sizes larger than 3.0 mm . The reason is that the out-of-plane fibre waviness, which is one of the consequences of the induced gaps, becomes more significant in relatively large gap zones. This effect can significantly contribute to the compressive strength reduction of the defective composite laminates. However, structures with a defect size larger than 3.0 mm are rejected in the production line in many practical aerospace applications. Thus, the IDLM method can still be a robust tool for damage assessment of defective composite structures in industrial applications. Furthermore, a knockdown factor or a modification on the geometry can be applied to the structures with large or aligned defects to consider the effect of fibre waviness. Figure 5-18(b) shows the contour of GP for zero plies, and it is shown that the IDLM method is not required mesh refinement in the vicinity of the gap area

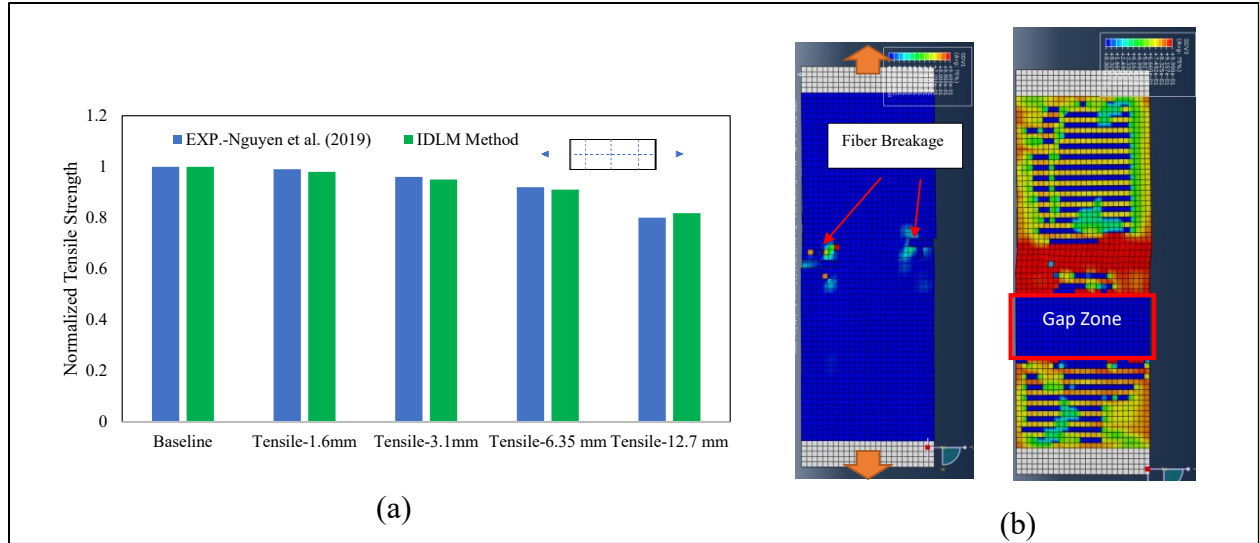


Figure 5-17 (a) Comparison of the tensile strength of the defective composite laminate; present study versus the experiment [34] (b) fibre breakage and matrix crack pattern at zero and ninety plies

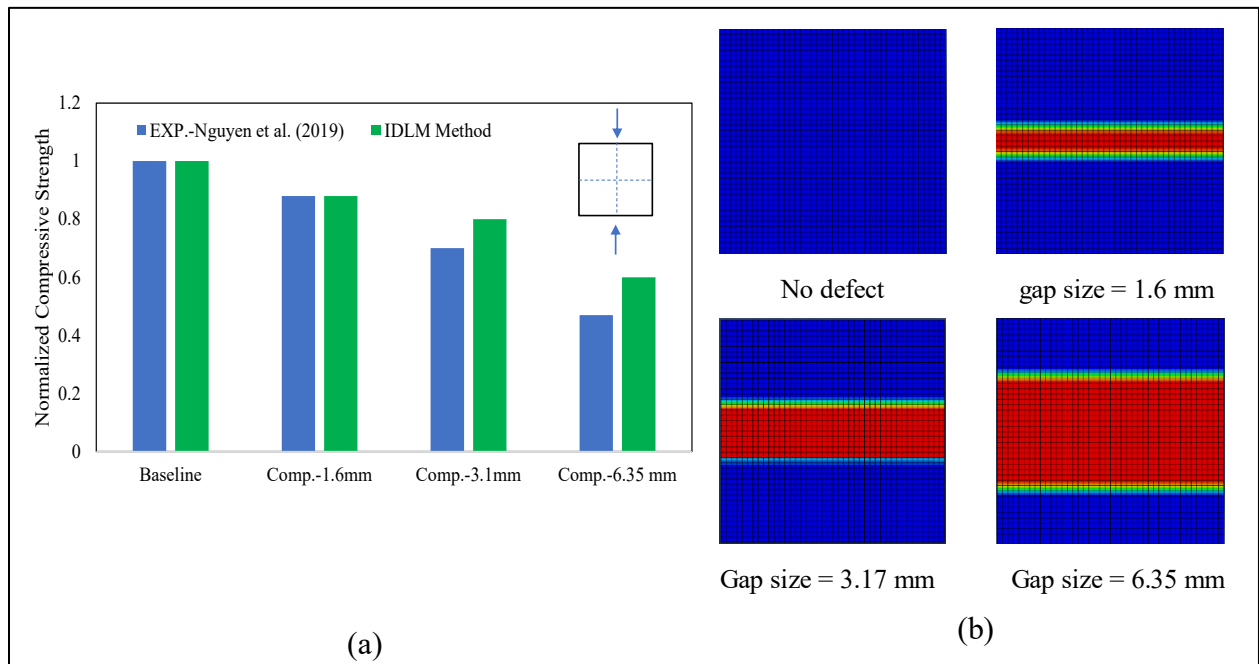


Figure 5-18 (a) Comparison of the compressive strength of the defective composite laminate; present study versus the experiment [34] (b) gap pattern of the defective specimens at zero plies

5.4 Concluding Remarks

In this chapter, a multiscale Induced Defect Layer Method was presented to include the induced manufacturing gap in the numerical damage analysis of the composite laminate fabricated by the

AFP technique. Despite the current techniques limited to the coupon testing of samples with limited gap areas, this method is an advanced and robust macro-meso method that can be embedded in the FE commercial software for structural analysis of the composite structures with distributed defects. The macro model is based on CDM approaches. The intralaminar damage parameters at the material points are calculated by a novel homogenization technique at the meso level. This method can conduct the damage analysis at the sub-cell level of the presented RUC by using the GMC method. Thus, both intralaminar composite damages and local resin-pocket plasticity and failure can be assessed simultaneously at the defective areas of the composite structures. For this purpose, the proposed method has been facilitated with a geometrical parameter, GP, which represents the gap area in the material points. Using this parameter brings the advantage of applying the FE mesh without distinguishing the composite and gap defects individually. Thus, computational stress analysis of the composite structures manufactured by the AFP technique can be performed with satisfactory performance and reasonable computational time.

The obtained results showed that the IDLM is an effective method for continuum damage analysis of the defective composite structures manufactured by the AFP technique. In order to verify the method, the obtained results were compared with the experimental results of the samples subjected to both in-plane and out-of-plane loading. It was shown that the results are in good agreement with the experimental results.

One of the presented method's concerns might be the degree of reliability for the structures with aligned or large gap sizes. It was shown that the presented method estimates a conservative strength reduction for the defective composite structures with gap sizes larger than 3.0 mm , where the out-of-plane fibre waviness plays a significant role in the strength reduction. However, because composite structures with large gap sizes or missing tows are rejected in many real cases in aerospace applications, the IDLM method can still be a robust tool for damage assessment of defective composite structures.

CHAPTER 6

Impact Damage Assessment of Defective Composite Laminates: Experimental Studies and Numerical Simulations

This work has been submitted to the *Journal of Composite Structures*

6. Impact Damage Assessment of Defective Composite Laminates: Experimental Studies and Numerical Simulations

In this chapter, damage assessment of the impacted defective laminate is conducted by performing a series of numerical studies and numerical simulations. The main question addressed in this chapter is the combined effect of tow-gaps and impact damages on the residual strength reduction of the laminates under compressive loads. It has been shown in the literature that LVI damages, especially the delamination, significantly reduce the compressive strength of composite laminates. On the other hand, induced tow-gap defects can also reduce the compressive strength of intact laminates. Thus, the main challenge is the interaction mechanism of tow-gap and impact damage and the combined effect on the residual strength reduction and failure of defective laminates.

For this purpose, the Compression After Impact (CAI) test was chosen to evaluate the impacted laminates' residual compressive strength. The impacted samples from chapter 3 were fixed in a standard CAI fixture and were subjected to the compressive load. The in-plane strain of the laminates under loads was also evaluated using Digital Image Correlation (DIC) technique to investigate whether the tow defects can change the strain contour of the specimen under compressive loads.

The secondary objective of this chapter is to evaluate the IDLM efficiency as a robust numerical method for damage assessment of defective laminates manufactured by AFP. This method was shown in chapter 5 as an enhanced method that can capture an arbitrary distribution of gaps over multilayer composite laminates. It was also shown that it is an effective method for 3D stress analysis of defective composite laminates. In this chapter, the IDLM results are verified by the experimental results of this study. It includes the impact force versus time, impact delamination pattern, compression after impact stress versus strain, and failure modes of the samples under CAI load.

Results show that the combined effect of gap and impact damage on the CAI effect of defective laminates is significant and should not be neglected. This effect seems critical for thin laminates due to the change in the failure mode under compressive load. Although the direct effect of the induced gap is the compressive strength reduction, change in the failure mode amplifies this effect. It is also shown that the IDLM is a powerful tool for the FE explicit analysis of composite laminates with distributed gaps.

Summary

AFP tow-gap causes local thickness consolidation and creates relatively large resin pockets. Both effects can affect the impact response and residual compressive strength of composite structures. Although the effect of tow-gap on the in-plane response of composite plates has been widely studied, there is still a lack of knowledge in damage assessment of defective composite plates subjected to Low-Velocity Impact (LVI) loading. In this study, a series of experimental Compression After Impact (CAI) tests are carried out on the standard carbon/epoxy composite plates subjected to impact loads to investigate the effect of impact damage and gap defect on the residual strength reduction. Effect of the curing process on the gap formation is evaluated by measuring the Induced Gap Shrinkage Factor (IGSF) using microscopic observation. This factor is used for numerical simulation of the defective composite plates. Digital Image Correlation (DIC) technique is also performed to measure the in-plane strains of the specimen under compressive loading.

Furthermore, a numerical investigation is carried out by implementing Induced Defect Layer Method (IDL) model. The numerical studies contain LVI and CAI results, including the impact response, impact damage, and final failure of impacted specimens under compressive loading. Results show that the induced gaps play a significant role in the residual compressive strength reduction of thin composite plates, which is significant at low-velocity impact loading. It is also shown that IDL is a robust meso-macro damage method for damage analysis of the composite laminates with manufactured gaps.

6.1 Introduction

There has been an increased demand for utilizing automated manufacturing techniques in the composite industry in recent years. The automated Fibre Placement (AFP) technique is a fast-growing fabrication technique, especially in the aerospace and automotive industries. AFP can fabricate large structures with high precision, making it a practical alternative for traditional hand-layup techniques. The flexibility of mounting two modular lay-up heads for both thermoplastic and thermoset composite fibre tows and fibre steering on complex shapes [7] are two advantages of this technique. These advantages make AFP a distinctive technique from other automated techniques such as Automated Tape Laying (ATL) [11].

However, this new technology has brought several concerns about the structural integrity of composite structures by introducing new types of manufacturing defects induced during the fibre tow deposition [11, 12, 17, 19, 21, 26]. Fibre tow-gap in one of the most probable types of defects are detected between two adjacent fibre tows. The induced gap size observed during the fibre deposition is a multivariant parameter that functions the materials system, complexity of the composite structure, curing process, and fibre tow's width. The maximum gap size can be theoretically assumed as the tow's width identical to the tow drop; however, the allowable gap width is less than 2.0-3.0 mm in the industry application [101].

Tow-gap is a structural level defect that may cause local thickness consolidation, create relatively large resin pockets [25, 46, 93], and reduce the strength of the composite laminates. The experimental studies can be categorized by the works performed on in-plane [28, 34–38, 100], out-of-plane [33, 93, 101], and also fatigue loading [41] conditions. While experimental studies reveal that tensile strength is less likely reduced by the existence of the tow-gap [28, 35], it was shown

[28, 36–38, 65] that gap defects reduce the compressive strength up to 30%. Note that dimension and distribution of gaps play a significant role in strength reduction; Therefore, considerable strength reduction variations can be found in the literature.

Composite laminates are vulnerable to impact loads due to the low out-of-plane strength of composite materials [111]. Low-Velocity Impact (LVI) is the low energy impact that might occur during the manufacturing or service maintenance of aircraft structures. It may cause Barely Visible Impact Damage (BVID) in composite structures [112]. Although the impact damage is not a catastrophic failure, it significantly affects the post-impact residual strength and structural integrity of composite structures. CAI residual strength is usually the most vulnerable structural property of composite aircraft parts which is drastically affected by impact damages. This is mainly because of the local instability in the delaminated areas of impacted structures [113].

On the other hand, it was discussed earlier in the introduction that induced gaps reduce the compressive strength. Thus, the interaction of impact damage and the induced gap might intensify the CAI residual strength reduction of the laminates manufactured by the AFP technique. In addition, due to the local thickness consolidation, defective composite laminates are more vulnerable in out-of-plane loading conditions and impact loading. An experimental study [101] on the flexural behaviour of standard and short beams with 2.0 *mm* gaps demonstrated that tow-gap reduces both flexural stiffness and strength of the beams by 30-35%. It was also shown that the gap areas are prone to be a source of delamination initiation and reduce the interlaminar shear strength by around 13%.

Both flexural stiffness and strength reductions caused by defects play significant roles in the impact behaviour of the defective composite laminates. A comparative study [93] on the effect of gap on the impact resistance of thin defective composite laminates shows that impact response and damage threshold of thin composite laminate with gaps are reduced due to the tow-gaps in composite specimens. In this study, a series of experimental LVI tests were performed on quasi-isotropic Carbon/Epoxy laminate. Effect of gap on the impact response was evaluated by embedding 2.0 *mm* gaps between fibre courses, which provided 8% volumetric gaps in the laminates. Test samples were subjected to 5 J - 15 J of impact loads, and it was shown that defective samples experience up to 15% less impact response comparing with the baseline. A reduction of the damage threshold load can also be expected for the defective samples. A similar study on the damage resistant and CAI residual strength of variable stiffness composite laminates but under medium impact energy (15 J - 45 J) was performed in Ref. [33]. It was shown that the effect of gap is more relevant to LVI energy. Effect of continuous tow-gaps on the CAI strength of thick laminates subjected to 18 J impact load was studied in Ref. [47], and it was shown that the location of the gaps might affect the delamination pattern of impacted structures. However, up to the knowledge of authors, no research studied the effect of automated manufacturing gaps and impact damage on CAI of thin composite laminates subjected to low-velocity impact loading.

The primary objective of this chapter is to conduct a comparative study on the interaction of induced manufacturing tow-gaps and impact damage on the compression after impact strength of impacted composite laminates. In other words, the interaction of both impact and the tow-gap defects on the compressive strength of the thin laminates are evaluated to understand the importance of gaps in damage analysis of impacted thin Carbon/Epoxy plates. The secondary objective of this study is to evaluate the robustness of the Induced Defect Layer Method (IDLM) for complex 3D stress and damage analyses of defective composite laminates. It was shown in

Ref. [114] that IDLM can successfully evaluate the mechanical behaviour and failure of composite laminates with tow-gaps under in-plane loading conditions. In this work, impact and CAI behaviours of defective laminates manufactured by the AFP technique are numerically studied using this method.

This study includes experimental and numerical investigation on the composite plate with an average of 8% pre-cured volumetric gaps. The experimental studies mainly focus on the CAI tests, and numerical simulation includes the results of both impact and compression after impact loading conditions.

6.2 Experimental Investigation

6.2.1 Fabrication Process

Two Carbon/Epoxy composite laminates with the dimension of $480 \times 430 \text{ mm}^2$ were fabricated with both hand-layup and AFP techniques and have been cured for six hours in an autoclave under pressure of 0.6 MPa, with a curing temperature of 180°C according to the manufacture manual. An Aluminum caul plate was placed on the top of the composite plate during the curing to reduce the out-of-plane waviness [65, 72]. Cycom 977-2 HTS 40 fibre tows and prepreg sheet were used for fabrication with AFP and Hand-layup techniques, respectively.

The laminate with defects was fabricated by ZX103L Kawasaki fibre placement machine, a six-axis articulated robot arm provided by Automated Dynamic Inc, as shown in Figure 6-2(a). The robot places four fibre tows at a time which is called a fibre course. The width of each fibre course for the selected material system is equal to 25.4 mm . The tow gaps with a width of 2.0 mm (Figure 6-2(b)) were then induced between the fibre courses with 5 mm ply-staggering to avoid overlapping gaps in adjacent layers with the same fibre angle. The plate with no defects (baseline) was fabricated with the hand-layup technique. During the ply deposition, the debulking process was performed to ensure an even consolidation in the plate and remove trapped air between plies. This process was carried out after ply one, every subsequent three plies, and final ply. The cured plates were then cut into the standard dimension of $150 \times 100 \text{ mm}^2$ by a diamond power saw for performing LVI and CAI tests. Note that in this chapter, the samples with no defects and defects are referred to as baseline and AFP-G, respectively.

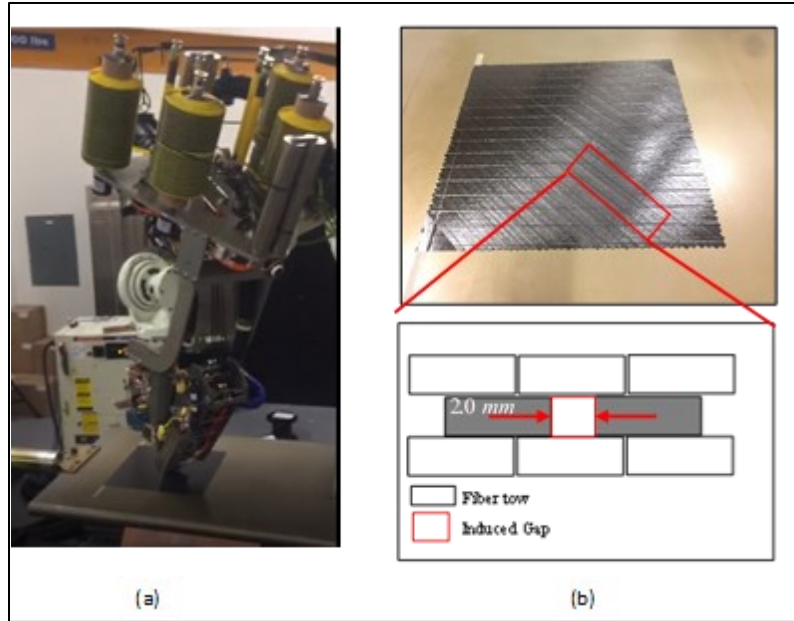


Figure 6-1 (a) Fibre deposition by AFP robot head (b) 2.0 mm tow-gap between the fibre courses

6.2.2 Impact Test

Low-velocity impact tests were performed using CEAST 9340 Instron machine at three levels of Impact Energy (IE), 5 J, 10 J, 15 J based on ASTM D7136 standard (Figure 6-2(a)). The impact machine has been facilitated with an advanced data acquisition device that can record the data with a sampling frequency of 4000 kHz. Ultrasonic C-Scan tests were then carried out on the impacted specimens to map the projected delamination area. The scanning was performed using two 5 MHz transducers with 1.0 mm resolution on the samples immersed in distilled water. This chapter mainly focuses on the CAI tests in the experimental sections, and complementary details for the LVI test results can be found in 3.4.

6.2.3 Compression after impact test

The compressive residual strength of the impacted composite plates was measured by performing experimental CAI tests according to ASTM D7137 standard. For this purpose, specimens were fixed in a standard CAI fixture and were subjected to compressive load using an MTS universal testing machine with a maximum load capacity of 100 kN. The loading process continued with a loading rate of 1.0 mm/min until final failure, where the applied load dropped by 30%. The DIC technique was carried out to measure the strain values of the back surface of the impacted samples (The surface that was not hit by the impactor). Figure 6-2 (b). shows the CAI setup, including the MTS machine and DIC device.

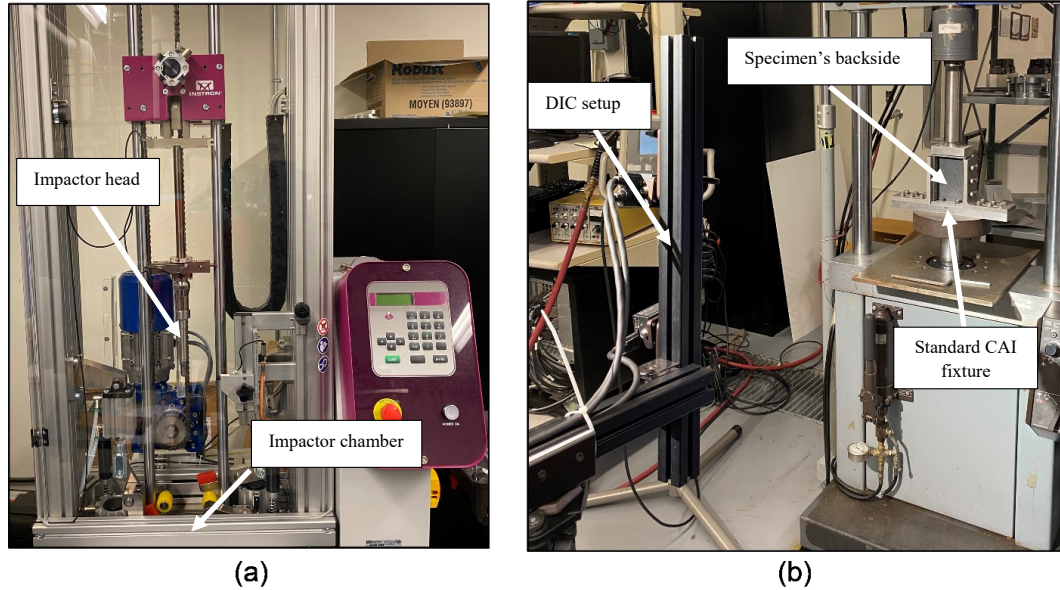


Figure 6-2 (a) CEA9340 Instron machine for impact test (b) CAI test setup, 100 kN MTS machine, and DIC camera

6.3 Numerical Studies

Interlaminar and intralaminar damage modes that are caused by impact load interact with each other. For instance, matrix cracks and fibre breakage might induce delamination. Although the current FE approaches [115, 116] can satisfactorily evaluate the damage parameters of the regular composite laminates, the interaction of the induced gap and impact/post-impact damages is of interest to the current study.

For this purpose, IDLM is used to evaluate the damage parameters of defective composite laminates. This method is a robust multi-scale method, developed in Ref.[114] for damage analysis of composite structures with randomly distributed tow-gaps under in-plane and out-of-plane loading conditions. This method eliminates restrictions of the FE built-in approaches [36, 40, 117], where composite laminates and gap defects are required to be modelled with individual material properties. Thus, any arbitrary FE mesh pattern can be mapped over the composite laminates. Besides the intralaminar damage modes (matrix cracks and fibre breakages), IDLM evaluates the plasticity and resin failure at gap areas. For this purpose, IDLM performs stress homogenization on a Representative Unit Cell (RUC) with sub-cells of variable lengths, where the length is a function of gap percentage (GP) at material points. A bilinear softening damage model [82] with 3D Hashin failure criteria [81] and elasto-plastic failure model [102] is used to calculate the damage parameters in composite and resin sub-cells, respectively.

Impact and post-impact simulations were performed using ABAQUS/Explicit software. The IDLM was used as a user material subroutine (VUMAT) to evaluate the constitutive law at material points. The solid brick element C3D8R was used for meshing the solid parts to avoid the shear locking problem. Figure 6-3(a) shows the FE solid model and its boundary conditions for impact simulation. The composite plate has meshed one element per ply (16 solid elements through the thickness). The ply thickness of the cured baseline sample is 0.13 mm, and a consolidation factor

(bulk factor) of 0.93 was applied to the thickness of the AFP-G samples. More details on the calculation of the consolidation factor are discussed in the result section.

Ply interfaces were simulated by 8-node cohesive elements (COH3D8) with a thickness of 0.01 *mm*. Finer mesh with a minimum length of 1.0 *mm* was applied in the impact zone, providing a total of 193,000 elements for the laminated composite plate. Figure 6-4(a) shows the top view of the FE composite plate. The impactor and fixed points were simulated using a discrete rigid body model, and an elastic linear model with steel material was used to simulate the fixture base. The impactor head was meshed with tetrahedral elements to obtain better contact convergence at the impact area. The contact behaviour was simulated using the general contact algorithm with the Coulomb friction model [75] with a contact friction coefficient of 0.3, an acceptable value for metal-laminate contact [64, 76, 77]. The enhanced hourglass control was set to the enhanced to diminish the noise on the results, and no mass scaling was applied to the model during impact simulation.

An intermediate step between the LVI and CAI simulations was considered to damp out the kinetic energy of the plate caused by the impact load. For this purpose, viscous pressure (Eq.(1)) is applied on both sides of the plate as follows by developing an ABAQUS VDLOAD script [118].

$$P = -c_v(\bar{v} \cdot \bar{n}) \quad (1)$$

where P is applied pressure, c_v is the viscosity, \bar{v} is the surface point velocity, and \bar{n} is the unit outward normal to the surface at the point. The recommended value for c_v can be defined as following [118]:

$$c_v = 0.015 \rho c_d \quad (2)$$

where ρ is the density and c_d is dilatational wave speed in the composite material.

Figure 6-3.(b) shows the boundary conditions of the FE model for CAI analysis. As can be seen, a displacement load is applied on the top assembly, and side plates prevent the specimen from buckling. Fixed support, top assembly, and side plates have been modelled with steel material.

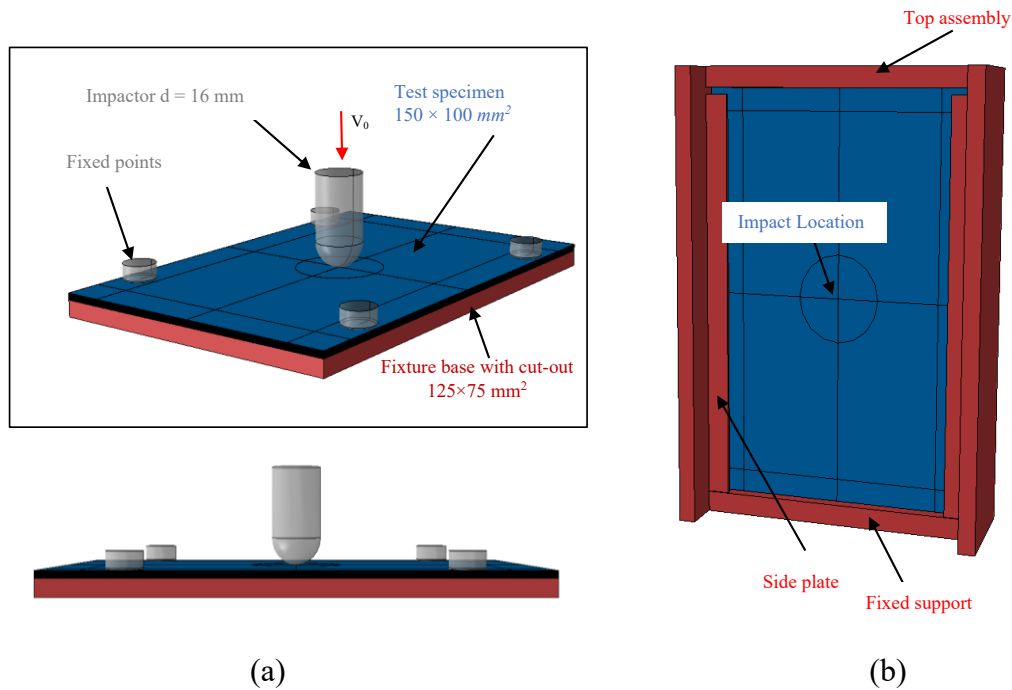


Figure 6-3 Boundary conditions for (a) low-velocity impact (b) Compression after impact simulation

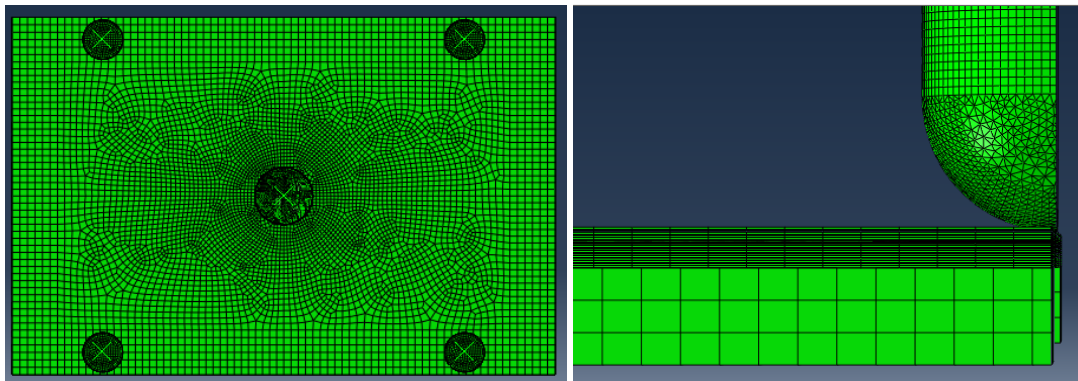


Figure 6-4 (a) Top view of Composite plate FE mesh (b) Tetrahedral elements for rigid body impactor

6.4 Results and Discussion

6.4.1 Induced Gap shrinkage factor (IGSF) and Consolidation Factor (CF)

Induced gaps cause two consequent effects that degrade the mechanical performance of the structures. (1) Material inhomogeneity forms relatively large resin pockets, mainly affecting the damage initiation and propagation in the structure. (2) Thickness reduces the flexural stiffness and might cause a local out-of-plane fibre waviness. These two effects affect each other because of in-ply and out-of-ply fibres movement during the curing process (Figure 6-5). In other words, if fibres

can freely move in the thickness direction, the Consolidation Factor (CF) increases. The top ply can also fill in the gap area in the adjacent layer and shrink the gap sizes. This scenario can mainly occur for a thermoset material system cured in an autoclave under high pressure.

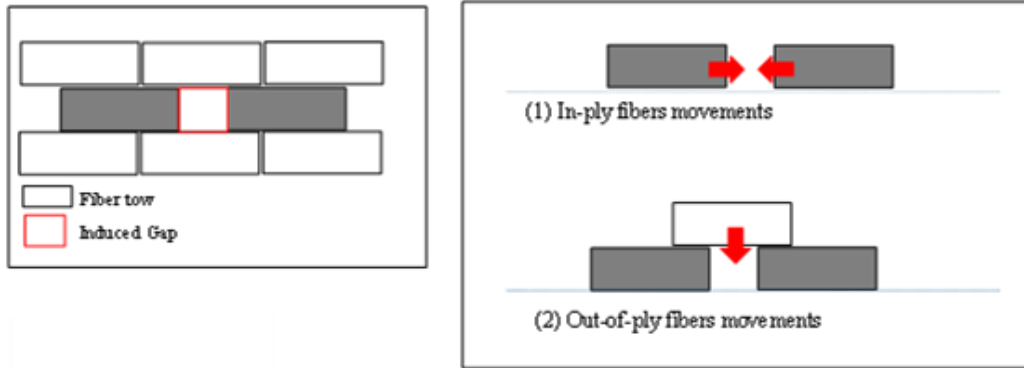


Figure 6-5 Gap shrinkage due to in-ply and out-of-ply fibres movement

Although CF is a geometrical parameter that can be applied by modifying the laminate geometry, IGSF might vary by location and the initial dimension of the gaps. In other words, the post-cured dimensions of the gaps with the same pre-cured dimensions might vary after the curing process. Figure 6-6 shows the post-cured gap dimension at two different spots of the studied composite samples. While the pre-set gaps have a dimension of 2000 microns, the post-cured gap size is around 450 microns. The post-cured shape and dimension of gaps is a function of several parameters such as stacking sequence, material system, and initial gap size. Due to the lack of a comprehensive database of the effect of these parameters on the gap shape, no general and precise rule can be applied to estimate the shape/sizes of randomly distributed gaps in composite laminates.

On the other hand, non-destructive techniques such as ultrasonic C-scan cannot detect the gap patterns in the laminates. Although several numerical studies [30, 31] assume the gap sizes do not change after the curing process (IGSF = 1.0), In this study, an average IGSF was selected for the numerical study of defective composite samples. For this purpose, microscopic observation was performed on twenty different gap spots at different layers of cured composite laminates, and the length of the resin pocket areas was measured. Note that the gap areas are not necessarily formed in an ideal rectangular shape. In this study, the average length of the area where the Fibre Volume Fraction drops by 50% is considered post-cured gap length, and it is assumed that the gap width through the ply thickness is uniform.

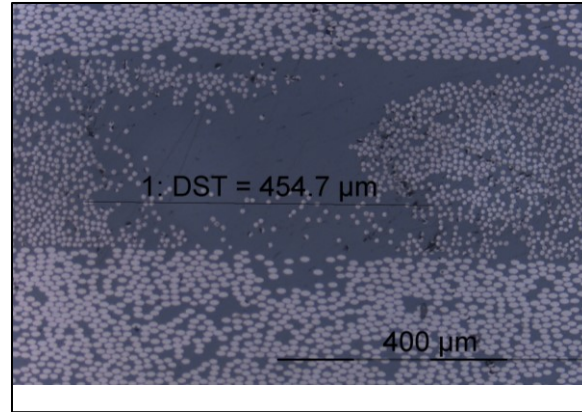


Figure 6-6 Resin pocket at gap zones at 90° ply

Figure 6-7 shows the statistical results of the studied defective composite laminate's tow-gap lengths with an average gap length of 2000 micron. The maximum and minimum observed gap lengths are around 660 microns and 270 microns, respectively, and the average gap length is around 460 microns with a standard deviation of 94 microns. Thus, an IGSF of 0.23 was selected for numerical studies of the defective samples. The CF value of 0.93 was also applied to the laminate thickness reported in Ref. [93].

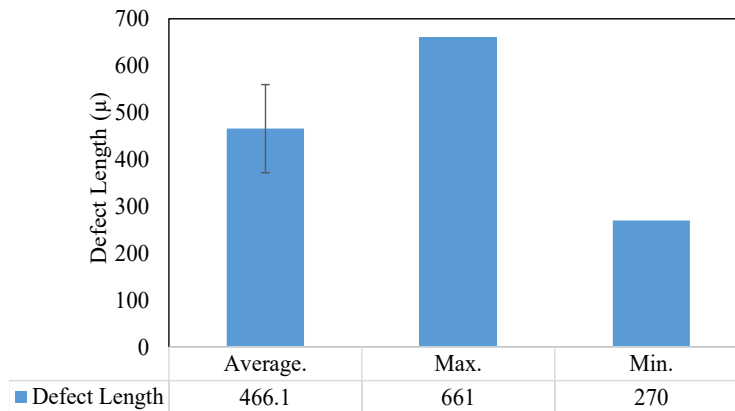


Figure 6-7 Statistical results of the tow-gap length obtained from the different spots of the AFP-G samples

6.4.2 Low-Velocity Impact Results

A comparison of impact force versus time graphs between the numerical simulations and the experimental results has been demonstrated in Figure 6-8 for IE = 5 J, 10 J, and 15 J. It can be seen that IDLM can predict the impact force for both baseline and defective samples with a good agreement. Furthermore, by comparing the baseline and defective samples with the same IE, it can be said that the impact force is reduced for AFP-G samples by around 17%. Figure 6-9 demonstrates the numerical result of IE versus time for both baseline and defective samples. No significant difference between the results of the baseline and defective samples is observed. Thus, it can be concluded that the damage dissipation due to the presence of the resin pocket is less significant than the CF for the impact response of the composite laminates. However, the resin pocket might be related to the change of intralaminar damage pattern [101]. Figure 6-10 compares the delamination pattern of both defective and baseline samples. It can be seen that the defective

samples experience higher projected delamination. Although the rate of the change might not be of interest for impact analysis, it might have a consequence effect on the post-impact behaviour of the composite plates, which will be discussed in detail in the CAI results section.

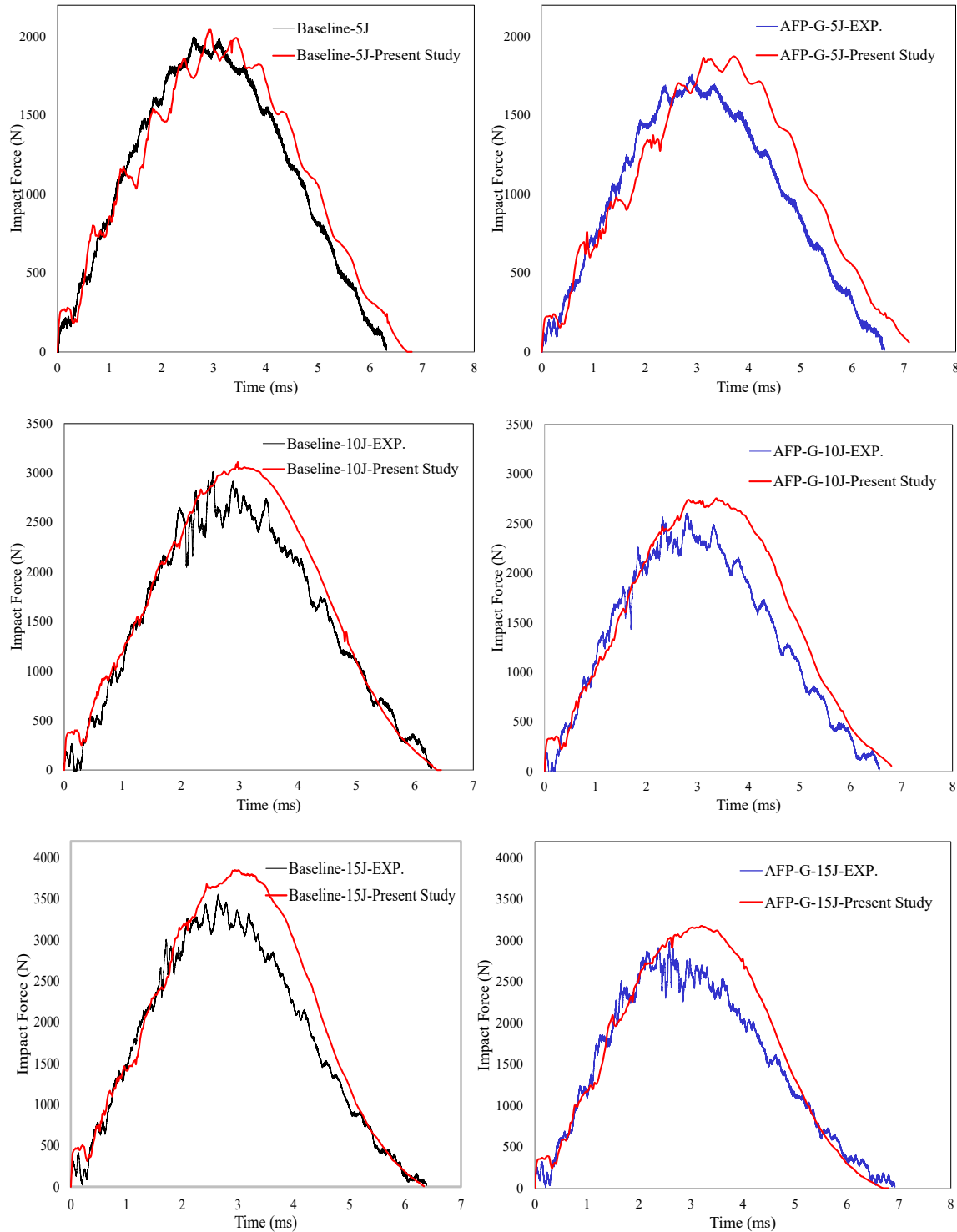


Figure 6-8 Comparison of impact force versus; experimental and numerical results for IE= 5 J, 10 J, and 15 J

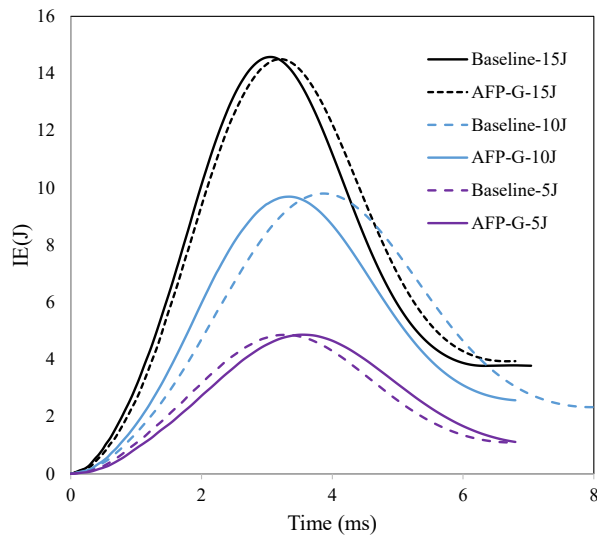


Figure 6-9 Numerical results of the impact energy versus time for both baseline and defective samples

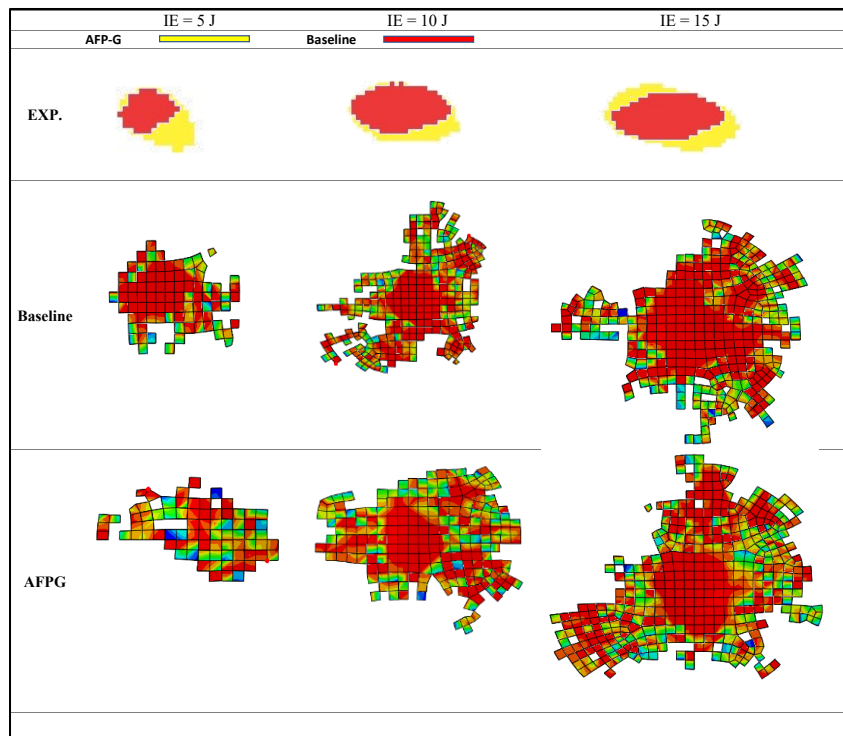


Figure 6-10 Numerical results of the projected delamination pattern for baseline and AFP-G samples

Figure 6-11(a) shows the contour of delamination initiation for the cross-section of the numerical sample under $IE = 15\text{ J}$. It is shown that the impact causes delamination between all plies at the

impact area. On the other hand, the resin failure at the gap areas close to the impact point has been demonstrated in Figure 6-11(b), which shows the IDLM can estimate the resin failure in the defect areas as one of the failure types of defective plates manufactured by AFP technique. The contour of GP for FE elements containing the gap areas has also been shown in Figure 6-11(c). Because of a finer mesh at the impact zone, the value of GP for central elements is higher than far-from-impact elements. Note that the elements with GP= 0.0 have been removed from the contour to demonstrate the gap zones in multi-layers. It is also important to note that the IDLM is not limited to the continuous tow gaps, and damage analysis of the composite laminates with any arbitrary pattern of the gaps can be performed using this method.

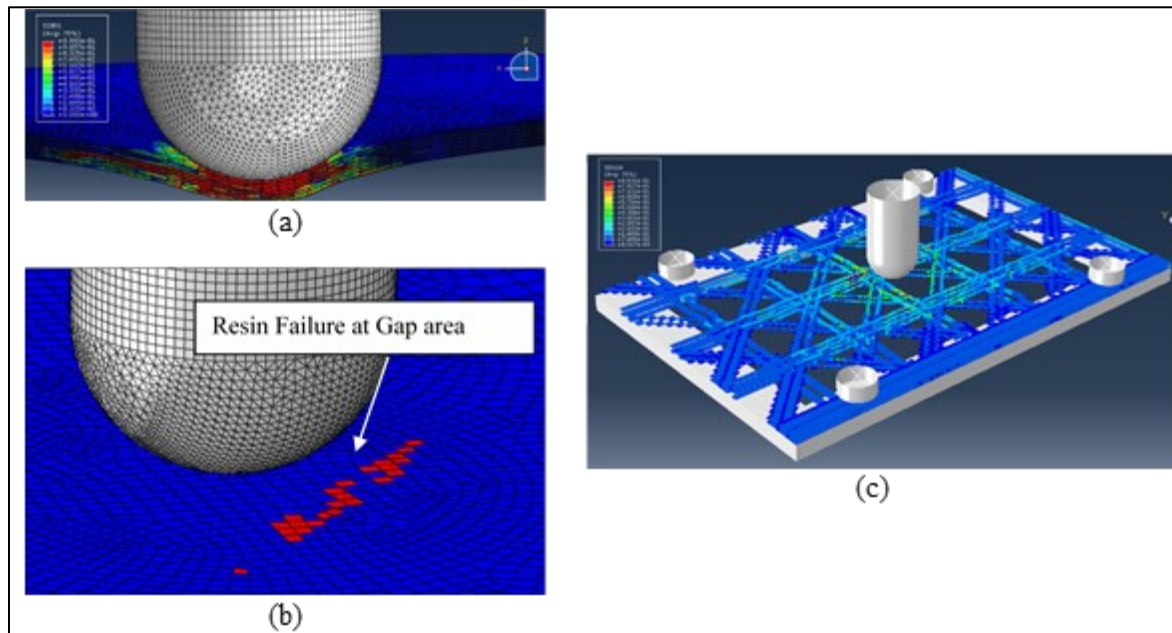


Figure 6-11 (a) Cross-section view of the deformed specimen under impact loading for IE = 15 J (b) Resin failure at gap areas close to the impact zone(c) Gap areas mapped on the FE elements

6.4.3 Effect of Induced gap on Delamination Initiation and Propagation

Although gaps create free volumes during the fibre deposition, they are filled with resin and fibres during the curing process. Thus, gap areas are transformed to (1) relatively large single or multiple resin pockets and (2) low fibre volume fraction composite zones [93]. In addition, it was shown in chapter 4 that the gap area can be a source of delamination initiation for the short beam under flexural loading. That is probably because the resin area provides a lower shear strength level than the non-defective composite material. Thus, higher interlaminar shear stress can be expected at the gap zones.

On the other hand, the resin area may cause stress relaxation in structures and act as a crack delamination blunter [47, 101]. Figure 6-12 shows the effect of distributed gaps on the delamination pattern between composite plies. It is shown that gap areas can change the dimension and angle of delamination. The change is more highlighted between the lower plies, where a higher

delamination area is expected. Note that both FE samples have the same thickness, and no consolidation factor has been applied to the defective plate. The contour of GP for all composite plies has been demonstrated in Figure 6-12. Non-gap areas have been removed from the contour. The value of GP is calculated for every material point using a mapping algorithm [119].

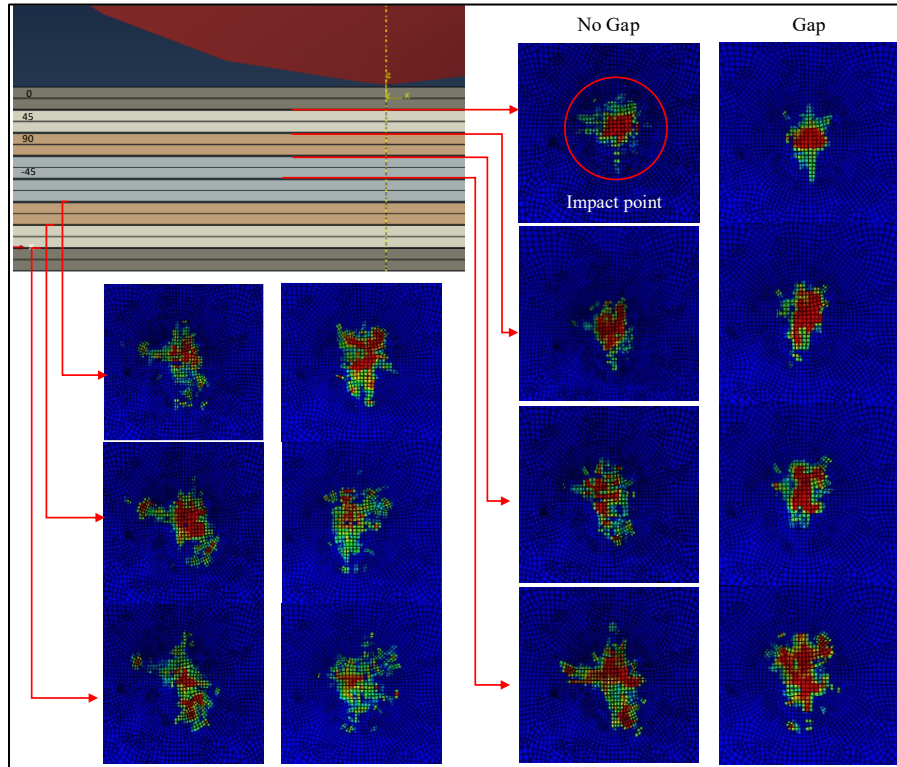


Figure 6-12 Effect of tow-gaps on the delamination patterns of the laminated under IE = 10 J

In order to investigate the effect of induced gap on the delamination propagation, the location of gap lines has been mapped on the interface plies in Figure 6-13. It seems that the delamination is stopped when it reaches the lower ply gap lines (red dash line); however, the upper ply gap line (solid red line) does not have a significant effect on the delamination pattern.

In other words, the location of the induced gap plays a significant role in the delamination behaviour of the composite laminates under impact loading. If the gap locates where the delamination is prone to occur (for example, where the maximum interlayer shear stress is found), it can accelerate the delamination initiation. It is probably because the resin failure and matrix cracks at the gap areas can reduce the interlaminar shear strength [101] and induce the delamination initiation. However, if the gap is located in the vicinity of the zone where delamination is initiated (gap does not cause the delamination initiation), it might impede the delamination propagation. It seems that the plasticity that occurs in the resin pockets at the vicinity of the impact loads causes stress relaxation at the gap areas. As the inter-ply crack (delamination) reaches the plastic zone, the plastic area might act as a crack stopper [120]. However, enhanced numerical studies are required to understand the interaction of plasticity and delamination

propagation and investigate the effect of resin plasticity on the interlaminar crack growth parameters (strain energy release rate, stress intensity factor).

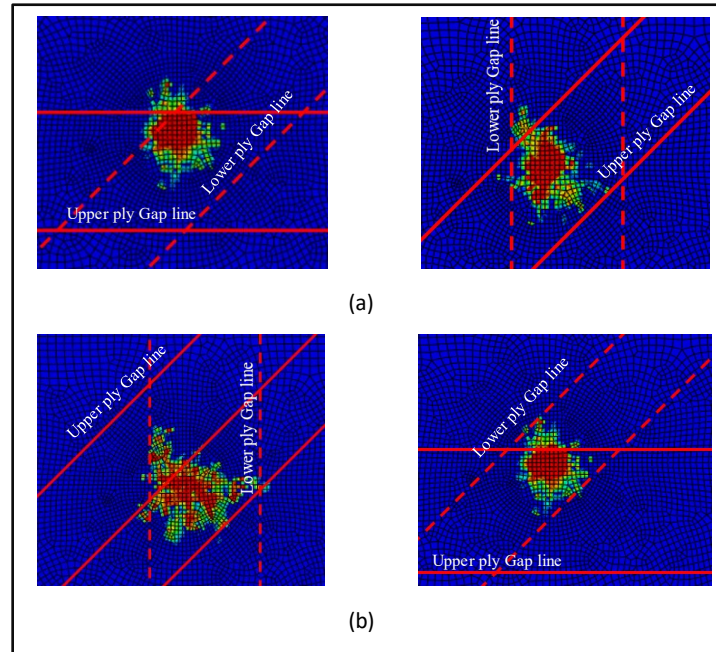


Figure 6-13 Effect of upper and lower ply gap lines on the delamination propagation of the laminates under low-velocity impact loads

6.4.4 Compression After Impact (CAI)

Figure 6-14 shows the graphs of compressive stress versus strain for both experimental results and numerical simulations. By comparing the results of impacted baseline and defective samples, it can be understood that the presence of induced gaps in impacted samples cannot be neglected. For instance, while the compressive strength of the impacted baseline specimen under $IE = 5$ J has reached 220 MPa, the AFP-G sample has experienced a lower compressive strength with the value of 197 MPa. However, the residual compressive strength reduction rate is not the same for different levels of IEs. It is also shown that the IDLM method can predict the stress-strain behaviour of the impacted plates with a good agreement.

Furthermore, it can also be seen that the compressive strength of the defective samples does not follow the same trend as that of the baseline samples. The graphs of CAI strength versus IE and versus delamination length have been plotted in Figure 6-15 to understand better the interaction of both impact damage and tow gaps on the CAI strength of the samples. Figure 6-15(a) shows that the impact damage reduces the CAI strength of baseline samples. However, the IE level does not significantly affect the amount of reduction, which agrees with the results of Ref. [121]. On the other hand, induced gaps have reduced the compressive strength of the samples in the presence of impact damage. The CAI strength of the defective sample under $IE = 5$ J has been decreased by 30 MPa, which is around 13% less than the strength of the baseline impacted samples.

Figure 6-15(b) illustrates the compressive strength versus delamination length and the corresponding failure mode under compressive loading. It can be seen that all specimens except

the AFP-G-15J have been failed under fibre breakage, which is mainly observed for impacted thin composite laminates [122–124]. The failure occurs far away from damage close to the fixing side of the plate, as shown in Figure 6-16(a). Interestingly, the AFP-G-15 fails under multiple delamination areas at the vicinity of the impact ((Figure 6-16b)). The reason for that can be related to the larger delamination area of the sample. The delamination length of the defective impacted sample is around 25 mm, which is larger than the baseline impacted sample by a factor of 1.25.

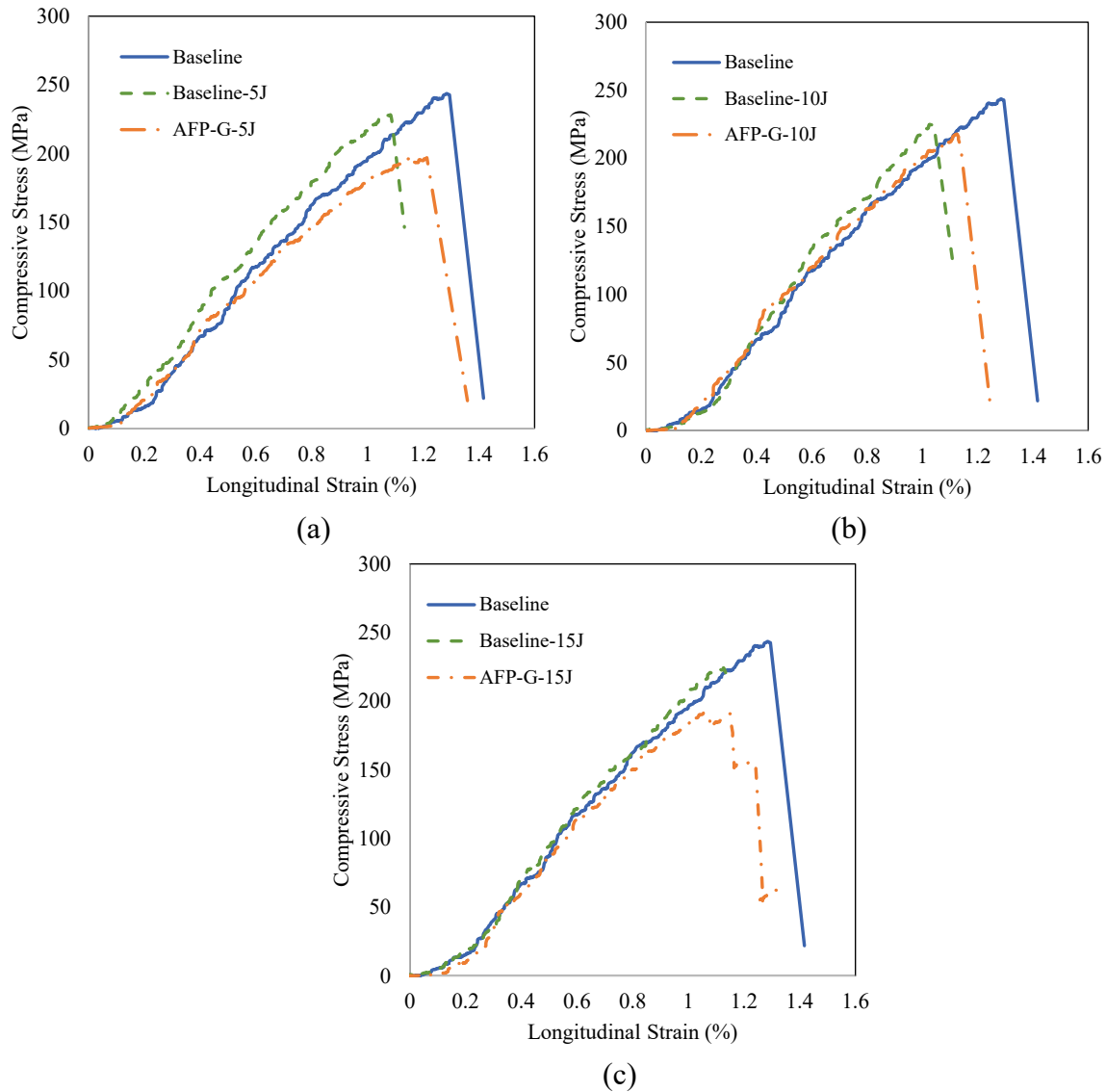


Figure 6-14 Compressive stress versus longitudinal strain for the specimens under (a) IE = 5 J, (b) IE = 10 J, (c) IE = 15 J

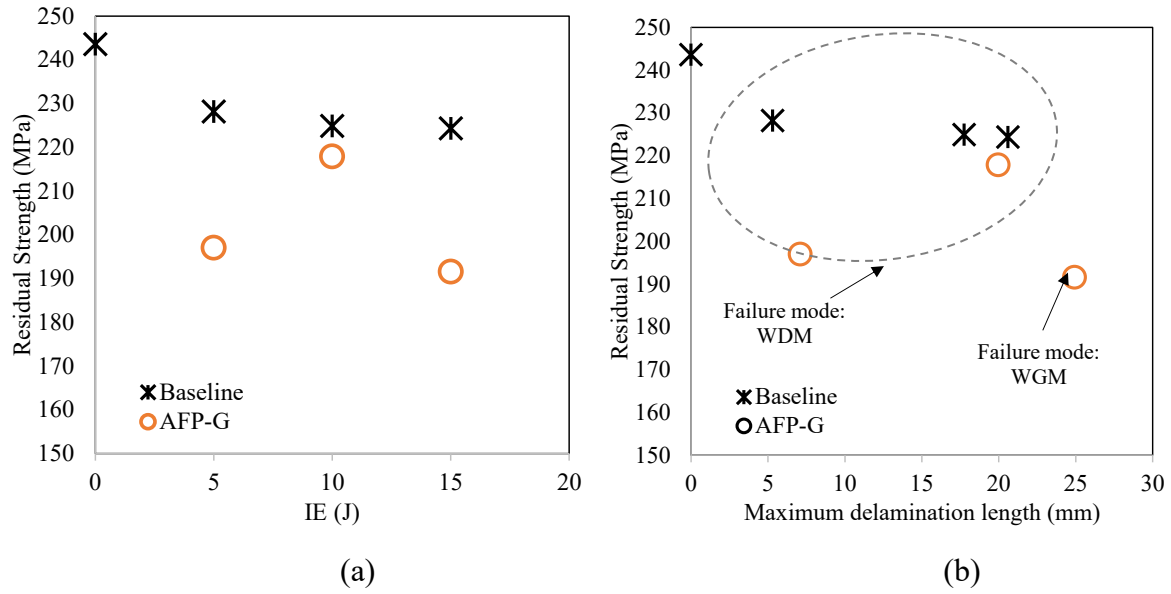


Figure 6-15 Residual strength versus (a) Impact Energy (b) Maximum delamination length

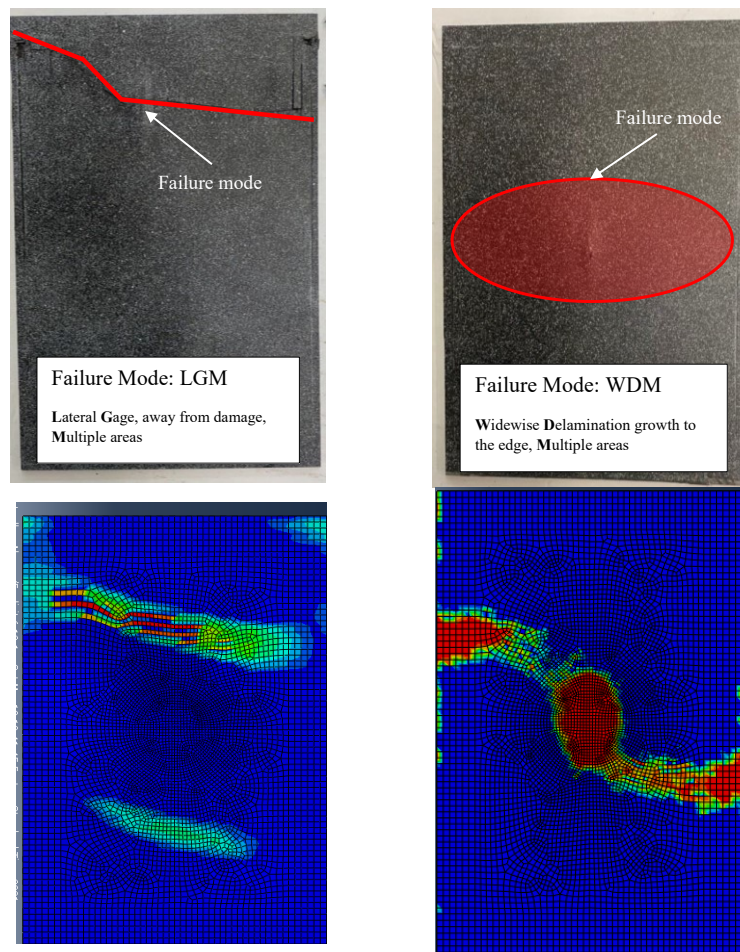


Figure 6-16 Observed failure modes of the impacted samples (a) Lateral gage away from damage (b) Widespread delamination

In-plane strain contours of the specimens were compared for the intact and impacted samples under $IE = 5 \text{ J}$ (Figure 6-17). The contours were captured from DIC results of the back side of the composite plates at a longitudinal displacement load equal to 1.15 mm . It was shown that the longitudinal strain (ϵ_{xx}) patterns have been changed at impacted samples; however, no significant difference is observed in ϵ_{yy} and ϵ_{xy} contours. Furthermore, no significant difference is observed between the in-plane strain contours of impacted baseline and AFP-G samples due to the similarity of failure mode of both samples, which is fibre breakage, as discussed earlier in this section.

The same result but for $IE = 15 \text{ J}$ has been demonstrated in Figure 6-18 for baseline and AFP-G sample at displacement load of 1.03 mm . It is shown that the in-plane strain distribution of the AFP-G sample is dissimilar to the baseline due to the multiple delamination failure. For instance, the amount of longitudinal strain at the vicinity of the impact zone is positive because of the local buckling caused by delamination at the impact area.

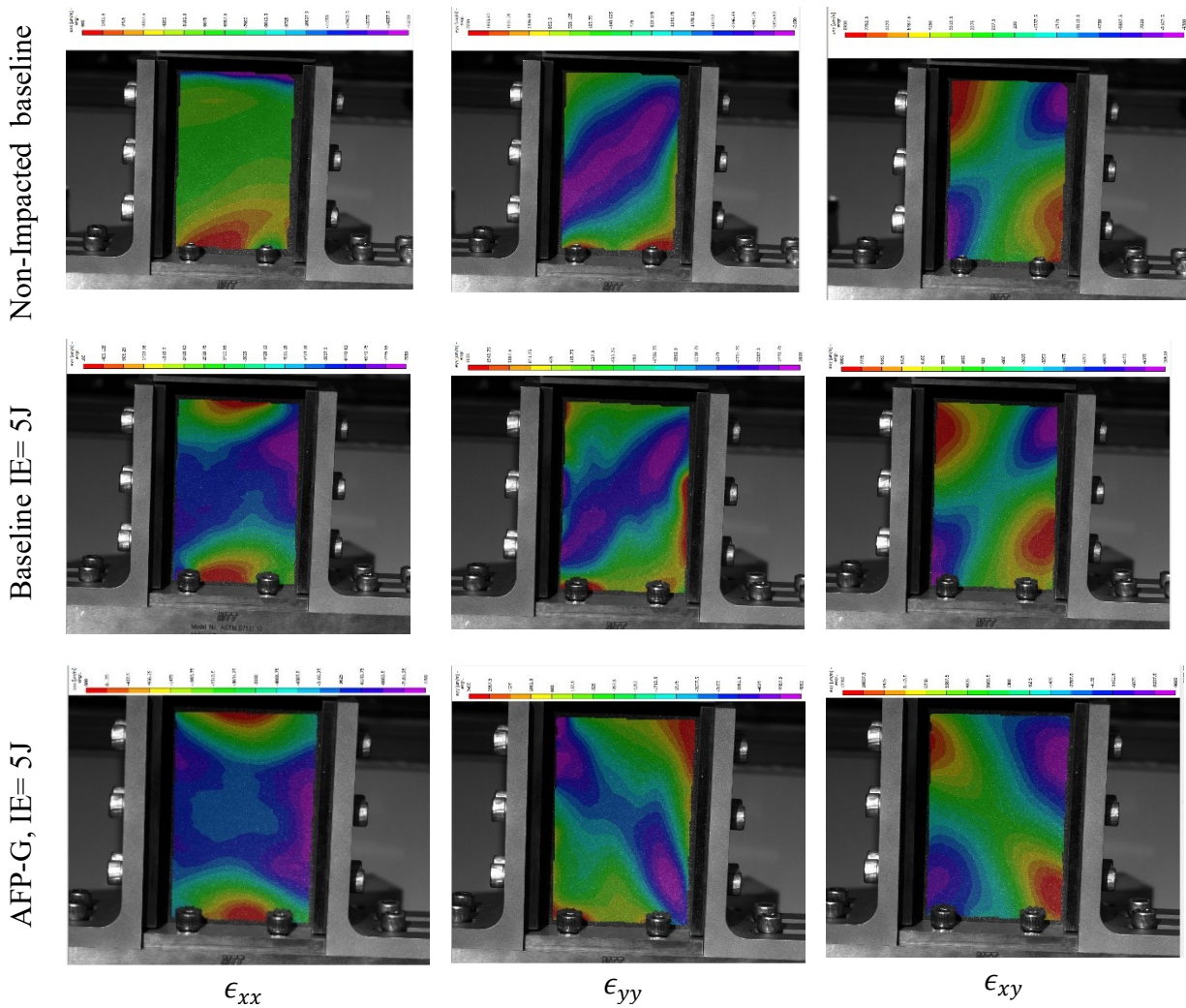


Figure 6-17 Comparison of in-plane strain contours between non-impacted and impacted samples under $IE = 5 \text{ J}$ at displacement load equal to 1.15 mm

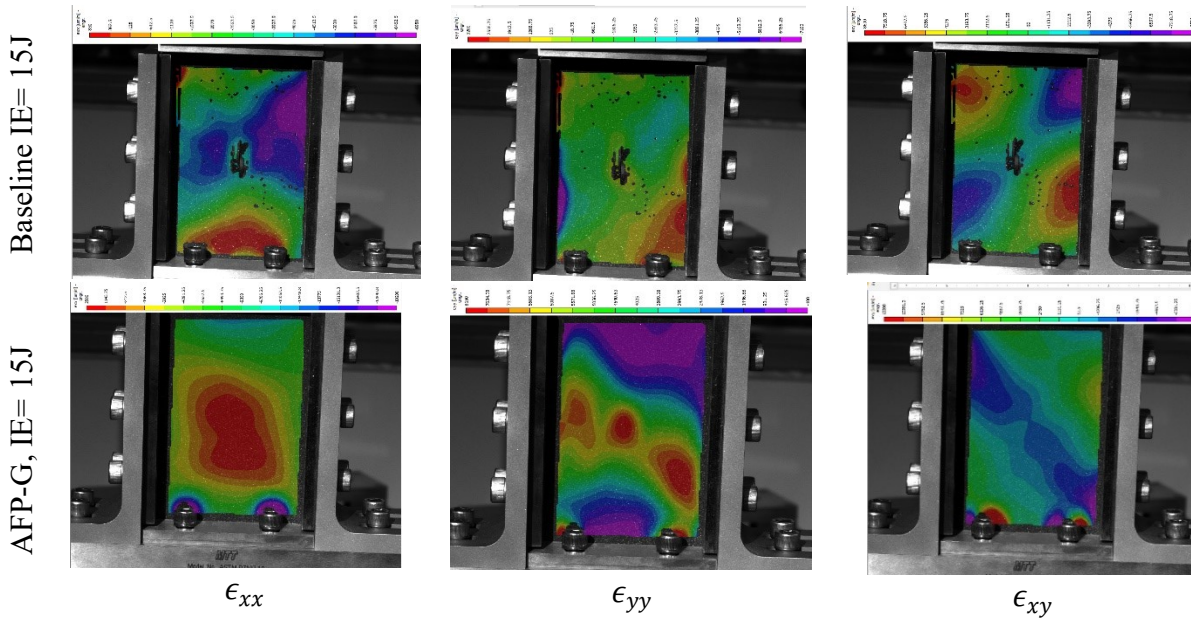


Figure 6-18 In-plane strain contours for impacted samples under $IE = 15$ J at displacement load equal to 1.03 mm

In conclusion, it can be said that the worst-case scenario for the impacted plates is the case that the induced gaps cause the change of the failure mode under CAI load. In this case, a significant CAI strength reduction might be expected. In addition, because the impact delamination is expected to be larger for the defective plates, the post-fatigue behaviour of these plates is also an interesting subject of the experimental studies.

6.5 Concluding Remarks

In this chapter, experimental and numerical studies were performed to investigate the effect of fibre tow-gaps on the Low-velocity impact and Compression After Impact of thin composite laminates. For this purpose, a quasi-isotropic composite laminate with 2 mm tow gaps at all plies was fabricated using the AFP technique. The induced gaps create around 8% volumetric gap inside the laminate before the curing process. The effect of the autoclave curing on the gap forming was investigated by performing microscopic observation was performed on the gap area, and it was shown that an average IGSF and a CF of 0.25 and 0.93 is expected during the curing process. Although these factors might vary by the stacking sequence and material system, they can be used for numerical studies of thermoset materials cured in an autoclave in the cases that the experimental result is not available.

It was shown that the composite plates experience a lower impact force by around 17% for IE less than 15 J. However, a larger projected delamination length can be expected for the defective samples. Because no significant difference in the graphs of the impact energies of the baseline and defective samples, it can be concluded that the impact response of the sample is more affected by the consolidation factor rather than resin pockets formed in gap zones. However, the delamination pattern can be changed due to the presence of the gap areas.

The experimental results on the CAI strength of the defective impacted specimens demonstrated that the effect of tow gaps is not negligible for composite laminates subjected to LVI. It was shown that the interaction of impact damage and automated manufacturing defects on the CAI strength reduction of thin composite laminates is significant. While the impact reduced the CAI strength by around 15% for the baseline sample under $IE = 5$ J, a 28% reduction was observed for the defective sample under the same IE. Impact damage and tow-gap interaction might also cause an early failure due to the change in the failure mode of the impacted plated under compressive loads. While thin plates usually are failed under fibre breakage during the CAI test, which is similar to the failure mode of the non-impacted plates, the presence of the defects might cause a multiple delamination failure. It is probably because the defects might cause a higher area of delamination. This effect accelerates the failure of the plate under compressive loading, as shown for the sample under $IE = 15$ J. In addition, it was shown that the graph of CAI strength versus IE is not similar for the baseline and defective samples. The CAI strength is negligibly affected by the level of IE for the baseline samples. However, due to the change in the failure mode, CAI strength varies by IE for defective plates. Because of the limited number of test specimens in this study, more experimental studies are required to investigate the effect of the induced gaps on the failure mode of impacted thin composite plates under CAI load.

Numerical studies were carried out using IDLM, a robust meso-macro method for continuum damage analysis of the composite plates with arbitrary tow-gap patterns. This method can evaluate the resin failure and plasticity at the gap areas, composite matrix cracks, and fibre breakage using a novel homogenization technique at material points. IDLM had been formerly implemented for quasi-static in-plane behaviour of the defective plates. In this study, it was shown that IDLM successfully evaluates the impact response, projected delamination pattern, and also the CAI strength of defective composite plates with a good agreement with the experimental results

CHAPTER 7
Conclusions and Future Work

7. Conclusions and Future Work

7.1 Conclusions

In this thesis, mechanical performance and failure of composite laminates manufactured by the Automated Fibre Placement technique were studied. The research studied the damage mechanism and failure of thin thermoset Carbon/Epoxy composite laminates subjected to out-of-plane and impact loads. While several inherent defect types can be found in the laminates manufactured by the AFP technique, induced tow-gap was chosen for this study. This inherent defect is found in complex-shaped composite structures and might significantly affect the in-plane and out-of-plane strengths of composite laminates. To address this issue, several experimental tests were performed to investigate the effect of tow-gaps on the strength reduction of the laminates under flexural and impact loads. Besides, a new meso-macro scale method was developed for damage analysis of defective laminates with arbitrarily distributed gaps due to the lack of a robust computational model.

Results indicated that tow gaps might affect the quality of the final composite parts in structural and material levels. That is why applying a single knockdown factor might not be effective for including this defect into failure studies of defective laminates. It was also demonstrated that the effect of gap on low-velocity impact and compression after impact of laminates manufactured by the AFP technique should not be neglected. In addition, it was shown that the Induced Defect Layer Method (IDLM) can empower the FE packages for damage analysis of defective structures with arbitrarily distributed induced gaps. More details on the results are as follows.

For the experimental studies, a quasi-isotropic laminate with a stacking sequence of $[0_2/45_2/90_2/-45_2]_s$ was fabricated using the AFP technique. Cycom 977-2/HTS40 was selected as the material system. A 2.0 mm tow-gaps were then induced in all layers of composite plies between each fibre course that generated an average of 8% volumetric pre-cured gap in the whole laminate. A similar laminate but manufactured with the hand-layup technique was considered as a baseline sample. This sample is a gap-free laminate that is used as an experimental reference specimen.

A series of microscopic observations were performed to investigate the effect of curing on the final forming of the gap areas. Results showed that the shape and the dimension of the gap area are changed during the curing process in the autoclave. Furthermore, it was shown that an Induced Shrinkage Factor (IGSF) and a Consolidation Factor (CF) are required for numerical studies of defective laminates. For this study, an average IGSF and a CF of 0.25 and 0.93 are selected based on the statistical analysis on several gap spots.

Laminates were then cut into desired dimensions, and low-velocity impact tests with IE of 5 J, 10 J, and 15 J were performed using an Instron Impact machine with a standard hemispherical head. Results showed that the defective samples experience up to 17% lower maximum impact force than baseline samples. It was also shown that the delamination threshold load of defective samples, which is a laminate property, was changed for different impact loads. This observation and expecting a larger projected delamination area for defective samples (compared to the baselines) strengthen the idea that the gap areas might be a source of delamination initiation.

The impact samples were then subjected to the Compression After Impact (CAI) tests using a standard MTS machine. A DIC technique was then applied to the backside of the impacted plate

to measure the in-plane strain during the compressive loading. Results showed that the impact damage reduces the compressive residual strength; however, the impact energy level does not significantly affect the amount of reduction. It was also shown that the effect of automated induced gaps on the residual strength reduction of the impacted plate should not be neglected. For instance, a compressive strength reduction of 28% was measured for the defective sample compared to a 15% reduction for the baseline sample subjected to IE of 5 J. Tow-gaps can also affect the failure mode of the impacted sample under compressive loading, especially for thin composite laminates. It was shown that the larger delamination area for the defective sample subjected to IE of 15 J could alter the failure mode of the sample and caused multiple delamination damage, which is rarely observed in thin Carbon/Epoxy composite laminates.

From the numerical aspect of the study, it was shown that the currently developed methods cannot be used to simulate the defective composite laminates. Due to the relatively large widespread resin-pockets caused by tow-gaps, the assumption of heterogeneous material with uniform carbon fibre and resin distribution is no longer valid. Thus, the composite laminate theory may not be applied to the material points in the gap zones. Furthermore, the developed FE models, such as ply-by-ply deposition techniques, are limited to the coupon studies of the defective samples.

In order to overcome this issue, a meso-macro scale method called Induced Defect Layer Method (IDLM) was developed in this research study to include the effect of the induced manufacturing gaps on the damage analysis of defective composite laminates. This method is based on CDM approaches and can be embedded in the FE commercial software. IDLM uses a novel homogenization technique for intralaminar damage analysis of large composite structures with defects. This method has been facilitated with a geometrical parameter that represents the gap in the material point and the unit-cell. Thus, no mesh refinement is required in the gap areas of multi-layers composite that have computational time advantages compared to the current methods. Numerical studies were then carried out by integrating the IDLM method into the ABAQUS FE package. Results were compared with obtained experimental results, and it was shown that IDLM is an effective method for stress and damage analyses of composite structures with distributed induced gaps.

7.2 Future Work

The potential future work can be described as below:

- This research study was carried out on thermoset material systems. The resin pockets in the gap area might be shaped differently for thermoplastic materials due to the absence of an autoclave curing process. Thus, future research could investigate the effect of tow-gap on thermoplastic material systems.
- Future work could focus on thick composite laminates and study the impact and post-impact behaviour of defective laminates.
- Because the gap areas form relatively large resin areas, the effect of temperature and residual stress might be of interest for future work.
- A detailed micro analysis study on the effect of different parameters such as autoclave pressure, stacking sequence on the resin pockets formation can be carried out.

- The AFP defects have a random distribution in real practical applications. Although the focus of this study and similar studies is on the material characterization and understanding the failure mechanism in the presence of the gaps, a stochastic study can be performed to address the relationship between the AFP technique parameters and gap patterns during the lay-up deposition.

References

- [1] Airbus SAS. "Global Market Forecast 2019-2038".
- [2] Boeing. "Commercial market outlook: 2018--2037".
- [3] Campbell FC. "Ply Collation: A Major Cost Driver". In: *Manufacturing Processes for Advanced Composites*. Elsevier, 2004, pp. 131–173.
- [4] Lossie M, Van Brussel H. "Design principles in filament winding". *Compos Manuf* 1994; 5: 5–13.
- [5] Colombo C, Vergani L. "Optimization of filament winding parameters for the design of a composite pipe". *Compos Part B Eng* 2018; 148: 207–216.
- [6] Crosky A, Grant C, Kelly D, Legrand X, Pearce G. "Fibre placement processes for composites manufacture". In: *Advances in Composites Manufacturing and Process Design*. Elsevier Inc., 2015, pp. 79–92.
- [7] Harik R, Saidu C, Williams SJ, Gurdal Z, Grimsley B. "Automated fiber placement defect identity cards: cause, anticipation, existence, significance, and progression". In: *SAMPE 18-Long Beach*. 2018.
- [8] Kozaczuk K. "AUTOMATED FIBER PLACEMENT SYSTEMS OVERVIEW". *Trans Inst Aviat* 2016; 245: 52–59.
- [9] Mostakima Mafruha Lubna, Zaheeruddin Mohammed, Manik Chandra Biswas MEH. "Fiber-Reinforced Polymer Composites in Aviation". In: *Fiber-Reinforced Polymers: Processes and Applications (ISBN: 978-1-53619-049-6)*. Nova Science Publishers, Inc. New York, 2021, pp. 177–210.
- [10] Lukaszewicz DH-JA, Ward C, Potter KD. "The engineering aspects of automated prepreg layup: History, present and future". *Compos Part B Eng* 2012; 43: 997–1009.
- [11] Parmar H, Khan T, Tucci F, Umer R, Carlone P. "Advanced robotics and additive manufacturing of composites: towards a new era in Industry 4.0". *Materials and Manufacturing Processes* 2021; 1–35.
- [12] Oromiehie E, Prusty BG, Compston P, Rajan G. "Automated fibre placement based composite structures: Review on the defects, impacts and inspections techniques". *Compos Struct* 2019; 224: 110987.
- [13] Izco L, Isturiz J, Motilva M. "High Speed Tow Placement System for Complex Surfaces with Cut / Clamp / & Restart Capabilities at 85 m/min (3350 IPM)". *SAE Tech Pap*. Epub ahead of print 12 September 2006. DOI: 10.4271/2006-01-3138.
- [14] Hale, R.D.; Moon, R.S.; Lim, K.; Schueler, K.; Yoder A. S. "*Integrated Design and Analysis Tools for Reduced Weight, Affordable Fiber Steered Composites*". Lawrence, KS, 2004.
- [15] Debout P, Chanal H, Duc E. "Tool path smoothing of a redundant machine: Application to Automated Fiber Placement". *Comput Des* 2011; 43: 122–132.

References

- [16] Blom AW, Lopes CS, Kromwijk PJ, Gürdal Z, Camanho PP. "A theoretical model to study the influence of tow-drop areas on the stiffness and strength of variable-stiffness laminates". *J Compos Mater* 2009; 43: 403–425.
- [17] Bakhshi N, Hojjati M. "An experimental and simulative study on the defects appeared during tow steering in automated fiber placement". *Compos Part A Appl Sci Manuf* 2018; 113: 122–131.
- [18] Wehbe R, Tatting B, Rajan S, Harik R, Sutton M, Gürdal Z. "Geometrical modeling of tow wrinkles in automated fiber placement". *Compos Struct* 2020; 246: 112394.
- [19] Heinecke F, Willberg C. "Manufacturing-Induced imperfections in composite parts manufactured via Automated Fiber Placement". *J Compos Sci*; 3. Epub ahead of print 2019. DOI: 10.3390/jcs3020056.
- [20] Orifici AC, Herszberg I, Thomson RS. "Review of methodologies for composite material modelling incorporating failure". *Compos Struct* 2008; 86: 194–210.
- [21] Belhaj M, Hojjati M. "Wrinkle formation during steering in automated fiber placement: Modeling and experimental verification". *J Reinf Plast Compos* 2018; 37: 396–409.
- [22] Sacco C, Baz Radwan A, Anderson A, Harik R, Gregory E. "Machine learning in composites manufacturing: A case study of Automated Fiber Placement inspection". *Compos Struct* 2020; 250: 112514.
- [23] Chen M, Jiang M, Liu X, Wu B. "Intelligent inspection system based on infrared vision for automated fiber placement". In: *Proceedings of 2018 IEEE International Conference on Mechatronics and Automation, ICMA 2018*. Institute of Electrical and Electronics Engineers Inc., 2018, pp. 918–923.
- [24] Maass D. "Progress in automated ply inspection of AFP layups". *Reinf Plast* 2015; 59: 242–245.
- [25] Cemenska J, Rudberg T, Henscheid M. "Automated In-Process Inspection System for AFP Machines". *SAE Int J Aerosp*; 8. Epub ahead of print 15 September 2015. DOI: 10.4271/2015-01-2608.
- [26] Bakhshi N, Hojjati M. "Effect of compaction roller on layup quality and defects formation in automated fiber placement". *J Reinf Plast Compos* 2020; 39: 3–20.
- [27] Wehbe R, Sacco C, Baz Radwan A, Albazzan M, Harik R. "Influence of process parameters in AFP fiber steering on cylinders: Constant curvature paths". *Compos Part C Open Access* 2020; 2: 100036.
- [28] Croft K, Lessard L, Pasini D, Hojjati M, Chen J. "Experimental study of the effect of automated fiber placement induced defects on performance of composite laminates". *Compos Part A Appl Sci Manuf* 2011; 42: 484–491.
- [29] Del Rossi D, Cadran V, Thakur P, Palardy-Sim M, Lapalme M, Lessard L. "Experimental investigation of the effect of half gap/half overlap defects on the strength of composite structures fabricated using automated fibre placement (AFP)". *Compos Part A Appl Sci Manuf* 2021; 150: 106610.

References

- [30] Fayazbakhsh K, Arian Nik M, Pasini D, Lessard L. "Defect layer method to capture effect of gaps and overlaps in variable stiffness laminates made by Automated Fiber Placement". *Compos Struct* 2013; 97: 245–251.
- [31] Falcó O, Mayugo JA, Lopes CS, Gascons N, Costa J. "Variable-stiffness composite panels: Defect tolerance under in-plane tensile loading". *Compos Part A Appl Sci Manuf* 2014; 63: 21–31.
- [32] Ghayour M, Hojjati M, Ganesan R. "Effect of manufacturing flaws on the behavior of composite beams manufactured by Automated Fibre Placement (AFP) process". In: *The Fourth International Symposium on Automated Composite Manufacturing ACM4*. 2019.
- [33] Falcó O, Lopes CS, Mayugo JA, Gascons N, Renart J. "Effect of tow-drop gaps on the damage resistance and tolerance of Variable-Stiffness Panels". *Compos Struct* 2014; 116: 94–103.
- [34] Nguyen MH, Vijayachandran AA, Davidson P, Call D, Lee D, Waas AM. "Effect of automated fiber placement (AFP) manufacturing signature on mechanical performance of composite structures". *Compos Struct* 2019; 228: 111335.
- [35] Lan M, Cartié D, Davies P, Baley C. "Influence of embedded gap and overlap fiber placement defects on the microstructure and shear and compression properties of carbon–epoxy laminates". *Compos Part A Appl Sci Manuf* 2016; 82: 198–207.
- [36] Sawicki AJ, Minguet PJ. "Effect of intraply overlaps and gaps upon the compression strength of composite laminates". In: *Collection of Technical Papers - AIAA/ASME/ASCE/AHS/ASC Structures, Structural Dynamics and Materials Conference*. AIAA, 1998, pp. 744–754.
- [37] Nimbal SS, Banker MM, Roopa A, Varughese B, Sundaram R. "Effect of gap induced waviness on compressive strength of laminated composites". *Mater Today Proc* 2017; 4: 8355–8369.
- [38] Guin WE, Jackson JR, Bosley CM. "Effects of tow-to-tow gaps in composite laminates fabricated via automated fiber placement". *Compos Part A Appl Sci Manuf* 2018; 115: 66–75.
- [39] Marouene A, Legay P, Boukhili R. "Experimental and numerical investigation on the open-hole compressive strength of AFP composites containing gaps and overlaps". *J Compos Mater* 2017; 51: 3631–3646.
- [40] Falcó O, Lopes CS, Naya F, Sket F, Maimí P, Mayugo JA. "Modelling and simulation of tow-drop effects arising from the manufacturing of steered-fibre composites". *Compos Part A Appl Sci Manuf* 2017; 93: 59–71.
- [41] Elsherbini YM, Hoa S V. "Experimental and numerical investigation of the effect of gaps on fatigue behavior of unidirectional carbon/epoxy automated fiber placement laminates". *J Compos Mater* 2017; 51: 759–772.
- [42] Elsherbini YM, Hoa S V. "Fatigue threshold-stress determination in AFP laminates containing gaps using IR thermography". *Compos Sci Technol* 2017; 146: 49–58.

References

- [43] Li X, Jones MI, Woigk W, Hallett SR, Wisnom MR. "Modelling the effect of interacting gaps and overlaps in automated fibre placement (AFP) manufactured laminates". *Sci Eng Compos Mater* 2015; 22: 115–129.
- [44] Noevere AT, Collier CS. "Mapping AFP manufacturing data from VCP to hypersizer for stress analysis and optimization". In: *AIAA/ASCE/AHS/ASC Structures, Structural Dynamics, and Materials Conference, 2018*. American Institute of Aeronautics and Astronautics Inc, AIAA, 2018. Epub ahead of print 2018. DOI: 10.2514/6.2018-0228.
- [45] Zhou W, Cheng Q, Xu Q, Zhu W, Ke Y. "Deformation and fracture mechanisms of automated fiber placement pre-preg laminates under out-of-plane tensile loading". *Compos Struct* 2021; 255: 112948.
- [46] Nguyen MH, Davidson P, Waas AM. "Experimental and numerical study on the tensile failure behavior of toughened-interlayer composite laminates with automated fiber placement (AFP) induced gap and overlap defects". *Int J Mater Form* 2020; 1–15.
- [47] Rhead, A. T.; Dodwell, T. J.; Butler R. "The effect of tow gaps on compression after impact strength of robotically laminated structures". *C Comput Mater Contin* 2013; 35: 1–16.
- [48] Hoa S V. "*Principles of the Manufacturing of Composite Materials*". DEStech Publications, Incorporated, <https://books.google.ca/books?id=BipITS70dw0C> (2009).
- [49] Abrate S. "Impact on Laminated Composites: Recent Advances". *Appl Mech Rev* 1994; 47: 517.
- [50] Abrate S. "Impact on Laminated Composite Materials". *Appl Mech Rev* 1991; 44: 155–190.
- [51] Olsson R. "Analytical prediction of large mass impact damage in composite laminates". *Compos Part A Appl Sci Manuf* 2001; 32: 1207–1215.
- [52] Minak G, Abrate S, Ghelli D, Panciroli R, Zucchelli A. "Low-velocity impact on carbon / epoxy tubes subjected to torque – Experimental results , analytical models and FEM analysis". *Compos Struct* 2010; 92: 623–632.
- [53] Olsson R. "Analytical model for delamination growth during small mass impact on plates". *Int J Solids Struct* 2010; 47: 2884–2892.
- [54] Olsson R. "Analytical prediction of damage due to large mass impact on thin ply composites". *Compos Part A Appl Sci Manuf* 2015; 72: 184–191.
- [55] Ghayour M, Ganesan R, Hojjati M. "Interlaminar shear strength of the Carbon/Epoxy composites containing gaps induced by Automated Fiber Placement process". In: *11th Canadian-International Conference on Composites (CANCOM)*. 2019.
- [56] González EV, Maimí P, Camanho PP, Lopes CS, Blanco N. "Effects of ply clustering in laminated composite plates under low-velocity impact loading". *Compos Sci Technol* 2011; 71: 805–817.
- [57] Abdulhamid H, Bouvet C, Michel L, Aboissière J, Minot C. "Experimental study of compression after impact of asymmetrically tapered composite laminate". *Compos Struct* 2016; 149: 292–303.

References

- [58] Li N, Chen PH. "Micro–macro FE modeling of damage evolution in laminated composite plates subjected to low velocity impact". *Compos Struct* 2016; 147: 111–121.
- [59] Wang K, Zhao L, Hong H, Zhang J. "A strain-rate-dependent damage model for evaluating the low velocity impact induced damage of composite laminates". *Compos Struct* 2018; 201: 995–1003.
- [60] Li X, Ma D, Liu H, Tan W, et al. "Assessment of failure criteria and damage evolution methods for composite laminates under low-velocity impact". *Compos Struct* 2019; 207: 727–739.
- [61] Abrate S. *Impact on composite structures*. New York, NY, USA : Cambridge University Press, 1998.
- [62] Yudhanto A, Wafai H, Lubineau G, Goutham S, et al. "Revealing the effects of matrix behavior on low-velocity impact response of continuous fiber-reinforced thermoplastic laminates". *Compos Struct* 2019; 210: 239–249.
- [63] Yang P, Shams S, Slay A, Brokate B, Elhajjar R. "Evaluation of temperature effects on low velocity impact damage in composite sandwich panels with polymeric foam cores". *Compos Struct* 2015; 129: 213–223.
- [64] Lopes CSS, Camanho PPP, Gürdal Z, Maimí P, González EV V. "Low-velocity impact damage on dispersed stacking sequence laminates. Part II: Numerical simulations". *Compos Sci Technol* 2009; 69: 937–947.
- [65] Woigk W, Hallett SR, Jones MI, Kuhtz M, Hornig A, Gude M. "Experimental investigation of the effect of defects in Automated Fibre Placement produced composite laminates". *Compos Struct* 2018; 201: 1004–1017.
- [66] Hyer MW, Lee HH. "The use of curvilinear fiber format to improve buckling resistance of composite plates with central circular holes". *Compos Struct* 1991; 18: 239–261.
- [67] Marouene A, Boukhili R, Chen J, Yousefpour A. "Buckling behavior of variable-stiffness composite laminates manufactured by the tow-drop method". *Compos Struct* 2016; 139: 243–253.
- [68] Gürdal Z., Tatting B. F., Wu K. C. "Variable stiffness panels, Effects of stiffness variation on in-plane and bending responses". *Compos Part A Appl Sci Manuf* 2005; 39: 911–922.
- [69] Lopes CS, Gürdal Z, Camanho PP. "Variable-stiffness composite panels: Buckling and first-ply failure improvements over straight-fibre laminates". *Comput Struct* 2008; 86: 897–907.
- [70] Setoodeh S, Abdalla MM, IJsselmuiden ST, Gürdal Z. "Design of variable-stiffness composite panels for maximum buckling load". *Compos Struct* 2009; 87: 109–117.
- [71] Rouhi M, Ghayoor H, Fortin-Simpson J, Zacchia TT, Hoa S V., Hojjati M. "Design, manufacturing, and testing of a variable stiffness composite cylinder". *Compos Struct* 2018; 184: 146–152.
- [72] Lan M, Cartié D, Davies P, Baley C. "Microstructure and tensile properties of carbon-epoxy laminates produced by automated fibre placement: Influence of a caul plate on the effects

References

- of gap and overlap embedded defects". *Compos Part A Appl Sci Manuf* 2015; 78: 124–134.
- [73] ASTM D7264/D7264M-07. "D7264/D7264M: Standard test method for flexural properties of polymer matrix composite materials". *ASTM Stand* 2007; i: 1–11.
- [74] "ASTM D2344/D2344M: Standard test method for short-beam strength of polymer matrix composite materials and their laminates". *ASTM Stand*.
- [75] Wriggers P, Zavarise G. "Computational Contact Mechanics". In: *Encyclopedia of Computational Mechanics*. Chichester, UK: John Wiley & Sons, Ltd. Epub ahead of print 15 November 2004. DOI: 10.1002/0470091355.ecm033.
- [76] Ebina M, Yoshimura A, Sakaue K, Waas AM. "High fidelity simulation of low velocity impact behavior of CFRP laminate". *Compos Part A Appl Sci Manuf* 2018; 113: 166–179.
- [77] Bondyra A, Klasztorny M, Szurgott P, Gotowicki P. "Numerical modelling and experimental verification of glass-polyester mixed laminate beam bending test". *acta Mech Autom* 2012; 6: 1–18.
- [78] McCarthy CT, O'Higgins RM, Frizzell RM. "A cubic spline implementation of non-linear shear behaviour in three-dimensional progressive damage models for composite laminates". *Compos Struct* 2010; 92: 173–181.
- [79] Jumahat A, Soutis C, Jones FR, Hodzic A. "Fracture mechanisms and failure analysis of carbon fibre/toughened epoxy composites subjected to compressive loading". *Compos Struct* 2010; 92: 295–305.
- [80] Shi Y, Pinna C, Soutis C. "Modelling impact damage in composite laminates: A simulation of intra- and inter-laminar cracking". *Compos Struct* 2014; 114: 10–19.
- [81] Hashin Z. "Failure criteria for unidirectional fiber composites". *J Appl Mech* 1980; 47: 329–334.
- [82] Pham DC, Cui X, Ren X, Lua J. "A discrete crack informed 3D continuum damage model and its application for delamination migration in composite laminates". *Compos Part B Eng* 2019; 165: 554–562.
- [83] Shi Y, Swait T, Soutis C. "Modelling damage evolution in composite laminates subjected to low velocity impact". *Compos Struct* 2012; 94: 2902–2913.
- [84] Jumahat A, Soutis C, Hodzic A. "A graphical method predicting the compressive strength of toughened unidirectional composite laminates". In: *Applied Composite Materials*, pp. 65–83.
- [85] Canal LP, Segurado J, LLorca J. "Failure surface of epoxy-modified fiber-reinforced composites under transverse tension and out-of-plane shear". *Int J Solids Struct* 2009; 46: 2265–2274.
- [86] Bai X, Bessa MA, Melro AR, Camanho PP, Guo L, Liu WK. "High-fidelity micro-scale modeling of the thermo-visco-plastic behavior of carbon fiber polymer matrix composites". *Compos Struct* 2015; 134: 132–141.
- [87] Fiedler B, Hojo M, Ochiai S, Schulte K, Ochi M. "Finite-element modeling of initial matrix

References

- failure in CFRP under static transverse tensile load". *Compos Sci Technol* 2001; 61: 95–105.
- [88] Tschoegl NW. "Failure surfaces in principal stress space". *J Polym Sci Part C Polym Symp* 1971; 32: 239–267.
- [89] Melro AR, Camanho PP, Andrade Pires FM, Pinho ST. "Micromechanical analysis of polymer composites reinforced by unidirectional fibres: Part I – Constitutive modelling". *Int J Solids Struct* 2013; 50: 1897–1905.
- [90] Camanho P, Davila CG. "Mixed-Mode Decohesion Finite Elements in for the Simulation Composite of Delamination Materials". *Nasa* 2002; TM-2002-21: 1–37.
- [91] Benzeggagh ML, Kenane M. "Measurement of mixed-mode delamination fracture toughness of unidirectional glass/epoxy composites with mixed-mode bending apparatus". *Compos Sci Technol* 1996; 56: 439–449.
- [92] Camanho PP, Dávila GC. "*Mixed-mode decohesion finite elements for the simulation of delamination in composite materials*". 2002.
- [93] Ghayour M, Hojjati M, Ganesan R. "Effect of Tow Gaps on Impact Strength of Thin Composite Laminates Made by Automated Fiber Placement: Experimental and Semi-Analytical Approaches". *Compos Struct* 2020; 248: 112536.
- [94] Ghayour M, Hosseini-Toudeshky H, Jalalvand M, Barbero EJEJ. "Micro/macro approach for prediction of matrix cracking evolution in laminated composites". *J Compos Mater* 2016; 50: 2647–2659.
- [95] Ghayour M, Chitsaz N, Hosseini-Toudeshky H, Barbero EJ. "Enhanced variational approach for damage analysis of laminated composite". *Mech Adv Mater Struct* 2019; 27: 1483–1493.
- [96] Nartey M, Zhang T, Gong B, Wang J, et al. "Understanding the impact of fibre wrinkle architectures on composite laminates through tailored gaps and overlaps". *Compos Part B Eng* 2020; 196: 108097.
- [97] Oromiehie E, Garbe U, Gangadhara Prusty B. "Porosity analysis of carbon fibre-reinforced polymer laminates manufactured using automated fibre placement". *J Compos Mater* 2020; 54: 1217–1231.
- [98] Nixon-Pearson O, Belnoue J-H, Ivanov D, Potter K, Hallett S. "An experimental investigation of the consolidation behaviour of uncured prepregs under processing conditions". *J Compos Mater* 2017; 51: 1911–1924.
- [99] Krogh C, Glud JA, Jakobsen J. "Modeling the robotic manipulation of woven carbon fiber prepreg plies onto double curved molds: A path-dependent problem". *J Compos Mater* 2019; 53: 2149–2164.
- [100] Marouene A, Legay P, Boukhili R. "Experimental and numerical investigation on the open-hole compressive strength of AFP composites containing gaps and overlaps". *J Compos Mater* 2017; 51: 3631–3646.

References

- [101] Ghayour M, Ganesan R, Hojjati M. "Flexural response of composite beams made by Automated Fiber Placement process: Effect of fiber tow gaps". *Compos Part B Eng* 2020; 201: 108368.
- [102] Melro AR, Camanho PP, Andrade Pires FM, Pinho ST. "Micromechanical analysis of polymer composites reinforced by unidirectional fibres: Part II – Micromechanical analyses". *Int J Solids Struct* 2013; 50: 1906–1915.
- [103] Aboudi J, Arnold S, Bednarczyk B. "*Micromechanics of Composite Materials*". 1st ed. Elsevier Inc., 2013. Epub ahead of print 2013. DOI: 10.1016/C2011-0-05224-9.
- [104] Raghavan P, Li S, Ghosh S. "Two scale response and damage modeling of composite materials". *Finite Elem Anal Des* 2004; 40: 1619–1640.
- [105] Naghdinasab M, Farrokhabadi A, Madadi H. "A numerical method to evaluate the material properties degradation in composite RVEs due to fiber-matrix debonding and induced matrix cracking". *Finite Elem Anal Des* 2018; 146: 84–95.
- [106] Paley M, Aboudi J. "Micromechanical analysis of composites by the generalized cells model". *Mech Mater* 1992; 14: 127–139.
- [107] ABOUDI J. "The Generalized Method of Cells and High-Fidelity Generalized Method of Cells Micromechanical Models—A Review". *Mech Adv Mater Struct* 2004; 11: 329–366.
- [108] Bednarczyk BA, Aboudi J, Arnold SM. "Micromechanics Modeling of Composites Subjected to Multiaxial Progressive Damage in the Constituents". *AIAA J* 2010; 48: 1367–1378.
- [109] Aboudi J, Arnold SM, Bednarczyk BA, Aboudi J, Arnold SM, Bednarczyk BA. "The Method of Cells Micromechanics". In: cob Aboudi, Steven M. Arnold BAB (ed) *Micromechanics of Composite Materials*. Butterworth-Heinemann, pp. 147–226.
- [110] Fayazbakhsh K. "*The impact of gaps and overlaps on variable stiffness composites manufactured by automated fiber placement*". McGill University.
- [111] Cantwell W. "The impact resistance of composite materials - a review". *Composites* 1991; 5: 347–362.
- [112] Hampson PR, Moatamedi M. "A review of composite structures subjected to dynamic loading". *Int J Crashworthiness* 2007; 12: 411–428.
- [113] Richardson MO, Wisheart MJ. "Review of low-velocity impact properties of composite materials". *Compos Part A* 1996; 27: 1123–1131.
- [114] Ghayour M, Hojjati M, Ganesan R. "Induced defect layer method to characterize the effect of fiber tow gaps for the laminates manufactured by automated fiber placement technique:". <https://doi.org/10.1177/00219983211031649> 2021; 002199832110316.
- [115] Shah SZH, Karuppanan S, Megat-Yusoff PSM, Sajid Z. "Impact resistance and damage tolerance of fiber reinforced composites: A review". *Compos Struct* 2019; 217: 100–121.
- [116] Bogenfeld R, Kreikemeier J, Wille T. "Review and benchmark study on the analysis of low-velocity impact on composite laminates". *Eng Fail Anal* 2018; 86: 72–99.

References

- [117] Belnoue JP-H, Mesogitis T, Nixon-Pearson OJ, Kratz J, et al. "Understanding and predicting defect formation in automated fibre placement pre-preg laminates". *Compos Part A Appl Sci Manuf* 2017; 102: 196–206.
- [118] "Simulia. Abaqus 6.13 User's manual".
- [119] Ghayour M, Ganesan R, Hojjati M. "Induced Defect Layer Method to characterize the effect of fiber tow gaps for the laminates manufactured by Automated Fiber Placement Technique". *J Compos Mater*.
- [120] Kendall K. "Cracks: a century of toughness". In: *Crack Control*. Elsevier, 2021, pp. 1–29.
- [121] Sebaey TA, Mahdi E. "Using thin-ply to improve the damage resistance and tolerance of aeronautical CFRP composites". *Compos Part A Appl Sci Manuf* 2016; 86: 31–38.
- [122] Soto A, González E V., Maimí P, Martín de la Escalera F, Sainz de Aja JR, Alvarez E. "Low velocity impact and compression after impact simulation of thin ply laminates". *Compos Part A Appl Sci Manuf* 2018; 109: 413–427.
- [123] Sihm S, Kim RY, Kawabe K, Tsai SW. "Experimental studies of thin-ply laminated composites". *Compos Sci Technol* 2007; 67: 996–1008.
- [124] Yokozeki T, Kuroda A, Yoshimura A, Ogasawara T, Aoki T. "Damage characterization in thin-ply composite laminates under out-of-plane transverse loadings". *Compos Struct* 2010; 93: 49–57.